Fault-Tolerant Control with Applications to Aircraft Using Linear Quadratic Design Framework

Bin Yu

A Thesis
In the Department
of
Mechanical & Industrial Engineering

Presented in Partial Fulfillment of Requirements
For the Degree of
Doctor of Philosophy (Mechanical Engineering) at
Concordia University
Montreal, Quebec, Canada

February 2016

CONCORDIA UNIVERSITY
SCHOOL OF GRADUATE STUDIES

This is to certify that the thesis prepared

By: Bin Yu

Entitled: Fault-Tolerant Control with Applications to Aircraft Using Linear Quadratic Design Framework

and submitted in partial fulfillment of the requirements for the degree of

Ph.D.

complies with the regulations of the University and meets the accepted standards with respect to originality and quality.

Signed by the final examining committee:

Deborah Dysart-Gale — Chair

Ruxandra Mihaela BOTEZ — External Examiner

Amir G. Aghdam — External to Program

Brandon W. Gordon — Examiner

Wenfang Xie — Examiner

Youmin Zhang — Thesis Supervisor

Approved by

Chair of Department or Graduate Program Director

Feb. 29 , 2016

Dean of Faculty

Abstract

Fault-Tolerant Control with Applications to Aircraft Using Linear Quadratic Design Framework

Bin Yu, Ph.D.

Concordia University, 2016

Safety is one of the major concerns in the aviation community for both manned aircraft and unmanned aerial vehicles (UAVs). The safety issue of manned aircraft, such as commercial aircraft, has drawn great attentions especially after a series of disasters in recent decades. Safety and reliability issues of UAVs have also attracted significant attention due to their highly autonomous feature towards their future civilian applications. Focusing on the improvement of safety and reliability of aircraft, a fault-tolerant control (FTC) system is demanded to utilize the configured redundancy in an effective and efficient manner to increase the survivability of aircraft in the presence of faults/failures.

This thesis aims to develop an effective FTC system to improve the security, reliability, and survivability of the faulty aircraft: manned aircraft and UAVs. In particular, the emphases are focused on improving the on-line fault-tolerant capability and the transient performance between faults occurrence and control re-configuration.

In the existing fault-tolerant literature, several control approaches are developed to possess fault-tolerant capability in recent decades, such as sliding mode control (SMC), model reference adaptive control (MRAC), and model predictive control (MPC), just as examples. Different strategies have their specific benefits and drawbacks in addressing different aspects of fault-tolerant problems. However, there are still open problems in the fault-tolerant performance improvement, the transient behavior management, consideration of the interaction between FTC and fault detection and diagnosis (FDD), etc. For instance, MPC is recognized as a suitable inherent structure in synthesizing a FTC system due to its capability of addressing faults via solving constraints, reforming cost function, and updating model on-line. However, this on-line FTC capability introduces further challenges in terms of fault problem formulation, on-line computation, transient behavior before reconfiguration is triggered, etc. Designing an efficient FDD is also a challenge topic with respect to time response speed, accuracy, and reliability due to its interaction with a fault-tolerant controller.

In the control design framework based on linear quadratic (LQ) cost function formulation, faults can be accommodated in both passive and active way. A passive FTC system is synthesized with a prescribed degree of stability LQ design technique. The state of the

post-fault system is obtained through state-augmented extended Kalman filter (SAEKF), which is a combined technique with state and parameter estimation. In terms of reconfiguration capability, MPC is considered as a favorable active FTC strategy. In addition to MPC framework, the improvement of on-line computational efficiency motivates MPC to be used to perform fault-tolerant flight control. Furthermore, a Laguerre-function based MPC (LF-MPC) is presented to enhance the on-line fault-tolerant capability. The modification is based on a series of Laguerre functions to model the control trajectory with fewer parameters. In consequence, the computation load is reduced, which improves the real-time fault-tolerant capability in the framework of MPC. The FTC capability is further improved for accommodating the performance degradation during the transient period before the control reconfiguration. This approach is inspired by exponentially increasing weighting matrix used in linear quadratic regulator (LQR).

Two platforms are used to perform the evaluation of the designed FTC system. A quadrotor UAV, named the Qball-X4, is utilized to test FTC designed with exponentially increasing weighing matrix LQ technique and FDD designed with SAEKF. The evaluation is conducted under the task of trajectory tracking in the presence of loss of control effectiveness (LOE) faults of actuators. The modified MPC is utilized to synthesize an active FTC system to accommodate the elevator stuck fault of a Boeing 747-100/200 benchmark model. The exponentially increasing weighing matrix LQ technique is further implemented in LF-MPC framework to improve the fault-tolerant capability before the control reconfiguration. A time delayed FDD is integrated into the evaluation process to present the effectiveness of the proposed FTC strategies. The designed FTC system is evaluated under the emergency landing task in the event of failure of elevators.

Acknowledgement

I would like to express my gratitude to everyone who supported me throughout the course of my PhD study. I am thankful for their inspiring guidance, invaluably constructive criticism and friendly advice during my research. First I would like to express my greatest appreciation and gratitude to my supervisor, Prof. Youmin Zhang, for giving me the opportunity to work on the fault-tolerant control topic and also for his insightful guidance, encouragement and support throughout the research project. I would also like to thank my committee members: Prof. Wenfang Xie, Prof. Henry Hong, Prof. Amir G. Aghdam, who gave me insightful suggestions on my critical literature review and research proposal exams.

I would like to express the deep appreciation to Prof. Deborah Dysart-Gale for her help, support, and friendship during my stay at Concordia.

I would also be grateful to my parents, my brother, and sisters for their love, encouragements, and supports. In particular, I show my appreciate to my girlfriend Ms. Chen Wei for her support and love. It would be impossible to accomplish my PhD study without them being supporting me.

Last but not least, I would like to thank my colleagues and friends: Dr. Xiang Yu, Dr. Zhi Li, Dr. Ismael Minchala, Mr. Peng Lu, Mr. Hamed Badihi, Mr. Dongdong Zheng, Ms. Xian Wang, Mr. Dingyu Zhang, Dr. Yuansheng Zhou, Mr. Zhixiang Liu, Ms. Chi Yuan, Mr. Ban Wang, Ms. Yu Fu, Mr. Ali A.Hemmat, Mr. Tao Yu, Mr. Juqi Hu, and others, for their valuable discussions, friendship, and kind help.

Contents

List of Figures

List of Tables

Nomenclature

$.cg.$	Center of gravity
$\bar{c}$	Wing chord (m)
$\bar{q}$	Dynamic pressure, $\frac{1}{2}\rho V_{TAS}^2$ (N/m^2)
$\bar{u}$	Non-manipulated control input vector
β	Angle of sideslip
$\delta_{ail/r}$	Inboard aileron (left/right)
$\delta_{aol/r}$	Outboard aileron (left/right)
$\delta_{eil/r}$	Inboard elevator (left/right)
$\delta_{eol/r}$	Outboard elevator (left/right)
δ_{rl}	Lower rudder
δ_{ru}	Upper rudder
δ_{spi}	ith spoiler
ϕ	Roll angle
ψ	Yaw angle
σ	Horizontal stabilizer deflection
$\sigma_i(k)$	Control effectiveness
θ	Pitch angle

A_t State transition matrix

B_t Control matrix

C_D Drag coefficient

C_L Lift coefficient

C_m Pitching moment coefficient

C_t Output matrix

c_α, c_β Cosine-angle of attack & sideslip

F_x, F_z Body-axes aerodynamic forces along x and z axes (N)

h_e Geometric altitude (m)

ih Stabilizer

M_y Body-axes aerodynamic moments (N.m)

MAC Mean aerodynamic chord

p_b Roll rate about body x-axis

q Pitch rate (rad/s)

q_b Pitch rate about body y-axis

r_b Yaw rate about body z-axis

S Reference surface area

s_α, s_β Sine-angle of attack & sideslip

Tn Thrust force (N)

$u(t)$ Control inputs

u_0 Trim control efforts of a system

$u_m(k)^f$ Actuator fault at the time instant k

u_t Control effort vector of a system

V_{TAS} True airspeed (m/s)

x_0 Trim states of a system

x_e Horizontal position along with earth x-axis

x_t State vector of a system

y_e Horizontal position along with earth y-axis

EA Eigenstructure assignment

FDD Fault detection and diagnosis

FTC Fault-tolerant control

FTFC Fault-tolerant flight control

GARTEUR Group for aeronautical research and technology in Europe

GS Gain scheduling

GTM Generic transport model

IFAC International federation of automatic control

LMI Linear matrix inequality

LPV Linear parameter varying

LQ Linear quadratic

LQR Linear quadratic regulator

MF Model following

MM Multiple model

MPC Model predictive control

RECOVER REconfigurable COntrol for Vehicle Emergency Return

SAEKF States-augmented extended Kalman filter

SAKF States-augmented Kalman filter

SI Pseudo inverse

SMC Sliding model control

VSC Variable structure control

Chapter 1

Introduction

1.1 Motivation on Investigating Fault-Tolerant Control of Aerial Vehicles

Safety issue of aircraft is getting more and more attentions in recent decades due to a series of disasters, such as the crash of McDonnell-Douglas DC-10, American Airlines Flight AA191, Japan Airlines Flight JL123, United Airlines Flight UA 232, USAir Flight 427, United Airlines Flight 585, and El Al Flight 1862 in 1992 [3–5]. The consequences of these disasters introduce a great amount of loss, especially, with the expenses of individuals' lives. However, some disasters can be avoided if the faulty aircraft can be operated and landed safely with assistance of remaining functional actuators manipulated in a proper way. The 1989 Sioux City DC-10 case is one example, in which the pilot saved 185 people's lives by performing their reconfiguration with asymmetric thrust from the remaining engines to maintain the limited control in the presence of total hydraulic system failure. The ability of reconfigurable control improves the survivability of aircraft in the presence of faults/failures, which motivates the development of a system being capable of maintaining the stability and a certain degree of performance in the presence of faults.

In addition to manned aircraft, unmanned aerial vehicles (UAVs) have drawn increasing attentions during recent years, since they can be applied for both military and civil purposes in an efficient and low cost manner, such as reconnaissance, search and rescue [6], forest fire monitoring [7], pipeline monitoring [8], data collection [9], mapping [10], and product delivery [11], respectively. The problems of safety, reliability, and high autonomous capability are

naturally brought with the applications, which motivates the efforts to increase the reliability and safety of the systems. Without any proper actions, faulty UAVs can lead to catastrophic consequences, which may cause great danger to personnel on the ground when it is operated in the environment with great population density. Therefore, UAVs are highly demanded to possess fault-tolerant capability, which improves safety of UAVs not only in normal situation, but also in abnormal cases.

The safety concerns of manned and unmanned aircraft promote the research of fault-tolerant control (FTC) on aircraft with the same purpose of improving the safety, reliability, and survivability in the event of abnormal situations. A FTC scheme is thereby proposed to prevent the system breakdown using the configured redundancies [2, 12]. The design of GARTEUR Reconfigurable Control for Vehicle Emergency Return (RECOVER) is developed to investigate and validate the performance of the newly designed fault-tolerant flight control schemes when applied to a realistic, non-linear advanced flight control application. Moreover, the National Aeronautics and Space Administration (NASA) has developed a Generic Transport Model (GTM), which is a 5.5% scaled dynamic model of a Boeing 757, to advance and validate new technologies for transport aircraft, thereby, reducing the loss of control accidents resulting from adverse conditions [13–15]. These efforts and resources also motivate this research of using the RECOVER benchmark model (Boeing 747) to investigate FTC strategies for manned/unmanned aircraft. Last but not least, a quadrotor UAV platform named the Qball-X4 is available in Diagnosis, Flight Control and Simulation (DFCS) Lab at Concordia University, which brings the direct motivation of this study to test the FTC approach on the UAV platform.

1.2 Research Objectives and Main Contributions

The structure of a FTC system is well studied in the literature. In the framework of FTC, a great amount of control approaches are developed to possess FTC capability in recent decades, such as sliding mode control (SMC) [16–18], adaptive control (AC) [15, 19], and model predictive control (MPC) [4, 20, 21]. Different fault-tolerant strategies have their specific benefits and drawbacks in addressing different aspects of fault-tolerant problems. Despite the developed FTC strategies, there are still open problems in the fault-tolerant performance improvement [2, 22], such as the transient behavior management [23], the limited amount of recovery time [24], the post-fault information [25, 26], and consideration of

the interaction between FTC and FDD [27, 28]. For instance, the reconfigurable property of MPC for FTC has been extensively studied in recent two decades [29–31].

MPC is recognized as a suitable strategy in synthesizing a reconfigurable controller for FTC due to the inherent capability of solving constraints, reforming cost function, and updating model on-line. These updating and on-line solving properties can be combined with faults. However, this on-line FTC capability introduces further challenges in terms of fault problem formulation, on-line computation, transient behavior before reconfiguration triggered, etc. These problems in the framework of MPC-based FTC system are not well discussed, especially, on aircraft system. An efficient FDD is also a challenge topic with respect to time response speed, accuracy, and reliability due to its interaction with a fault-tolerant controller.

This research aims to find an effective FTC approach in the framework of linear quadratic (LQ) programming to improve the safety, reliability, and survivability of aircraft in the event of actuator faults/failure. The effectiveness of the designed FTC strategies are tested and evaluated based on unmanned/manned aircraft: 1) the Qball-X4 quadrotor UAV platform and 2) the RECOVER benchmark, which is a fixed-wing platform of a Boeing 747-100/200 benchmark model with more complexity compared to the Qball-X4 platform.

The contributions of this study are summarized as follows:

- Develop and implement an effective fault-tolerant controller within the framework of LQ techniques: linear quadratic regulator (LQR) and MPC;
- Develop a fault detection and diagnosis (FDD) system using states-augmented extended Kalman filter to solve the FDD problem in the sensorless environment;
- Improve the performance of the designed FTC system with respect to on-line fault-tolerant capability;
- Improve the transient performance before the control reconfiguration is triggered with prescribed degree of stability design;
- Demonstrate the effectiveness of the proposed FTC strategy with FDD against loss of control effectiveness (LOE) based on the Qball-X4 platform;
- Demonstrate the effectiveness of the proposed active FTC with the emergency task of landing aircraft in the event of actuator faults based on the RECOVER benchmark model, in which an imperfect FDD with time delay is included into the close-loop evaluation.

1.3 Literature Review

This section covers the basic concept for understanding the concept of a fault/failure of aircraft. Categories of faults and the behaviors of different faults are illustrated for the purpose of solving the consequences resulted from the faults. To address the faults problems, the strategies to compensate the performance degradation are illustrated in two main principles: passive FTC and active FTC [1, 2]. Passive FTC uses the robustness margin to accommodate faults while active FTC reconfigures the control efforts with respect to the post-fault systems. In general, a FDD unit is demanded in the process of control reconfiguration. The active FTC structure is introduced in a schematic overview. Finally, the state-of-the-art of FTC approaches with applications to aircraft are presented to further develop an effective FTC system.

1.3.1 Fault Definition and Classification

A fault/failure is previously defined in literature [32], which is further promoted as unifying terminology by the International Federation of Automatic Control (IFAC) technical committee as follows [33–36]: "A fault is an unpermitted deviation of at least one characteristic property or parameter of the system from the acceptable/usual/standard condition. A failure is a permanent interruption of a system's ability to perform a required function under specified operating conditions. A failure can be treated as a severe sequence of a fault in terms of the property of the abnormal condition." Hence, the term fault/failure will be considered as 'fault' in general in this thesis.

The classification of faults has different categories according to various criteria. In terms of faults occurrence location, faults are categorized in three types: actuator faults, sensor faults, and other component faults. In terms of time characteristic, faults are also characterized as abrupt, incipient and intermittent as shown in Fig. 1.1. Abrupt faults occur instantaneously perhaps due to hardware damage, which can be severe since the stability/performance of the controlled system might be affected. Incipient faults represent slow parametric changes as result of aging. These faults are more difficult to be detected compared to abrupt fault since the symptom of this type of fault is not significant. Intermittent faults occur only at some randomly intervals, for instance, due to partially damaged wiring [1].

Based on the classification, it is convenient to understand the properties or behaviors of faults in the time sequence based on the fault occurrence location. This is particularly

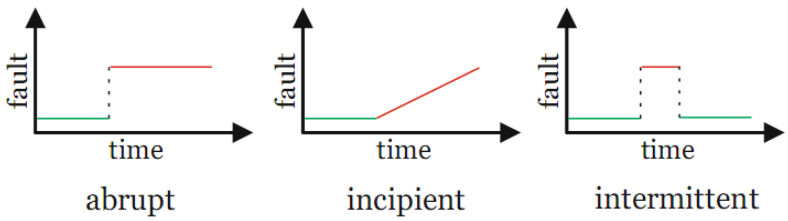

Figure 1.1: Fault classification with respect to time

important in addressing FTC problems with respect to the faulty components. In this thesis, abrupt actuator faults are the main concerns, and corresponding FTC strategies are implemented to accommodate the performance degradation due to these types of faults. In general, actuator faults can be represented as partial, such as LOE, or total loss of control (LOC), such as stuck, runaway, and floating of control surfaces. LOE of actuators means performance deteriorates in terms of the actuator's effectiveness, which might be caused by partial loss of a control surface, or pressure reduction in hydraulic lines [37]. Stuck fault is a failure condition when an actuator is lock at some fixed position and immovable. This might be caused by a mechanical jam, due to the lack of lubrication. Float fault is a failure condition when the control surface moves freely without providing any moment to aircraft. This might be induced by the loss of mechanical link. Since there is not any forces/moments generated from the floating control surface, the deflection of the control surface should be coincident with angle of attack. Runaway (hardover) fault is a failure condition, where the control surface moves to its maximum position limit or blowdown limit at its maximum rate. It might not be the same position between the maximum physical deflection of the control surface and the runaway position. This runaway fault might be induced by an electronic component failure, in which case a large wrong signal is sent to the actuator leading the control surface deflect to its maximum position. Runaway can be treated as a special stuck failure at its extreme position. The described faults [38] are shown in Fig. 1.2 for a clear overview, where t_F is the fault occurrence time and $\delta_{max}, \delta_{min}$ denote the maximum and minimum value of the actuator, respectively.

The faults studied in RECOVER benchmark model with different FTC strategies are listed in Table 1.1. The maneuver of operating reconfiguration is given in the second column of Table 1.1. The criticality of the faults mostly depends on the control redundancy of a system, which can be used to reconfigure the control maneuver. As listed in the table, the remaining control surfaces/efforts can still be used to accommodate faults, while the

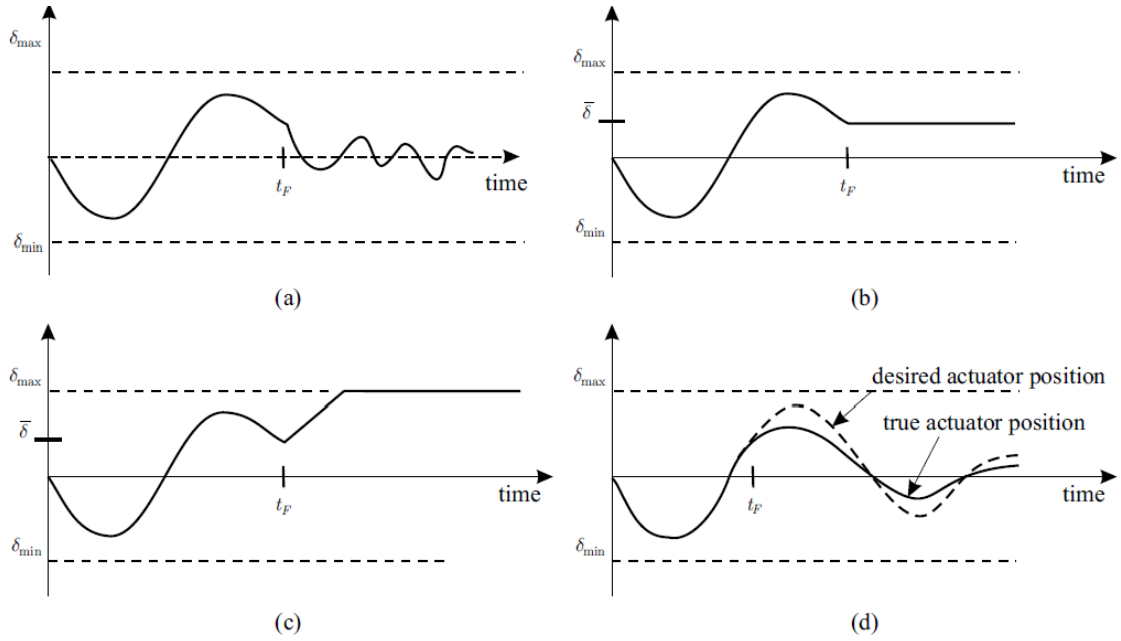

Figure 1.2: Floating fault (a), stuck fault (b), runaway fault (c), and loss of control effectiveness fault (d)

redundant parts are mostly in much more heavy duty mode than that in normal situation. For example, if faults occur in aileron, the spoilers can still be used to accommodate faults by the reconfiguration with assistance of FTC strategies. The spoilers work in a more aggressive way than that in a fault-free situation.

Table 1.1: Failure modes and the relevant control effects

Fault mode	Reconfiguration	Criticality
No failure	N/A	N/A
Stuck or erroneous elevator	Stabilizer; Symmetric ailerons; Differential thrust	Major
Stuck or erroneous aileron	Ailerons (remaining); Spoilers	Major
Elevator/stabilizer runaway	Ailerons (remaining); Flaps; Thrust; Use of static stability	Major
Stuck, erroneous or rudder runaway	Remaining surfaces; Asymmetric thrust	Catastrophic
Loss of vertical tail surface	Differential thrust; Differential speed brakes	Catastrophic
Engine separation and structural damage	Remaining surfaces; Remaining engines; Remaining sensors	Catastrophic

1.3.2 Fault-Tolerant Control Systems

A FTC system aims to improve the safety, reliability, and survivability of aircraft by accommodating the performance degradation induced by various faults. Conventionally, the fault-tolerant task of aircraft is performed with hardware redundancy. However, this strategy brings great weight to aircraft introducing further challenges, such as strength of structure, cost of aircraft, fuel efficiency. Moreover, it is not realistic to equip redundant system components in some aircraft due to the space and weight limitations. FTC is an effective way to reduce the above mentioned problems. In general, FTC systems are categorized into two types: passive and active FTC systems [2]. In a passive FTC system, a fault is accommodated and compensated by a fixed control with its robustness property. In most cases, faults to be accommodated in the passive FTC framework are known during the design process. The philosophy of a passive FTC system is to make the controller robust enough to resist all the pre-specified faults. Therefore, a passive FTC system only performs well with respect to specific known faults and cannot address faults exceeding the robustness margin efficiently. A passive FTC system has limited ability to accommodate faults due to the non-flexible property. However, the benefit of this strategy is that less computational burden is required to perform the fault-tolerant tasks. In this regard, it is a feasible method to be implemented in a time-critical system. Compared to a passive FTC system, an active FTC system is a more flexible control system to deal with various faults by the reconfiguration of controller. The essential of the reconfiguration is to utilize the redundancy of the faulty parts to compensate the performance degradation induced by the fault/ failure of components. The fault-tolerant task with control reconfiguration is usually performed with the assistance of a FDD module. Although, active FTC strategy can address faults with more complexity according to the updated fault information from a FDD unit. Meanwhile, it also brings challenges in algorithms and implementations, such as the reconfiguration approaches, the FDD strategies, and the combination of FDD and reconfigurable control. Each of the mentioned problems includes more specific challenges, such as reliability of algorithm, uncertainty resistance, real-time performance, as well as other challenges presented in [2]. Based on the knowledge of passive FTC strategy philosophy, the passive FTC structure is fixed without significant difference compared to conventional controller. Therefore, the schematic diagram of an active FTC system of aircraft is only presented as shown in Fig. 1.3. A FDD module, a reconfiguration mechanism, and a reconfigurable fault-tolerant controller are combined together and cooperate functionally as an active FTC system marked in the rectangular area in Fig. 1.3. Conventionally, the majority of the FDD research is only for

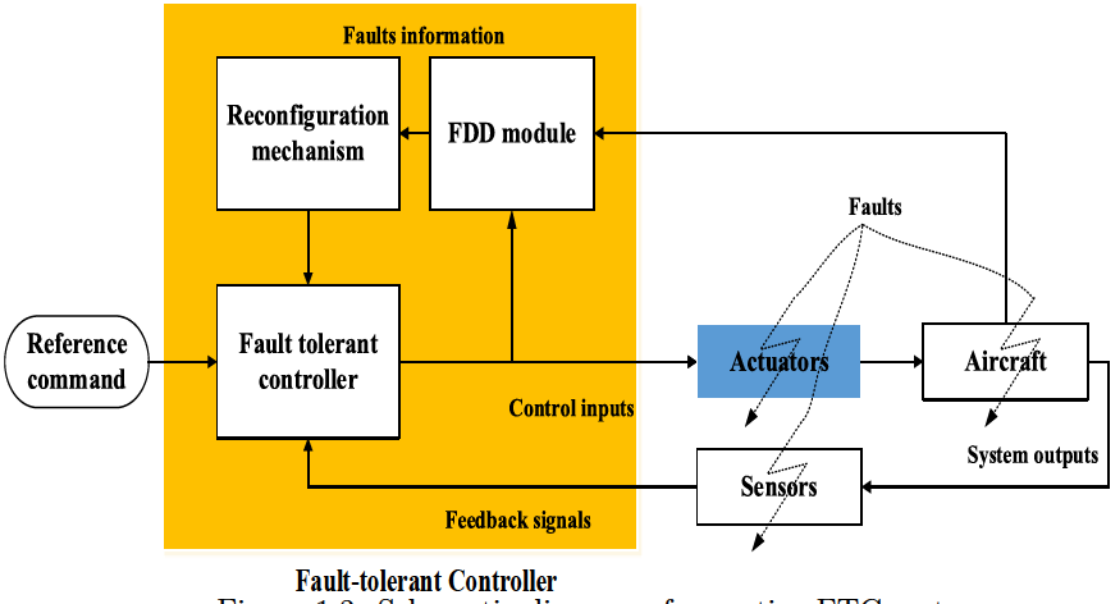

Figure 1.3: Schematic diagram of an active FTC system

monitoring and fault detection purpose [34, 39, 40], not for the application of FTC. However, FDD is critical to the performance of active FTC, as it is in the control loop and provides the information of faults, which determines the reconfiguration of the fault-tolerant controller. An assumption is given in most of literature that FDD provides the accurate information for reconfigurable control. It is not the case in reality. Therefore, the synthesis of integrated/combined FDD and FTC strategy is still an active and challenging problem due to time delay of the FDD, uncertainty of diagnosed fault information, faulty alarm, etc [2]. Moreover, the FTC approach is mostly model-based methodology, which usually need system states obtained from observer. Overall, two problems in synthesizing a FDD unit for the model-based FTC strategies are summarized as: the unmeasured states and the fault information.

Fault Detection and Diagnosis Approaches

Faults are inevitable and unpredictable in aircraft components. To detect the faulty components, the voting scheme with hardware redundancy is adopted conventionally, which is usually costly due to using extra expensive sensors. Furthermore, for some UAVs and manned aircraft, multiple-hardware redundancy is hard to implement due to the lack of operating space, unavailable environment, etc. Therefore, an increasing number of researches

focus on the development of analytical redundancy to detect and diagnose faults. In some sensorless environment, a FDD approach, which makes use of mathematical model of the monitored component/system to diagnose faults, is appropriate and favorable to overcome the cost problem and weight limitations of the conventional hardware voting method. Generally, FDD approaches fall into two categories: model-based and data-based schemes. Each of the two schemes can further be categorized into two types: qualitative and quantitative schemes.

The model-based FDD scheme is shown in Fig. 1.4. In particular, a quantitative model-

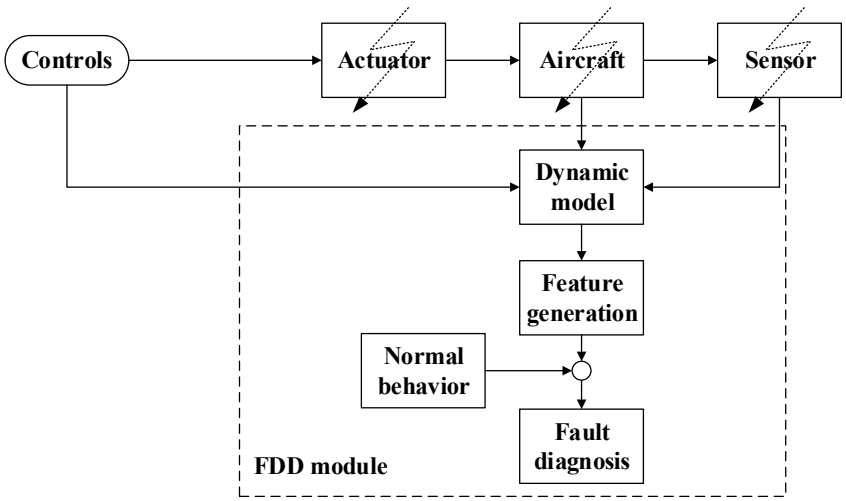

Figure 1.4: Overview of a FDD scheme

based FDD is more favorable for the FTC system design since most FTC approaches are model-based methods. In the framework of a quantitative model-based FDD, there are three common used techniques exist to generate the residual: 1) state estimation approach, 2) parameter estimation, 3) parity space [2, 35, 41]. In addition to the three techniques applying individually, combinations of these three techniques are more suitable to carry out FDD tasks [2, 42, 43]. Several criteria are listed to evaluate FDD approaches: 1) ability to handle different type of faults, 2) ability to provide quick detection, 3) isolation, 4) identification, 4) suitable for FTC, 6) identifiability for multiple faults, 7) suitability to nonlinear systems, 8) robustness of noises and uncertainties, 9) computational complexity [2]. Based on the aforementioned criteria , the existing quantitative model-based approaches are presented in Table 1.2.

It is shown that the combination of parameter identification and state estimation tech-

Table 1.2: Quantitative model-based approaches regarding FDD evaluation criteria [2]

Features of various FDD methods.

Criteria\method	State estimation				Parameter estimation RLS and variants	Simultaneous state and parameter estimation		Parity space
	Single		Multiple					
	Observer	Kalman filter	Observers	Kalman filter		Extended Kalman filter	Two-stage Kalman filter	
Fault sensor	√	√	√	√	*	√	√	√
Actuator	+	+	+	√	√	√	√	+
Type structure	+	+	+	√	√	√	√	+
Speed of detection	√	√	√	√	*	√	√	√
Isolability	×	×	√	√	√	√	√	√
Identifiability	×	×	+	*	√	√	√	*
Suitability for ftc	×	×	√	√	√	√	√	×
Multiple faults identifiability	−	−	√	√	√	√	√	*
Nonlinear systems	×	×	+	√	+	√	√	√
Robustness	−	−	*	*	+	+	+	√
Computational complexity	√	√	*	*	√	*	√	√

Note: (√) favorable; (*) less favorable; (×) not favorable; (+) applicable; (−) not applicable.

niques are more suitable for the application of FDD [2].

Fault-Tolerant Control Approaches

Table 1.3: Active fault-tolerant methods

Optimization	LQ, H∞, linear matrix inequality (LMI), and model predictive control (MPC)
Switching	Multiple model (MM), gain scheduling (GS), linear parameter varying (LPV), variable structure control (VSC), sliding model control (SMC)
Matching	Pseudo inverse (PI), eigenstructure assignment (EA)
Following	Model following (MF), MPC
Compensation	Additive compensation and adaptive compensation

In the literature, the FTC approaches fall into the following techniques: LQ, pseudo inverse, gain scheduling, linear parameter varying, model reference adaptive control, eigenstructure assignment, multiple-model, feedback linearization or dynamic inversion, H_∞ robust control, model predictive control, variable structure/sliding mode control, and intelligent control, which are summarized in Table 1.3 based on reconfiguration mechanisms for a FTC system [2].

Various control methodologies have been exploited for the FTC system design of aircraft,

such as MM [44], control allocation (CA) [16, 45, 46], SMC [17, 47–49], non-linear dynamic inversion (NDI) [50], and MPC [4, 51]. MM method is an active FTC approach, which is based on a finite set of linearized models that describe the system in different flight conditions, such as, in the case of a faulty condition. A group of control laws are pre-designed based on the known possible faults, and the key to this method is to develop a mechanism to determine the global control action based on the multiple models. This method is highly attractive for FTC while only a finite number of anticipated faults can be accommodated effectively due to the finite number of models. SMC is another effective way to design a fault-tolerant controller, which can accommodate structural failure by modifying the plant dynamics. This approach is a robust control technique, which requires to tune the controller to the point that can accommodate all priori known faults. The conservative method might be not appropriate for the control of aircraft in a fault-free situation as the parameters are tuned to balance the performance in both normal and faulty situations. Another drawback of the method is that it only works for LOE faults. It cannot counteract the stuck, floating, and runaway faults. CA is thereby proposed combing with SMC approach to overcome the drawback [16]. EA is to place the eigenvalues of a linear system using state feedback and then using the remaining degree of freedom to align the eigenvectors as accurately as possible. The idea is to exactly assign some of the most dominant eigenvalues while minimizing the 2-norm of the difference of eigenvalues between fault-free and faulty conditions. The drawback of this method is that model accuracy is critical for the eigenvalue assignment. No uncertainty from the model and FDD part is considered in EA process. NDI is an effective approach for the control of a non-linear system with combination of other control techniques, such as CA, adaptive control. With an appropriate modeling, a full-flight control system can be quickly and efficiently developed. MPC is widely used in the industry due to that it is good at dealing with multiple variables and handling the constraints [52–54]. It is compared among these methods and indicated that MPC has the most suitable architecture with all kinds of faults while changing the constraints, internal model, and the objective function [1, 4]. In addition, MPC can be modified to be robust [55, 56], adaptive [57, 58], and computational efficient [18, 59], which make MPC attractive in the application of FTC.

Particularly, the state-of-the-art of FTC evaluated in the GARTEUR benchmark model [60] are depicted in Fig. 1.5, in which several FTC strategies are compared in terms of robustness, adaptive property, the ability to deal with the type of failures, the fault model, and the designed model. As can be seen from Fig. 1.5, MPC presents attracting characteristics for FTC purpose, marked by either filled dots or empty circles, compared to the other

control methodologies, in terms of dealing with multiple faults, the capability of addressing constraints, and the application of using linear/non-linear models.

Method	Failures		Robust	Adaptive	Fault Model		Constraints	Model Type	
	Actuator	Structural			FDI	Assumed		Linear	Nonlinear
Multiple Model Switching and Tuning (MMST)		●		●	●			●	
Interacting Multiple Model (IMM)		●		●	●		○	●	
Propulsion Controlled Aircraft (PCA)	●		○			●		●	●
Control Allocation (CA)*	●					●	○	●	
Feedback Linearization	●	●		●	●				●
Sliding Mode Control (SMC)*	○[1]	●	●[2]				●		●
Eigenstructure Assignment (EA)		●				●		●	
Pseudo Inverse Method (PIM)		●				●		●	
Model Reference Adaptive Control (MRAC)*		●		●	●			●	○
Model Predictive Control (MPC)*	●	●	○	○	●	●	●	●	●

Comparison of reconfigurable control methods
* Evaluated in this Action Group
1: Can handle partial loss of effectiveness of actuators, but not complete loss
2: Assumes robust control can handle all forms of structural failures

Figure 1.5: State-of-the-art of FTC [1]

Basically, MPC is a form of control in which the current control action is obtained by solving an optimization problem on-line at each sampling instant [61]. MPC gets great success in the process industries in chemical plants and oil refineries. Due to its success in the process industry and the advantages mentioned earlier, MPC is attracting more and more attentions in aerospace with the development of the computational speed. From the design point of view, MPC has several significant advantages, which include easy to be designed with state space model, easy to be tuned by the engineer, handling the constraints, and optimizing the objective function on-line with respect to timely information [53]. From the FTC point of view, MPC has the inherent properties to match the requirements of FTC [4]. Specially, faults for a system can be treated as constraints to the design of a fault-tolerant controller. Once MPC adopts the linear model as internal model to predict the future status of the system, the optimization problem can be solve in the LQ framework. In this sense, both MPC and LQR are the optimal control methods which can solve the problems formulated by the quadratic function. Considering that the LQ technique is a relative mature and successfully used as a modern control method in flight control, such as lateral autopilot control law of Boeing 767 and the Boeing version of Joint Strike Fighter [62], LQR is considered as a favorable approach in designing a FTC system using the robustness of LQR. In addition, LQR has inherent connection with MPC especially when the constraints of MPC is not activated. This motives the design of MPC can borrow ideas from LQR

technique to improve the fault-tolerant capability.

1.4 Thesis Organization

The thesis is organized as follows. Chapter 2 introduces the modelling process of actuator faults, the FDD approaches, and the basic concept of FTC strategy using LQ technique: LQR and MPC. Chapter 4 presents the process of designing a FTC system and a FDD module for a quadrotor UAV. The performance is investigated and validated by the Qball-X4 quadrotor platform. Chapter 5 introduces the non-linear model of a Boeing 747-100/200 airplane. The performance comparison between the linearized longitudinal model and nonlinear model of Boeing 747-100/200 is also presented with respect to the control surface deflections and thrusts. Chapter 6 synthesizes a FTC system with modified MPC to compensate the performance degradation induced by actuator faults, which is evaluated by aircraft emergency landing period. The FTC strategy is synthesized by Laguerre-function based MPC (LF-MPC), in consequence, the on-line fault-tolerant capability improves benefited from optimizing only a few coefficient parameters. Chapter 7 presents a LF-MPC based FTC approach with a prescribed degree of stability to improve the transient performance after abrupt fault occurrence. The degree of stability is obtained by modifying the cost function with exponentially increasing weighing matrices, in which case the robustness of FTC is improved without degrading the active fault-tolerant capability. Chapter 8 draws conclusions of the thesis and presents future works based on the performed current research.

Chapter 2

Fault Modeling and Fault-Tolerant Control within LQ Framework

This chapter presents the mathematical model of various actuator faults, FDD approaches with emphasizing Kalman filter based techniques, a FTC system schematic diagram, and the FTC strategy in the framework of LQ technique. Section 2.1 introduces the basic knowledge of fault modeling and presents the mathematical model of different types of actuator faults. Section 2.2 introduces FDD techniques with a focus on Kalman filter related techniques. Section 2.3 briefly introduces MPC algorithm and the fault-tolerant capability of MPC with the consideration of physical constraints. More specifically, the LQ technique is introduced at first due to its inherent connection with MPC. Based on the LQ framework and fault-tolerant consideration, constraints of MPC are further discussed. A variant of MPC named LF-MPC is introduced to function as an improved FTC strategy to accommodate the performance degradation induced by actuator faults. The fault-tolerant problem is formulated in the form of constraints in the LF-MPC framework and the control trajectory is approximated with a modeling method to reduce the computational burden since less optimized parameters are required to get control efforts. Section 2.4 summaries the contents of this chapter.

2.1 Fault Modeling

The considered modeling problem of actuators focuses on actuator faults. As discussed in Chapter 1, actuator faults of aircraft are classified into two types in terms of their behavior:

LOE of actuators and total actuator failures including stuck, runaway, and floating of control surfaces, etc. The actuator fault $u_m^f(k)$ at the time instant k is represented multiplicative model form with respect to the normal input $u_m(k)$ at the time instant k:

$$u_m^f(k) = u_m(k) + (I - \Sigma_A)(\bar{u} - u_m(k)), \tag{2.1}$$

where $u_m(k) \in \mathbb{R}^{l\times l}$ is the system input vector; $I \in \mathbb{R}^{l\times l}$ is the unit matrix; $\Sigma_A = diag\{\sigma_1(k), \sigma_2(k), \ldots, \sigma_l(k)\}$, where l is the dimension of actuators and $\sigma_i(k) \in [0, 1]$ is defined as the control effectiveness: $\sigma_i(k) = 0$ means completely losing its effectiveness of the ith actuator (i.e. failure); $\sigma_i(k) = 1$ represents 100% healthy of the ith actuator; and $\bar{u}$ is not a manipulated fault value.

For all $\sigma_i(k) = 0$, Eq. (2.1) is determined by the unknown fault value $\bar{u}$, which can be used to denote actuator stuck, runaway, and floating faults:

$$u_i^f(k) = \bar{u}_i. \tag{2.2}$$

Eq. (2.2) can denote the stuck fault with fixed input signal $\bar{u}$.

If $\bar{u}$ is the extreme (maximum/minimum) value of the acceptable input which is related to the flight condition

$$u_i^f(k) = \bar{u}_i = \begin{cases} u_{max} \\ u_{min}, \end{cases} \tag{2.3}$$

then, Eq. (2.3) can represent the runaway fault.

If $\bar{u}$ is related to the flight condition

$$u_i^f(k) = \bar{u}_i. \tag{2.4}$$

Eq. (2.4) can be used to represent the floating fault. A multiplicative format of fault modeling is convenient to express the partial LOE/LOC while it may cause the inconvenience of calculating the effective factors. The additive formulation of fault modeling [1, 37] is suitable for the application of FDD. Therefore, the expression in Eq. (2.1) is rewritten as Eq. (2.5) for FDD purpose:

$$u_m^f(k) = u_m(k) + F(u_m(k))\Gamma^a(k) + (I - \Sigma_A)\bar{u}, \tag{2.5}$$

where $\Gamma^a(k)$ is $[\gamma_1^a(k), \gamma_2^a(k), \ldots, \gamma_l^a(k)]$, $\gamma_i^a(k) = 1 - \sigma_i(k)$ $(i \in [1, l])$, and

$$F(u_m(k)) = \begin{bmatrix} -u_{m1}(k) & 0 & \cdots & 0 \\ 0 & -u_{m2}(k) & 0 & 0 \\ \vdots & \vdots & \ddots & \vdots \\ 0 & 0 & 0 & -u_{ml}(k) \end{bmatrix}. \tag{2.6}$$

In Eq. (2.5), $\Gamma^a(k)$ is defined as LOE factor and to be diagnosed for the fault-tolerant purpose.

2.2 Fault Detection and Diagnosis

In recent decades, all kinds of Kalman filter variants are developed and implemented to estimate the states and/or parameters for the purpose of FDD. Two-stage Kalman filter (TSKF) was proposed by [63] to estimate the constant bias of system model. An alternative approach is to estimate the random bias [64]. Optimal TSKF [65], is proposed to estimate the constant bias of the linear system under the noises with Gaussian distribution. The variant of optimal TSKF is further modified by modeling the LOE factor as a bias to detect and diagnose the LOE fault [37, 66–68]. Technically, TSKF is a method by augmenting fault information into a state vector based on the linear model, which is in the category of state-augmented Kalman filter (SAKF). The following subsections introduce the process of synthesizing FDD with SAKF.

2.2.1 System Model

The dynamics of aircraft can be represented in state-space model in the following general form:

$$\begin{cases} \dot{x}_t &= f_t(x_t, u_t) \\ y_t &= h_t(x_t), \end{cases} \tag{2.7}$$

where x_t is the state of aircraft, u_t is the control input, and y_t is the output response of aircraft. Linearizing Eq. (2.7) around the trim point(x_0, u_0), it can be obtained:

$$\begin{cases} \dot{x}_t \approx A_t x_t + B_t u_t \\ y_t \approx C_t x_t, \end{cases} \tag{2.8}$$

where

$$A_t = \frac{\partial f(x_t, u_t)}{\partial x_t}|(x_0, u_0), \qquad B_t = \frac{\partial f(x_t, u_t)}{\partial u_t}|(x_0, u_0), \qquad C_t = \frac{dh(x_t)}{dx_t}|x_0. \tag{2.9}$$

The model in Eq. (2.8) is also expressed in discrete form:

$$\begin{cases} x_m(k+1) = A_m x_m(k) + B_m u_l(k) \\ y_m(k) = C_m x_m(k), \end{cases} \tag{2.10}$$

where $x_m(k) \in \mathbb{R}^n$, $y_m(k) \in \mathbb{R}^m$, and $u_m(k) \in \mathbb{R}^l$ are the state, the output, and the input of the linearized system,respectively; and A_m, B_m, and C_m are the state matrix, the input matrix, and the output matrix, respectively.

2.2.2 Fault Detection and Diagnosis Scheme with SAKF

As the model-based FDD approach presents a deep insight into the dynamics process [2, 35], the model-based FDD system is thereby a very suitable method to detect and diagnose the fault when details of the post-fault system information are needed. The structure as

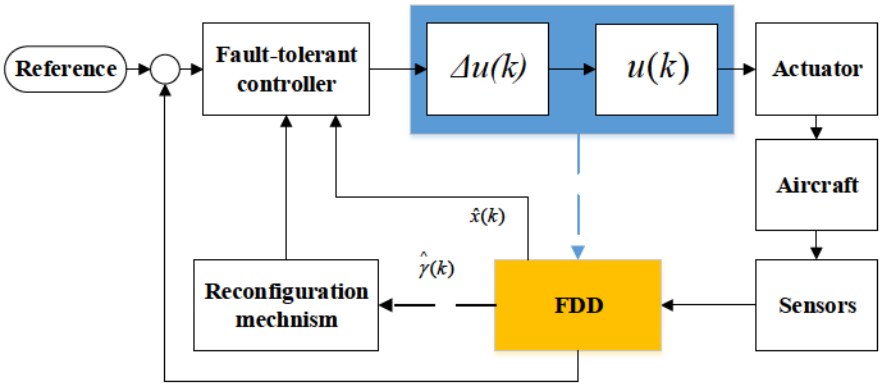

Figure 2.1: Schematic overview of FDD in a FTC system

shown in Fig. 2.1 presents a FTC system focusing on a FDD unit that simultaneously provides the states $\hat{x}_m(k)$ to the reconfigurable controller and the fault information $\hat{\gamma^a}(k)/\bar{u}(k)$ to the reconfigurable mechanism. The following focuses on the derivation of Kalman filter technique based FDD strategy, which emphasizes on the idea of simultaneously formalizing the fault

information and the post-fault states.

The system with the consideration of bias is presented as:

$$\begin{cases} x_{k+1} = Ax_k + Bu_k + Fb_k + \omega_k^x \\ b_{k+1} = b_k + \omega_k^b \\ y_k = Cx_k + Gb_k + \nu_k, \end{cases} \tag{2.11}$$

where $x_k \in \mathbb{R}^n$, $y_k \in \mathbb{R}^m$, and $u_k \in \mathbb{R}^l$ are the state vector, the observation vector, and the known inputs vector respectively, while $b_k \in R^p$ is the bias vector of unknown magnitude. Matrices A, B, C, F, and G have the appropriate dimensions. The noise sequence ω_k^x, ω_k^b, and ν_k are zero mean uncorrelated random sequences. k is the sampling time instant, and $k+1$ is the next sampling time instant. To detect bias using SAKF, Eq. (2.11) can be reformulated in conventional state space model as shown in Eq. (2.12):

$$\begin{cases} X_{k+1} = \bar{A}X_k + \bar{B}u_k + \bar{\omega_k} \\ y_k = \bar{C}X_k + \nu_k, \end{cases} \tag{2.12}$$

where

$$\bar{A} = \begin{bmatrix} A & F \\ 0 & I_p \end{bmatrix}, \bar{B} = \begin{bmatrix} B \\ 0 \end{bmatrix}, \bar{C} = [C\ G], \tag{2.13}$$

$$X_k = \begin{bmatrix} x_k \\ b_k \end{bmatrix}, \bar{\omega_k} = \begin{bmatrix} \omega_k^x \\ \omega_k^b \end{bmatrix}, \bar{\Omega} = E(\bar{\omega_k}\bar{\omega_j^T}) = \begin{bmatrix} \Omega^x & \\ 0 & \Omega^b \end{bmatrix} \delta_{kj}, \tag{2.14}$$

where δ_{kj} is the Kronecker delta. With the formulation in Eq. (2.12) the bias information can be estimated with the system state at the same time. To solve the FDD problem, a similar structure is applied to design FDD system to detect and diagnose the LOE of actuators [66]. Instead of estimating the constant bias, the dynamics of LOE factors are diagnosed in real-time by modifying the actuator fault expression.

The fault-free system is represented in Eq. (2.15):

$$\begin{cases} x_{k+1} = Ax_k + Bu_k + \omega_k^x \\ y_k = Cx_k + \nu_k. \end{cases} \tag{2.15}$$

With the consideration of post-fault scenarios, the post-fault system dynamics can be ex-

pressed in Eq. (2.16):

$$\begin{cases} x_{k+1} = Ax_k + Bu_k^f + \omega_k^x \\ y_{k+1} = Cx_k + \nu_k. \end{cases} \tag{2.16}$$

For the convenience of detecting and diagnosing faults, Eq. (2.16) can be rewritten as:

$$x_{k+1} = Ax_k + Bu_k + D_k(u_k)\gamma_k^a + \omega_k^x, \tag{2.17}$$

where $D_k(u_k) = BU_k$ and

$$\begin{aligned} U_k &= diag(-u_k^1, -u_k^2, \cdots, -u_k^l), \\ \gamma_k^a &= [\gamma_k^{a1}, \gamma_k^{a2}, \cdots, \gamma_k^{al}]. \end{aligned} \tag{2.18}$$

The dynamics of the LOE is expressed as the bias in a similar way as shown in Eq. (2.11) except that the number of detected parameters has to equal the number of actuators since each of them can be in faulty condition:

$$\gamma_{k+1}^a = \gamma_k^a + \omega_k^r. \tag{2.19}$$

To adopt SAKF for FDD design, Eq. (2.15) is rewritten in the standard form as shown in Eq. (2.20):

$$\begin{cases} X_{k+1} = \tilde{A}X_k + \tilde{B}u_k + \tilde{\omega}_k \\ y_k = \tilde{C}X_k + \nu_k, \end{cases} \tag{2.20}$$

where

$$\tilde{A} = \begin{bmatrix} A & D_k(u_k) \\ 0 & I_p \end{bmatrix}, \tilde{B} = \begin{bmatrix} B \\ 0 \end{bmatrix}, \tilde{C} = [C\ G] \tag{2.21}$$

$$X_k = \begin{bmatrix} x_k \\ \gamma_k^a \end{bmatrix}, \tilde{\omega_k} = \begin{bmatrix} \omega_k^x \\ \omega_k^{\gamma^a} \end{bmatrix}, \tilde{\Omega} = E(\tilde{\omega_k}\tilde{\omega_j^T}) = \begin{bmatrix} \Omega^x & 0 \\ 0 & \Omega^{\gamma^a} \end{bmatrix} \delta_{kj}. \tag{2.22}$$

Remark 2.1. *In comparison to the formulation in Eq.* (2.12) *and Eq.* (2.20)*, it is noted that the major difference is the state matrix.* $\bar{A}$ *is the time independent matrix, while* $\tilde{A}$ *is time dependent matrix because of the dependency of the time-varying control efforts, which makes more challenges in the diagnosing process.*

2.3 Fault-Tolerant Control

This section introduces the detail mechanism of a FTC system by analyzing the process of a fault-free system changing to a faulty system [12]. The system is fault-free until the time instant t_F and has afterwards a fault in one or several actuators. Hence, the whole set of actuators I is healthy in time interval $(0, t_F]$ and there is a subset I_F of faulty actuators in $[t_F, \infty)$. The whole set of actuators are composed of fault-free actuators and faulty actuator and denoted by $I = I_N U I_F$, where I_N is the subset of the fault-free actuators, I_F is aforementioned faulty actuator set. After the time instant of t_F, the post-fault system behavior is described by:

$$\dot{x}(t) = Ax(t) + \sum_{i \in I_N} B_i u_i(t) + \sum_{i \in I_F} \beta_i(u_i(t), \theta_i), \tag{2.23}$$

where $\beta_i(u_i(t), \theta_i)$ describes the contribution of the faulty actuator i. This vector may be known with unknown parameters θ_i or complete unknown depending on the considered faults, which are diagnosed by the FDD algorithms.

Two cases can be considered as far as the status of constraints are considered: 1) the fault tolerance analysis is done for given faults. Therefore, constraints are known and a fault-tolerant controller can be designed beforehand; 2) the analysis is done for any kind of fault which might occur during the system operation. Therefore, constraints have to be identified. The identification of the subset I_F of faulty actuators is done by fault detection algorithms and the functions $\beta_i(u_i(t), \theta_i), i \in I_F$ is further identified by fault diagnosis algorithms, which are included in a FDD module.

Based on the fault information known beforehand or detected on-line, two approaches are applied for the fault-tolerant purpose. The first one applies the per-designed control law to accommodate all the known faults either using passive FTC or active FTC depending on the reconfiguration behavior. The other one applies the active FTC based on the real-time calculation with respect to the fault information. In practice, the fault information is not known until it is provided by the FDD system. To make the process clear three time windows are presented: $[0, t_F]$, $[t_F, t_{FT}]$, and $[t_{FT}, \infty)$, which correspond to the fault-free period, the post-fault transient without fault-tolerant reconfiguration, and the post-fault period with fault-tolerant reconfiguration, respectively. In the period $[t_F, t_{FT}]$, the control efforts are calculated based on the fault-free case, while the control efforts are applied to the post-fault system, which might introduce instability of the controlled system. To address the problem,

one way is to design a passive FTC system to accommodate the performance degradation before applying reconfigurable control. The other is from FDD point of view to detect and diagnose faults as fast as possible to reduce the post-fault transient period. It is noticed that the time delay of FDD cannot be avoidable, no matter what advanced techniques are applied. One suitable FTC paradigm is to improve the FTC capability with the combination of increasing the transient performance and reducing FDD time delay before performing the efficient reconfiguration control efforts. This FTC diagram can be implemented in the framework of LQ design. In particular, the transient performance can be improved with exponentially increasing weighing matrix in the LQ design process. The control reconfiguration problem can be further addressed in a more flexible structure using MPC by on-line solving new constraints. Furthermore, the on-line FTC capability can be further enhanced within the framework of LF-MPC by reducing the optimized parameters without decreasing the control horizon.

2.3.1 Fault-Tolerant Control in the Framework of LQ Design

For the general and fixed horizon optimal control problem, two components are considered 1) the objective function, 2) the dynamics constraints. Suppose the system dynamics are represented as follows:

$$\begin{cases} \dot{x}(t) = f(x(t), u(t)) \\ x(t_0) = x_0, \end{cases} \tag{2.24}$$

where the following cost function is minimized to get the control $u(.)$ with the given time horizon $[t_0, t_f]$ under the dynamics constraint as shown in Eq. (2.24):

$$J(u(.), x_0, t_0, t_f) = \int_{t_0}^{t_f} L(x(t), u(t), t)dt + \phi(x(t_f)), \tag{2.25}$$

where the first term is the running cost which is used to penalize the transient state deviation and control effort and the second term is the final cost which is used to penalize the finite state. Define the Hamiltonian function:

$$H(x(t), u(t)) = L(x(t), u(t)) + \lambda^T f(x(t), u(t)). \tag{2.26}$$

The solution will be given by:

$$\begin{cases} \dot{\lambda} = -H_x = -\dfrac{\partial L}{\partial x} - \lambda^T \dfrac{\partial f}{\partial x} \\ \dot{x} = f(x(t), u(t)) \\ H_u = -\dfrac{\partial L}{\partial u} - \lambda^T \dfrac{\partial f}{\partial u} = 0 \\ \lambda^T(t_f) = \dfrac{\partial \phi}{\partial x}(x(t_f)) \\ x(t_0) = x_0 \end{cases},$$

where $H_x = \frac{\partial H}{\partial x}$, $H_u = \frac{\partial H}{\partial u}$.

In the LQ programming framework, the system can be represented in the form:

$$\begin{aligned} \dot{x}(t) &= A(t)x(t) + B(t)u(t) \\ &= A(t)x(t) + \sum_{i=1}^{l} B_i(t)u_i(t), \end{aligned} \tag{2.27}$$

where $x(t) \in \mathbb{X}^n$ is the state vector and $u(t) \in \mathbb{U}^l$ is the control vector. $u_i(t)$ is the ith control input. It is assumed that the pair $(A(t), B(t))$ is controllable. The following optimal control problem is considered:
1) The quadratic objective function to be minimized is:

$$J(u(.), x_0, t_0, t_f) = \int_{t_0}^{t_f} [x(t)^T Q_t x(t) + u(t)^T R_t u(t)]dt + x(t_f)^T S x(t_f). \tag{2.28}$$

2) The optimal problem is subjected to the dynamics of the system presented in Eq. (2.27), where $Q(t) \in \mathbb{R}^{n\times n}$ and $S \in \mathbb{R}^{n\times n}$ are symmetric positive semi-definite matrices, $R(t) \in \mathbb{R}^{l\times l}$ is symmetric positive definite matrix. x_0 can be obtained from the measurement, and t_0 and t_f are known fixed values. The control objective is to drive the state $x(t_0) = x_0$ to $\lim_{t_f\to\infty} x(t_f) = 0$, especially, at the final time t_f.

Theorem 2.1. *The cost function Eq.* (2.28) *is minimized using the control:*

$$u^*(t) = -R(t)^T B^T(t) P(t) x(t), \tag{2.29}$$

where $P(t) \in \mathbb{R}^{n\times n}$ is the solution to the following so-called continuous time Riccatti Differ-

ential Equation (CTRDE):

$$\begin{cases} -\dot{P}(t) = A^T(t)P(t) + P(t)A(t) - P(t)B(t)R^{-1}(t)B^T(t)P(t) + Q(t) \\ P(t_f) = S. \end{cases} \tag{2.30}$$

The minimum cost achieved using the above control is:

$$J^*(x_0, t_0, t_f) = \min_{u(.)} J(u, x_0)) = x_0^T P(t_0) x_0. \tag{2.31}$$

Consider now the case when the system is time invariant, i.e, $A(t) = A$, $B(t) = B$ in Eq. (2.27) and $Q(t) = Q$, $R(t) = R$ in Eq. (2.28) are constant matrices. The terminal cost is negligible provided that the time is infinite. Therefore the cost function becomes:

$$J(u(.), x_0) = \int_0^\infty [x^T(t)Qx(t) + u^T(t)Ru(t)]dt. \tag{2.32}$$

Remark 2.2. *LQ technique can be used to synthesize a real-time controller based on the most updated system information to solve non-linear problems.*

Remark 2.3. *The control strategies can be reformed with the consideration of the minimum cost. However, in general, the cost function is tend to obtain the the control efforts. The cost function value itself is not directly linked to the controlled system, especially to a complex system, such as aircraft system. Further efforts should be carried out in terms of the relationship between the cost function values and the physical meaning.*

Remark 2.4. *The terminal cost decreases with the increasing of the optimization time horizon. Meantime, the increasing of the terminal cost also decreases the time horizon in a specific manner. This is of paramount in the framework on-line optimization such as MPC.*

2.3.2 Philosophy of MPC

MPC is a form of a control scheme in which the current control effort is obtained at each time intervals by solving a finite horizon open-loop optimal control problem. Essentially, the current control to the system is the first control of the obtained optimal control sequence in the optimization process. Fig. 2.2 shows the working scheme of MPC. In general, the time line is divided into 3 intervals: past, present, and future. The idea of MPC is to generate controls based on the past and current information with considering the future

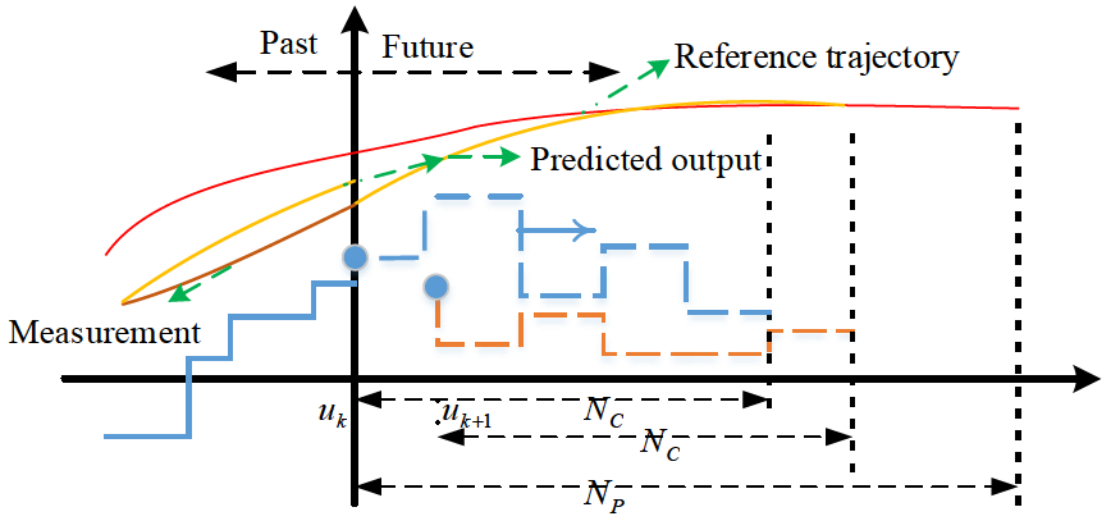

Figure 2.2: MPC working scheme

status. Given a reference, the control objective is to drive the controlled system to follow the reference or simply to stabilize the system. The past measurement and model of the controlled system are included in the past information. The controls at each interval are obtained by optimizing a cost function based on the open-loop system model and the current measurement. In general, the first control u_k obtained from the optimized control sequence $[u_k, u_{k+1}, \cdots, u_{k+p}]$ is applied into the controlled system. The rest of control efforts in the control sequence are discarded. Since the control efforts are obtained at each optimization interval and there are differences between measurements and predictions, the control action obtained in the next interval is always not the same as it was obtained in the last control sequence. Iotethat the control horizon N_c is less greater than the prediction control horizon N_p. It can be proved that with the same N_p in optimization formulation subjected to the same dynamics and other constraints, the overall cost decreases when N_c increases.

2.3.3 Fault-Tolerant Control Using MPC

MPC is proposed in solving fault problem of a system with different types of internal models, such as non-linear model [69–71], piecewise affine model [72–74], fuzzy method [75, 76]. Non-linear MPC is a promising research topic, but still not well developed limiting its applications on the high sample rate system. Linear MPC algorithm itself comes to be

a relative mature technique in terms of the structure and feasibility. While it is still in the development in terms of challenges, such as, on-line computational efficiency, robustness, and feasibility. It is more challenging to deal with the aforementioned challenges in the presence of faults. From the application point of view, MPC is still not widely used in the fast sampling rate system despite its success in the low-sampling process control area. The thesis aims to synthesize an effective FTC system by utilizing the most recent development technique in obtaining the optimized control trajectory. The linearized model is applied as an internal model to synthesize a FTC system. The system shown in Eq. (2.10) is used to derive internal model of MPC:

$$\begin{cases} x(k+1) = Ax(k) + B\Delta u(k) \\ y(k) = Cx(k) + r_s, \end{cases} \tag{2.33}$$

where $x(k) = [(x_m(k) - x_m(k-1))^T \ y_m(k)^T]^T$, $\Delta u(k) = [u_m(k) - u_m(k-1)]$, and A, B, and $C = [0 \ I_m]$ are the state matrix, the input matrix, and the output matrix, respectively. r_s is the reference command to the system. The block diagram for designing an active FTC system with MPC is given in Fig. 2.3.

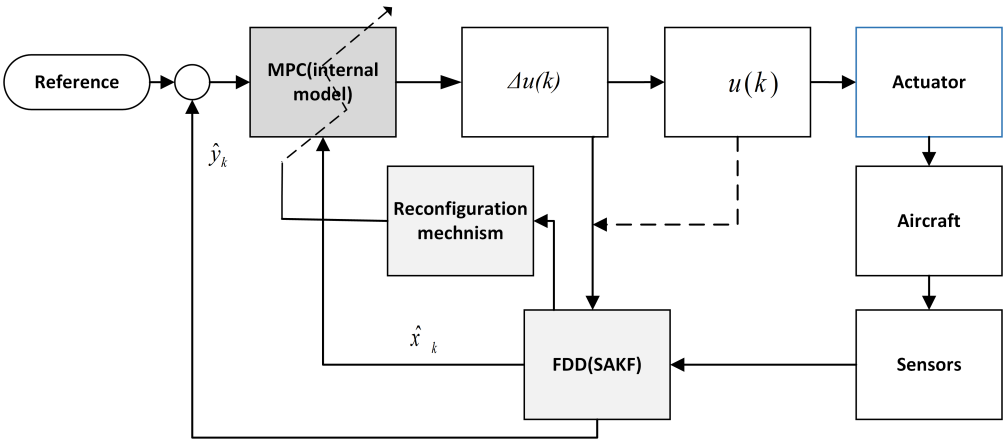

Figure 2.3: Block diagram for designing an active FTC system with MPC

The predictive state vector can be obtained by using the control trajectory:

$$\begin{cases} x(k+1|k) = Ax(k) + B\Delta u(k) \\ x(k+2|k) = Ax(k+1|k) + B\Delta u(k+1|k) \\ \qquad\qquad = A^2x(k) + AB\Delta u(k) + B\Delta u(k+1|k) \\ \qquad\qquad \vdots \\ x(k+N_p|k) = A^{N_p}x(k) + A^{N_p-1}B\Delta u(k) \\ \qquad\qquad + A^{N_p-2}B\Delta u(k+1|k) + \cdots \\ \qquad\qquad + A^{N_p-N_c}B\Delta u(k+N_c-1|k) \\ \qquad\qquad + (A^{N_p-N_c-1} + A^{N_p-N_c-2} + \cdots \\ \qquad\qquad + I)B\Delta u(k+N_c|k), \end{cases}$$

where N_p and N_c are the prediction and control horizons, respectively, which determine the smoothness of the predictive control trajectory, and $\Delta u(k+N_c) = 0$. This leads to the predictive output trajectory $Y = [y(k+1|k)^T, y(k+2|k)^T, \ldots, y(k_{N_p}|k)^T]^T$. Finally, the predictive output can be formalized as:

$$Y = Fx(k) + \Phi\Delta U, \tag{2.34}$$

where

$$\begin{aligned} F &= \begin{bmatrix} CA \\ CA^2 \\ CA^3 \\ \cdots \\ CA^{N_p} \end{bmatrix}, \\ \Phi &= \begin{bmatrix} CB & 0 & 0 & \cdots & 0 \\ CAB & CB & 0 & \cdots & 0 \\ CA^2B & CAB & CB & \cdots & 0 \\ \vdots & \vdots & \vdots & \vdots & \vdots \\ CA^{N_p-1}B & CA^{N_p-2}B & CA^{N_p-3}B & \cdots & CA^{N_p-N_c}B \end{bmatrix}. \end{aligned} \tag{2.35}$$

The cost function is

$$\begin{aligned} J &= (R_s - Y)^T Q (R_s - Y) + \Delta U^T R \Delta U \\ &= \sum_{i=1}^{N_p} (r_s(k+i|k) - y(k+i|k))^T Q_i (r_s(k+i|k) - y(k+i|k)) \\ &+ \sum_{j=0}^{N_c-1} (\Delta u(k+j|k)^T R_j \Delta u(k+j|k)), \end{aligned}$$

where R_s is the reference with $R_s = [r_s(k+1)^T,\ r_s(k+2)^T,\ \cdots,\ r_s(k+N_p)^T]^T$. Q and R are the block diagonal matrices with $Q_i (i \in [1, N_p])$ and $R_j (j \in [1, N_c])$, respectively. $Q_i \in \mathbb{R}^{m \times m}$ and $R_j \in \mathbb{R}^{l \times l}$ are the semidefinite matrix and the definite matrix, respectively, to balance the state and the input in the cost function.

The control trajectory in fault-free condition can be solved based on the cost function with dynamics constraints, which is denoted as:

$$\Delta U = \left(\Phi^T \Phi + R\right)^{-1} \left(\Phi^T R_s - \Phi^T F x(k)\right). \tag{2.36}$$

The receding horizon control strategy is used, thereby the real output control effort can be obtained from:

$$\Delta u = [I\ 0\ \cdots\ 0][\Phi^T \Phi + R]^{-1} (\Phi^T R_s r(k) - \Phi^T F x(k)). \tag{2.37}$$

Constraints On the Slew Rates and the Amplitudes of Actuators

The incremental variation of control signals is the changing rate of a control variable, which is tightly related to the property of actuators. Suppose that the upper limit of a changing rate is Δu_{max} and the lower limit is Δu_{min}, the boundary of a control change $\Delta u(k)$ at the time instant k can be expressed as follows:

$$\Delta u_{min} \leq \Delta u(k) \leq \Delta u_{max} \tag{2.38}$$

with

$$\begin{aligned} \Delta u(k) &= [\Delta u_1(k) \Delta u_2(k) \cdots \Delta u_l(k)], \\ \Delta u_{min} &= [\Delta u_{1_{min}} \Delta u_{2_{min}} \cdots \Delta u_{l_{min}}], \\ \Delta u_{max} &= [\Delta u_{1_{max}} \Delta u_{2_{max}} \cdots \Delta u_{l_{max}}]. \end{aligned} \tag{2.39}$$

For a specific actuator, the property of actuators can be known before the controller design. Specially, the upper limit and the lower limit deflection of an airfoil should be considered as constraints to the control signal, which can be expressed in the following expression:

$$u_{min} \leq u(k) \leq u_{max} \tag{2.40}$$

with

$$\begin{aligned} u(k) &= [u_1(k)\ u_2(k)\ \cdots\ u_l(k)], \\ u_{min} &= [u_{1_{min}}\ u_{2_{min}}\ \cdots\ u_{l_{min}}], \\ u_{max} &= [u_{1_{max}}\ u_{2_{max}}\ \cdots\ u_{l_{max}}]. \end{aligned} \tag{2.41}$$

Constraints on the Outputs

The constraints about the control signals are due to the physical dynamics or the limitation of actuators. However, the constrains on the outputs are due to the consideration of the control performance.

The output constraints are specified as:

$$y_{min} \leq y(k) \leq y_{max}, \tag{2.42}$$

where y_{min} and y_{max} are the minimum and maximum value of the outputs. The output constraints are related to the performance, which are not as serious as that about control signal. Usually a slack variable $s_v > 0$ is added to the constraints for feasibility purpose as shown in (2.42).

$$y_{min} - s_v \leq y(k) \leq y_{max} + s_v \tag{2.43}$$

with

$$\begin{aligned} y(k) &= [y_1(k)\ y_2(k)\ \cdots y_n(k)], \\ y_{min} &= [y_{1_{min}}(k)\ y_{2_{min}}(k)\ \cdots y_{n_{min}}(k)], \\ y_{max} &= [y_{1_{max}}(k)\ y_{2_{max}}(k)\ \cdots y_{n_{max}}(k)]. \end{aligned} \tag{2.44}$$

Note that n is the dimension of the outputs.

The control trajectory is generated in the form:

$$\Delta U = \left[\Delta u^T(k), \Delta u^T(k+1), \cdots, \Delta u^T(k+N_c-1)\right]^T. \tag{2.45}$$

The solutions to solve actuator faults can be concluded as:

$$\begin{cases} x_m(k+1) = A_m x_m(k) + B_m u^f(k) \\ \qquad\qquad = A_m x_m(k) + B_m u(k) + B_m(I - \Sigma_A)(\bar{u} - u(k))) \\ y_m(k) = y(k) \\ \qquad\qquad = C_m x_m(k) \\ u(k) \in (u_{min}, u_{max}) \\ \Delta u(k) \in (\Delta u_{mim}, \Delta u_{max}) \\ y(k) \in (y_{min}, y_{max}). \end{cases} \tag{2.46}$$

2.3.4 MPC Using Laguerre Functions

A well-known problem of MPC is that MPC has heavy a computational burden and the numerical problem when the predict horizon is large [77]. A Laguerre function based MPC is presented to reduce the computational burden by approximating the finite control trajectory with fewer optimization parameters. The control vector that is optimized in the design of a predictive controller is ΔU:

$$\Delta U = [\Delta u(k)^T, \Delta u(k+1)^T, \cdots, \Delta u(k+N_c-1)^T]^T, \tag{2.47}$$

where $\Delta U \in \mathbb{R}^{lN_c}$. At the time instant k, any element within the control trajectory ΔU can be represented using the discrete δ-function in conjunction with ΔU:

$$\Delta u(k+i) = [\delta(i), \delta(i-1), \cdots, \delta u(i-N_c+1)]\Delta U, \tag{2.48}$$

where

$$\begin{cases} \delta(i) = diag([\delta_1(i)\ \delta_2(i)\ \cdots \delta_l(i)]) = diag(\underbrace{[1\ 1\ \cdots\ 1]}_{l}) & i = 0 \\ \delta(i) = diag(\underbrace{[0\ 0\ \cdots\ 0]}_{l}) & i \neq 0. \end{cases} \tag{2.49}$$

The δ is used to capture the control trajectory.

The idea of approximating control trajectory is proposed in literature [53] to use a discrete polynomial function (a set of Laguerre functions) to approximate the control sequence $[\Delta u(k+i), \Delta u(k+i-1), \cdots, \Delta u(k+i-N_c+1)]$ in order to reduce the optimization parameters, which is critical character for the application of real-time FTC.

The basic design framework is to replace $\Delta u(k+i)$ with $L(i)^T\eta$ shown as:

$$\Delta u(k+i) = L(i)^T\eta \tag{2.50}$$

with $L^T(i) = diag([L_1(i)^T, L_2(i)^T, \cdots, L_l(i)^T])$ $(i \in [1, N_c])$, $\eta = [\eta_1^T\ \eta_2^T\ \cdots\ \eta_l^T]^T$.

Specially, the $L_q(i) = [l_{1_q}(i)\ l_{2_q}(i)\ \cdots\ l_{N_q}(i)]^T$ $(q \in [1,\ l])$ can be calculated iteratively by:

$$L_q(i+1) = A_{ql}L_q(i), \tag{2.51}$$

with $L_q(0)=\sqrt{\beta_q}[1\ -\alpha_q\ \alpha_q^2\ -\alpha_q^3\ \cdots\ (-1)^{N_q-1}\alpha_q^{N_q-1}]$, $\beta_q = 1-\alpha_q^2$ $(\alpha_q \in [0,1))$. N_q is the number of approximation factors of the q_{th} actuator. A_{ql} can be calculated off-line with the parameters α_q, N_q, N_c

$$A_{ql} = \begin{bmatrix} \alpha_q & 0 & \cdots & 0 \\ \beta_q & \alpha_q & \cdots & 0 \\ -\alpha_q\beta_q & \beta_q & \cdots & 0 \\ \vdots & \vdots & \vdots & \vdots \\ (-\alpha_q)^{N_q-2}\beta_q & (-\alpha_q)^{N_q-3}\beta_q & \cdots & \alpha_q \end{bmatrix}. \tag{2.52}$$

The system is represented using the expression shown in Eq. (2.50)

$$\begin{cases} x(k+j|k) = A^j x(k) + \sum_{p=0}^{j-1} A^{j-p-1}BL(p)^T\eta = A^j x(k) + \phi(j)^T\eta \\ y(k+j|k) = Cx(k+j|k) = CA^j x(k) + C\phi(j)^T\eta, \end{cases} \tag{2.53}$$

where $\phi(j)^T = \sum_{p=0}^{j-1} A^{j-p-1}BL(j)^T$ $(\ j \in [1, N_p])$.

It is shown that the $\Delta u(k+i)$ is replaced by the $L(i)^T\eta$, thus the parameter η is the only optimized parameters vector instead of ΔU. Note that the dimension of η is smaller than that of ΔU. $L(i)$ is determined by Eq. (2.51). By replacing ΔU, the formulation of cost function is denoted as:

$$J = \sum_{j=1}^{N_p}(r(k+j|k) - y(k+j|k))^T Q_j(r(k+j|k) - y(k+j|k)) + \eta^T R\eta. \tag{2.54}$$

By substituting Eq. (2.53) into the cost function Eq. (2.54), the cost function changes to

$$J = \eta^T(\sum_{j=1}^{N_p} \phi(j)Q\phi(j) + R_L)\eta + 2\eta^T(\sum_{j=1}^{N_p} \phi(j)QA^j)x(k) + \sum_{j=1}^{N_p} x^T(k)(A^T)^j QA^j x(k). \quad (2.55)$$

The cost function to be optimized can finally reduced as the following by dropping the constant terms:

$$J = \eta^T(\sum_{j=1}^{N_p} \phi(j)Q\phi(j) + R_L)\eta + 2\eta^T(\sum_{j=1}^{N_p} \phi(j)QA^j)x(k). \quad (2.56)$$

Constrains on the Slew Rates

Due to the physical constraints of an actuator, the slew rates should not exceed the actuator's limitations. The lower and upper limits on $\Delta u(k)$ are Δu_{min} and Δu_{max}:

$$\Delta u_{min} \leq \Delta u(k+i) \leq \Delta u_{max} \quad (2.57)$$

Eq. (2.57) can be rewritten with η based on Eq. (2.50):

$$\Delta u_{min} \leq L^T(i)\eta \leq \Delta u_{max}, \quad (2.58)$$

where $L^T(i) = diag([L_1^T(i)\ L_2^T(i)\ \cdots\ L_l^T(i)])$.

Constrains on the Amplitudes

It is similar to get the constrains on the amplitudes of the control signal. The increment of the control signal in a predictive control interval is

$$u(i) = \sum_{p=0}^{i-1} \Delta u(p), \quad (2.59)$$

then the inequality constraint for the future time i ($i = 1, 2, \cdots, N_c$) is expressed as:

$$u_{min} \leq S_L(i)\eta + u(k-1) \leq u_{max}, \quad (2.60)$$

where

$S_L(i) = diag([\sum_{j=0}^{i-1} L_1(j)^T,\ \sum_{j=0}^{i-1} L_2(j)^T,\ \cdots \sum_{j=0}^{i-1} L_l(j)^T])$, $u(k-1)$ is the previous control signal vector.

Constrains on the Outputs

The performance constraints at the prediction time instant $k+i$ can be shown as:

$$y_{min}(i) \leq CA^j x(k) + C\phi(i)^T \eta \leq y_{max}(i). \tag{2.61}$$

2.3.5 Constraints with Respect to Actuators Limitations and Performance of System Output

Define

$$\begin{aligned}
&S_L = [S_L(0)^T\ S_L(1)^T \cdots S_L(N_c)^T]^T,\\
&\Delta U_{max} = [\Delta u_{max}^T\ \Delta u_{max}^T\ \cdots \Delta u_{max}^T]^T\\
&\Delta U_{min} = [\Delta u_{min}^T\ \Delta u_{min}^T\ \cdots \Delta u_{min}^T]^T,\\
&L^T = [L(0)^T\ L(1)^T \cdots\ L(N_c)^T]^T,\\
&U(k-1) = [u_1(k-1)^T\ u_2(k-1)^T \cdots\ u_l(k-1)^T]^T,\\
&C_\phi = [(C\phi(1)^T)^T\ (C\phi(2)^T)^T \cdots (C\phi(N_p)^T)^T]^T.
\end{aligned} \tag{2.62}$$

In the prediction horizon N_c scope, the constraints about η is shown as:

$$\begin{bmatrix} M_1 \\ M_2 \\ M_3 \end{bmatrix} \eta \leq \begin{bmatrix} N_1 \\ N_2 \\ N_3 \end{bmatrix} \tag{2.63}$$

where

$$\begin{aligned}
M_1 &= \begin{bmatrix} L^T \\ -L^T \end{bmatrix}, \qquad N_1 = \begin{bmatrix} \Delta U_{max} \\ -\Delta U_{min} \end{bmatrix},\\
M_2 &= \begin{bmatrix} S_L \\ -S_L \end{bmatrix}, \quad N_2 = \begin{bmatrix} U_{max} - U(k-1) \\ U_{min} + U(k-1) \end{bmatrix},\\
M3 &= \begin{bmatrix} C_\phi \\ -C_\phi \end{bmatrix}, \quad N_3 = \begin{bmatrix} Y_{max} - Fx(k) \\ -Y_{min} + Fx(k) \end{bmatrix}.
\end{aligned} \tag{2.64}$$

Overall, the active FTC system using LF-MPC based technique design is to solve Eq. (2.56) subjected to dynamics constraints and constraints shown in Eq. (2.63) for both fault-free and post-fault scenarios.

2.4 Summary

This chapter introduces an active FTC system within LQ framework and extended Kalman filter. The FTC system is presented in the form of a schematic diagram, which aims to present the relative function of each module. Specifically, state estimation and fault diagnosis problems are solved simultaneously through the combination of state and parameter estimation approach using SAKF. The FTC strategy is analyzed with respect to the system situation impacted by the faulty actuators. Furthermore, the fault-tolerant strategy in the framework of LQ design is presented. MPC and LF-MPC algorithms are also illustrated in terms of addressing constraints with application to FTC.

Part I

Application to a Rotary-Wing Unmanned Aerial Vehicle

Chapter 3

Modeling of the Qball-X4

3.1 Introduction

The Qball-X4 is a platform for the evaluation of the newly designed fault-tolerant controller on the rotary-wing platform. It is available at Diagnosis, Flight Control & Simulation (DFCS) Lab in the Department of Mechanical and Industrial Engineering of Concordia University. This chapter introduces the Qball-X4 platform and the dynamics of a quadrotor UAV. Section 3.2 briefly presents the system description of the Qball-X4 platform. Section 3.3 presents the dynamics of the Qball-X4 with an emphasis on the dynamic model in height. The corresponding coordinates are also illustrated for the modeling purpose. Section 3.4 draws a summary.

3.2 System Description

The Qball-X4 shown in Fig. 3.1 is a rotary-wing platform suitable for a wide variety of UAVs research applications. The Qball-X4 is a quadrotor helicopter with 4 rotors fitted with 10-inch propellers. It is enclosed within a protective carbon fiber cage. The Qball-X4 is equipped with on-board sensors, Quanser's on-board avionics data acquisition card, and the embedded Gumstix computer. The on-board sensors include an inertial measurement unit (IMU) proving altitude (roll, pitch, and yaw) information and sonar for detecting the relative distance. The controller can be designed and implemented in the Matlab/Simulink environment, and then downloaded and executed on the on-board embedded micro-computer.

Figure 3.1: The quadrotor helicopter (Qball-X4)

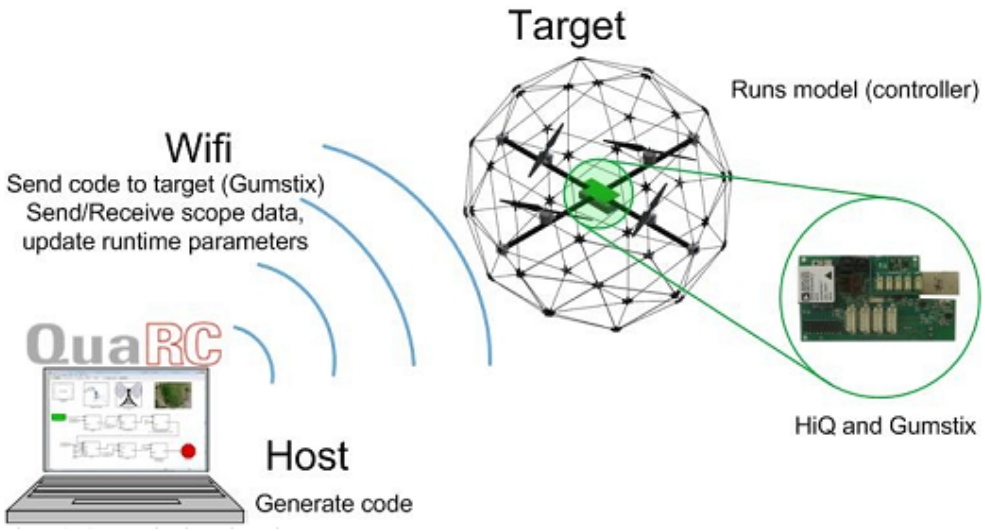

Figure 3.2: Qball-X4 platform communication scheme

The connection between the host and the target is wirelessly connected through WiFi as shown in Fig. 3.2 and the parameters about the Qball-X4 for using to design controllers are listed in Table 3.1 [78]. In addition to the IMU information for the attitude control, the OptiTrack motion tracking system is used for the controller to position the Qball-X4 as indoor positioning system.

Remark 3.1. *There is no extra sensor available to directly detect the actuator information.*

Table 3.1: Qball-X4 parameters

Parameter	Description	Value
K	Thrust gain	120
ω	Motor bandwidth	15 rad/s
L	Distance from motor to CG	0.2 m
K_ϕ	Thrust-to-moment gain	0.023
m	Mass	1.4 Kg
g	Gravity	9.81 m/s^2
J_x	Moments of inertia about x	$0.03Kg.m^2$
J_y	Moments of inertia about y	$0.03Kg.m^2$
J_z	Moments of inertia about z axis	0.04 $Kg.m^2$

The hardware configuration introduces challenges in the design of a FDD unit for actuators.

3.3 Modeling of the Qball-X4

The dynamics of the Qball-X4 UAV are discussed in this section. More specifically, the Qball-X4 dynamics are studied in a hybrid coordinate system: 1) inertial frame and 2) body frame, which are used to express the linear dynamics and the angular dynamics, respectively [79].

The inertial frame is assumed to be coincident with the body frame at the initial state. The most general axis system is known as a body frame ($ox_by_bz_b$) as shown in Fig. 3.3. The origin point o of the axes is fixed at a convenient reference point, which is coincident with the center of gravity (CG). Euler angles are defined based on the inertial frame and the body-frame. The procedural rotation process is depicted in Fig. 3.4 [80]. ($ox_0y_0z_0$) is the navigation frame based on the initial definition of the positioning system, ($ox_1y_1z_1$), ($ox_2y_2z_2$), and ($ox_3y_3z_3$) are the transient axes to the body frame. Euler angles ψ, θ, ϕ are defined in the rotation process in the following sequence: ($ox_0y_0z_0$) $\rightarrow$ ($ox_1y_1z_1$) $\rightarrow$ ($ox_2y_2z_2$) $\rightarrow$ ($ox_3y_3z_3$). Note that ($ox_3y_3z_3$) is coincident with the body frame ($ox_by_bz_b$).

The derivation process of the quadrotor dynamics can be found in [79, 81] with the results

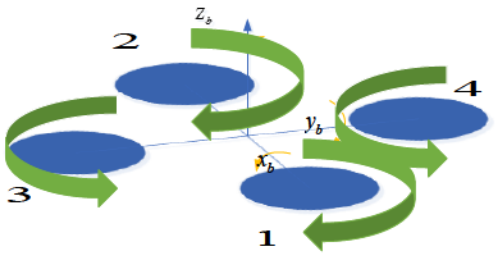

Figure 3.3: Body frame of the Qball-X4

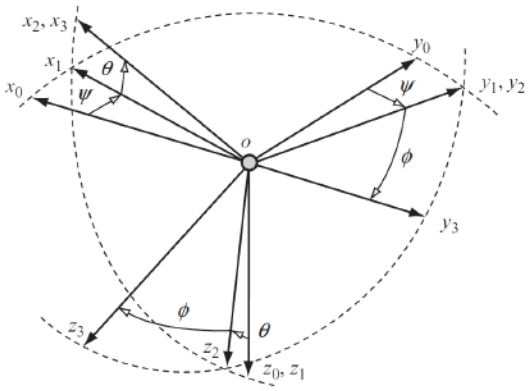

Figure 3.4: Euler angles

as shown in Eq. (3.1):

$$\begin{cases} m\ddot{x} = u_z(c_\phi s_\theta c_\psi + s_\phi s_\psi) - k_x\dot{x} \\ m\ddot{y} = u_z(c_\phi s_\theta s_\psi - s_\phi c_\psi) - k_y\dot{y} \\ m\ddot{z} = u_z(c_\phi c_\theta) - mg - k_z\dot{z} \\ J_x\dot{p} = u_p + (J_y - J_z)qr - J_T q\Omega - k_p p \\ J_y\dot{q} = u_q + (J_z - J_x)pr - J_T p\Omega - k_q q \\ J_z\dot{r} = u_r + (J_x - J_y)pq - k_r r, \end{cases} \tag{3.1}$$

where x, y, and z are the coordinates of the quadrotor in the inertial frame with the original point at the CG; m is the mass of the quadrotor; J_x, J_y, and J_z are the inertial moments about x, y, and z directions, respectively; ϕ, θ, and ψ are the roll, pitch, and yaw Euler angles with respect to the transient coordinates mentioned above; p, q, and r are the angular

velocities in the body-fixed frame. k_x, k_y, k_z, k_p, k_q, and k_r are the drag coefficients and are treated as constant. J_T is the inertial moment of each motor and Ω is the overall speed of propellers. By neglecting the drag terms at low speed condition, Eq. (3.1) is simplified further by:

$$\begin{cases} m\ddot{x} = u_z(c_\phi s_\theta c_\phi + s_\phi s_\psi) \\ m\ddot{y} = u_z(c_\phi s_\theta s_\psi - s_\phi c_\psi) \\ m\ddot{z} = u_z(c_\phi c_\theta) - mg \\ J_x\dot{p} = u_p + (J_y - J_z)qr - J_T q\Omega \\ J_y\dot{q} = u_q + (J_z - J_x)pr - J_T p\Omega \\ J_z\dot{r} = u_r + (J_x - J_y)pq, \end{cases} \tag{3.2}$$

with

$$\begin{cases} \Omega = -\Omega_1 - \Omega_2 + \Omega_3 + \Omega_4 \\ u_z = T_1 + T_2 + T_3 + T_4 \\ u_p = L(T_3 - T_4) \\ u_q = L(T_1 - T_2) \\ u_r = \tau_1 + \tau_2 - \tau_3 - \tau_4, \end{cases} \tag{3.3}$$

where Ω_i is the ith propeller's speed. The sign of u_p is defined by the sign of the difference between thrust T_3 and T_4, respectively; while the sign of u_q is defined with sign of the difference between T_1 and T_2. T_i $(i = 1, 2, 3, 4)$ is the thrust generated by the ith motor of 4 equipped motors. L is the distance from the center of motor to CG. τ_i is the torque from the ith motor. The angular velocities in the inertial frame (Euler rates) can be related to those in the body frame as follows:

$$\begin{bmatrix} \dot{\psi} \\ \dot{\theta} \\ \dot{\phi} \end{bmatrix} = \begin{bmatrix} 1 & s_\phi t_\theta & c_\phi t_\theta \\ 0 & c_\phi & -s_\phi \\ 0 & -s_\phi/c_\phi & c_\phi c_\theta \end{bmatrix} \begin{bmatrix} p \\ q \\ r \end{bmatrix}. \tag{3.4}$$

Note that the initial position of the Qball-X4 may not be coincident the navigation frame. This may affect the control performance if according to the assumptions $\phi = 0$, $\theta = 0$, and $\psi = 0$ at the initial states. When the Qball-X4 takes off on the ground, the assumption of $\phi = 0$ and $\theta = 0$ hold; However $\psi = 0$ may not hold. To overcome the flaw, the taking-off direction of the Qball-X4 is arbitrarily specified to have a fixed relationship to the navigation frame or the difference should be compensated. The relationship of inertial frame and the

navigation frame is presented as:

$$\begin{bmatrix} x_I \\ y_I \\ z_I \end{bmatrix} = \begin{bmatrix} c_{\theta_{IC}} & 0 & s_{\theta_{IC}} \\ 0 & 1 & 0 \\ -s_{\theta_{IC}} & 0 & c_{\theta_{IC}} \end{bmatrix} \begin{bmatrix} c_{\phi_{IC}} & s_{\psi_{IC}} & 0 \\ -s_{\psi_{IC}} & c_{\phi_{IC}} & 0 \\ 0 & 0 & 1 \end{bmatrix} \begin{bmatrix} x_c \\ y_c \\ z_c \end{bmatrix} \tag{3.5}$$

with $\theta_{IC} = -\pi/2$, $\psi_{IC} = -\pi/2$, where (x_I, y_I, z_I) is coincident with (x_0, y_0, z_0). (x_c, y_c, z_c) stands for the navigation frame given by the position systems. Therefore, the arbitrary direction of the Qball-X4 x_I faces to the z_c direction, y_I is coincident with X_c, and z_I is coincident with Z_c.

The lifts are generated with actuators and propellers controlled by the electrical speed controller (ESC) using pulse width modulation (PWM) signal. The dynamics of the actuator related to PWM input are the following as shown in Fig. 3.5:

$$v_i = \begin{cases} \dfrac{0.05\omega}{s+\omega}, & u_{PWM} > 1 \\ \dfrac{u_{PWM}}{s+\omega}, & 0.05 < u_{PWM} < 1 \\ 0, & u_{PWM} < 0.05 \end{cases} \tag{3.6}$$

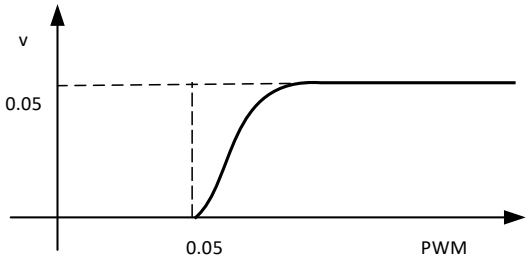

Figure 3.5: Actuator dynamics

As can be seen in Fig. 3.5, there is a dead zone between 0 and 0.05 in a DC motor actuator. This dead zone leads to the non-linearity of actuators. However, the non-linearity problem due to the dead zone can be solved easily by shifting the coordinator. Let $u_i(t) = u_{PWM_i}(t) - 0.05$, substituting the term in Eq. (3.6), the non-linear dynamics of the actuator changes to linear representation:

$$v_i(t) = \frac{\omega}{s+\omega} u_i(t), \qquad 0 < u_i < 0.05 \tag{3.7}$$

The transfer function between the lift generated by each actuator and corresponding PWM input is:

$$\begin{cases} T_i(t) = \dfrac{K\omega}{s+\omega} u_i(t) \\ \tau_i = K_\psi u_i, \end{cases} \tag{3.8}$$

where $u_i(t)(i = 1, 2, 3, 4)$ is the PWM input in ith channel of actuators, K_ψ is the torque coefficient. $x_z(t) = [z(t)\ \dot{z}(t)\ \nu_z(t)]$ is defined as the state vector related to height directional motion, $\dot{x}_z(t) = [\dot{z}(t)\ \ddot{z}(t)\ \dot{\nu}_z(t)] = [v_z(t)\ \dot{v}_z(t)\ \dot{\nu}_z(t)]$, the dynamics of the Qball-X4 in the fault-free case are represented as in Eq. (3.9):

$$\dot{x}_z(t) = f(x_z(t)) + B_c u(t). \tag{3.9}$$

The mathematical model of the Qball-X4 with actuator faults can be expressed in Eq. (3.10):

$$\begin{aligned} \dot{x}_z(t) =& f(x_z(t)) + B_c u^f(t) \\ =& f(x_z(t)) + B_c(u(t) + (I - \Sigma_A)(\bar{u} - u(t))), \end{aligned} \tag{3.10}$$

where

$$f(x_z(t)) = \begin{bmatrix} 0 & 1 & 0 \\ 0 & 0 & \frac{1}{m} * c_\phi c_\theta \\ 0 & 0 & -\omega \end{bmatrix} \begin{bmatrix} z(t) \\ \dot{z}(t) \\ \nu_z(t) \end{bmatrix} + \begin{bmatrix} 0 \\ -g \\ 0 \end{bmatrix}, \tag{3.11}$$

$$B_c = \begin{bmatrix} 0 & 0 & 0 & 0 \\ 0 & 0 & 0 & 0 \\ K\omega & K\omega & K\omega & K\omega \end{bmatrix}. \tag{3.12}$$

3.4 Summary

This chapter presents the rotary-wing platform available for testing the newly designed FTC system. The configuration of the Qball-X4 platform is introduced in terms of the computing resources, sensors, the positioning system, etc. The available hardware resources are significant in the FTC system design process since some sensor information can not be assumed in the real application. The dynamics of the Qball-X4 are illustrated and the dynamics in height are obtained for the fault-tolerant controller and the FDD unit design in the next chapter.

Chapter 4

Fault-Tolerant Control with Application to a Quadrotor UAV

4.1 Introduction

This chapter develops a new approach of a FTC system for a quadcopter using LQ technique in synthesizing a fault-tolerant controller and state-augmented extended Kalman filter (SAEKF) technique to carry out FDD task. The fault-tolerant controller is designed using improved LQ technique with a prescribed degree of stability. The FDD unit is synthesized with the combination of parameter identification and state estimation techniques in the framework of extended Kalman filter. The emphases of the chapter are 1) the fault-tolerant controller with the improved LQ technique using an increasing exponential weighting matrix; 2) the new SAEKF framework as a FDD module for FTC, which provides state and fault information in both fault-free and post-fault situations, with application to a quadrotor UAV; 3) the FDD approach design with the consideration of the system's non-linearity. The organization of this chapter is as follows. Section 4.2 presents the scheme of FTC for the Qball-X4. Section 4.3 presents the derivation process of SAEKF with the consideration of the non-linearity in height channel. Section 4.4 details the validation process and the performance with trajectory tracking task under three different scenarios in simulation environment. Section 4.5 draws conclusions of this chapter.

4.2 Fault-Tolerant Control Design Using LQ Technique

LQ is a modern control technique which is applied for the model flight control system [62]. However, no simple relation exists between the two weighting matrix Q and R and the close-loop eigenvalues of the post-fault system. In general, the weights are usually determined through trial and error. A remedy method combines the LQ technique with the time-varying weighting matrix together to get prescribed degree of stability of the controlled system for FTC design. To this end, an exponentially weighted matrix is introduced to balance the states and control input along the optimization window. Asymptotic stability is achieved through exponential data weighting and modification of the weight matrices.

The idea of using exponential data weighting is mentioned in [53, 82]. The discrete counterpart to $e^{\lambda_{\alpha_w} t}$ for all $t > 0$ is the geometric sequence $e^{\lambda_{\alpha_w} j T_s}$ $[j = 0, 1, 2, \cdots]$. The discretized model is obtained from Eq. (3.10):

$$\begin{cases} x(k+1) = Ax(k) + Bu(k) \\ y(k) = Cx(k). \end{cases} \tag{4.1}$$

The classical cost function is set as:

$$J_0 = \frac{1}{2} \sum_{k=0}^{\infty} x(k)^T Q x(k) + u(k)^T R u(k). \tag{4.2}$$

For the FTC design, the exponential weighting matrix is introduced. Therefore, the cost function with exponential weighting matrix is denoted as:

$$J = \frac{1}{2} \sum_{k=0}^{\infty} e^{-2k\lambda_{\alpha_w} T_s} x(k)^T Q x(k) + e^{-2k\lambda_{\alpha_w} T_s} u(k)^T R u(k), \tag{4.3}$$

where T_s is the sample time of the controller, $\lambda_{\alpha_w} < 0$ is the parameter to tune the weighting matrix. Define $\alpha_w = e^{\lambda_{\alpha_w} T_s}$, the cost function in Eq. (4.3) changes to

$$J = \frac{1}{2} \sum_{k=0}^{\infty} \alpha_w^{-2k} x(k)^T Q x(k) + \alpha_w^{-2k} u(k)^T R u(k). \tag{4.4}$$

Theorem 4.1. *Subject to the same system in Eq.* (4.1)*, the optimal solutions of controls by minimizing the cost function in Eq.* (4.4) *has a* α_w *degree of stability than that of controls by*

minimizing the cost function in Eq. (4.2).

Define $\hat{x}(k) = \alpha_w^{-k} x(k)$ and $\hat{u(k)} = \alpha_w^{-k} u(k)$, then Eq. (4.4) changes to

$$J = \frac{1}{2} \sum_{k=0}^{\infty} \hat{x}(k)^T Q \hat{x}(k) + \hat{u}(k)^T R \hat{u}(k), \tag{4.5}$$

subject to

$$\hat{x}(k+1) = \frac{A}{\alpha_w} \hat{x}(k) + \frac{B}{\alpha_w} \hat{u}(k). \tag{4.6}$$

The system's controller is the solution of the Riccati equation in Eq. (4.7) minimizing cost function Eq. (4.5) subjected to Eq. (4.6).

$$\frac{A}{\alpha_w}[P - P\frac{B}{\alpha_w}(R + \frac{B^T}{\alpha_w} P \frac{B}{\alpha_w})^{-1} \frac{B^T}{\alpha_w} p] \frac{A}{\alpha_w} + Q - P = 0. \tag{4.7}$$

The designed controller using exponential weighting matrix LQ technique is $K = (R + \alpha_w - 2B^T P B)^{-1} \alpha_w^{-2} B^T P A$. With the designed feedback controller, the closed-loop system turns to

$$\hat{x}(k+1) = \alpha_w^{-1}(A - BK)\hat{x}(k). \tag{4.8}$$

Substituting $\hat{x}(k)$ by $\alpha_w^k x(k)$, Eq. (4.8) can be rewritten by:

$$x(k+1) = (A - BK)x(k). \tag{4.9}$$

As the system in Eq. (4.8) is designed to be stable,

$$|\lambda_{max}(\alpha_w^{-1}(A - BK))| < 1, \tag{4.10}$$

where λ_{max} is the maximum eigenvalue of the closed-loop system. Recall that $\lambda_{\alpha_w} < 0$, so $\alpha_w < 1$. The actual close-loop system has eigenvalues

$$|\lambda_{max}(A - BK)| < \alpha_w. \tag{4.11}$$

Therefore, the designed controller K has at least α_w degree of stability, which makes it superior for the design of FTC system.

Remark 4.1. *For designing FTC with exponential weighting matrix, the appropriate pa-*

rameter α_w can guarantee the stability of the controlled system with a prescribed degree of stability in addition to tune the values of weighting matrices Q and R.

4.3 Fault Detection and Diagnosis Design with SAEKF

Kalman filter variants can be used to address the actuator fault detection problem as aforementioned. However, this technique relies on the linear model, which is not the real case for the application of aircraft. To address the non-linearity, non-constant fault, and post-fault state estimation problems, this section proposes SAEKF, which is capable of providing the up-to-date post-fault states of the system and the magnitude or behavior of the faults. The non-linear dynamic model is discretized as Eq. (4.12) with process noise $\omega(k)$ and measurements noise $\nu(k)$ at the time instant k, respectively:

$$\begin{cases} x(k+1) = f(x(k)) + Bu(k) + \omega(k) \\ z(k) = Hx(k) + \nu(k), \end{cases} \tag{4.12}$$

where $x(k) = [x_z(k)\ v_z(k)\ \nu_z(k)] \in \mathbb{R}^3$ is the states vector of the system at the time instant k, $z(k) = x_z(k) \in \mathbb{R}^1$ represents the measurements at the time instant k, $x(0) \sim N(x(0), P^x(0))$, $\omega(k) \sim N(0, Q^x)$ and $\nu(k) \sim N(0, R^x)$ denote the process and the measurements noise with Gaussian distribution, respectively, and

$$E(\begin{bmatrix} \omega_k \\ \nu_k \end{bmatrix} [\omega_j\ \nu_j]) = \begin{bmatrix} \Omega & 0 \\ 0 & V \end{bmatrix} \delta_{kj}. \tag{4.13}$$

The states and measurements can be approximated with the model of the system as follows:

$$\begin{cases} \hat{x}^-(k) = f(\hat{x}(k-1)) + Bu(k-1) \\ \hat{z}(k) = H\hat{x}^-(k), \end{cases} \tag{4.14}$$

where $\hat{x}^-(k)$ is the priori state estimate at k, $\hat{x}(k-1)$ is a posteriori state estimate at the time instant $k-1$. Extended Kalman filter process can be summarized in Table 4.1 and Table 4.2, where $A = \frac{\partial f}{\partial x}|_{x(k)=x_t(k)}$ with $x_t(k)$ the equilibrium point of the system in hovering condition.

Table 4.1: EKF time update equations

$\hat{x}^-(k)$	$= f(\hat{x}(k-1)) + Bu(k-1)$
$P^-(k)$	$= AP(k-1)A^T + Q^x$

Table 4.2: EKF measurement update equations

$K(k)$	$= P^-(k)H^T(HP^-(k)H^T + R^x)^{-1}$
$\hat{x}(k)$	$= \hat{x}^-(k) + K(k)(z(k) - H\hat{x}^-(k))$
$P(k)$	$= (I - K(k)H)P^-(k)$

The post-fault system is presented as:

$$\begin{cases} x(k+1) = f(x(k)) + Bu(k) + BF(u(k))\Gamma^a(k) + \omega^x(k) \\ \Gamma^a(k+1) = \Gamma^a(k) + \omega^{\gamma^a} \\ z(k) = Hx(k) + \nu(k), \end{cases} \tag{4.15}$$

where $x(k)$ is still the state vector, $z(k)$ the measurement vector, $u(k)$ the known control input vector, $\Gamma^a(k)$ denotes the actuator faults which are unknown and to be diagnosed. The noise sequence $\omega^x(k)$, $\omega^{\gamma^a}(k)$, and $\nu(k)$ are zero mean uncorrelated random sequences.

For identifying LOE factors, the augmented system is composed as in Eq. (4.16):

$$\begin{cases} x_e(k+1) = f_e(x_e(k)) + B_e u(k) + \begin{bmatrix} \omega^x(k) \\ \omega^{\gamma^a}(k) \end{bmatrix} \\ z_e(k) = \begin{bmatrix} H & 0 \\ 0 & I \end{bmatrix} x_e(k) + \nu(k), \end{cases} \tag{4.16}$$

where $x_e(k+1) = [x(k+1)^T\ \Gamma^a(k+1)^T]^T$, $x_e(k) = [x(k)^T\ \Gamma^a(k)^T]^T$, $I \in \mathbb{R}^{m \times m}$ is identity matrix, and

$$f_e(x_e(k)) = \begin{bmatrix} f(x(k)) + B(F(u))\Gamma^a(k) \\ I \end{bmatrix} \qquad B_e = \begin{bmatrix} B \\ 0 \end{bmatrix} \tag{4.17}$$

with $x_e(0) \sim N(\bar{x}_e(0), P_e(0))$, $\omega(k)^x \sim N(0, Q^x)$, and $\omega(k)^{\gamma^a} \sim N(0, Q^{\gamma^a})$, where

$$x_e(0) = [x(0)^T, \Gamma^a(0)^T]^T, \tag{4.18}$$

$$P_e(0) = \begin{bmatrix} P^x(0) & P^{x\Gamma^a} \\ P^{\Gamma^a x} & P^{\Gamma^a}(0) \end{bmatrix},$$

$$[\omega^x(k)^T \omega^r(k)^T \ \nu(k)]^T \sim N(0, \begin{bmatrix} Q^x & & \\ & Q^{\Gamma^a} & \\ & & V \end{bmatrix}),$$

where $x_e(0)$ is the initial value of the augmented state vector with

$$\begin{cases} E(x_e(0)) = \bar{x}_e \\ E(x(0) - \bar{x}(0))(x(0) - \bar{x}(0)^T) = P^x(0) > 0 \\ E\gamma^a(0) = \bar{\gamma^a}(0) \\ E(\gamma^a(0) - \bar{\gamma^a}(0))(\gamma^a(0) - \bar{\gamma^a}(0)) = P^{x\gamma^a}(0). \end{cases} \tag{4.19}$$

The process in Table 4.1 and Table 4.2 with the augmented model is used to update the estimate of the system states and the LOE factors simultaneously based on the updated measurements.

4.4 Simulation Results

4.4.1 Test Scenarios

To investigate and validate the proposed framework with SAEKF for FDD purpose, the test scenarios are adopted and described as follows: 1) the Qball-X4 takes off automatically with fault-free duty and hovers in the pre-specified height; 2) the Qball-X4 continues to follow a circular trajectory while different faults are injected into the four motors in the tracking process; 3) the Qball-X4 lands automatically after the task of the trajectory tracking. The fault scenarios include 1) Scenario 1: fault-free, 2) Scenario 2: 10% LOE, 3) Scenario 3: 20% LOE. Various algorithms (SAEKF, EKF, and KF for FDD) are used for evaluation and comparison purpose as indicated in Table 4.3.

The reference trajectory starts from 1) zero height reference for $15s$ meaning the Qball-X4 staying on the ground; 2) steps to the height in $1m$; 3) after $10s$, circulates in radians $r = 1m$ with angular rate at $\omega = 0.2rad/s$ with an abrupt LOE fault injected at $30s$ (keeping circulating with angular rate at $\omega = 1rad/s$ for the comparison of the performance of the proposed SAEKF with KF for FDD purpose); and 4) after that, keeps $1m$ height and finally

Table 4.3: Tested fault scenarios

Task / Scenarios	Trajectory tracking	SAEKF	EKF	KF_{FDD}
Fault-free	✓	✓	✓	✓
Abrupt 10% LOE	✓	✓	✓	✓
Abrupt 20% LOE	✓	✓	✓	✓

✓means that the task is finished or the algorithm is validated

lands on the nearly ground at $0.3m$. The circular trajectory is illustrated in x and y direction:

$$\begin{cases} x = 1 + rsin(\omega(t - t_0) + \phi_x) \\ y = rsin(\omega(t - t_0)), \end{cases}$$

where r is radians, ω denotes phase frequency, t_0 is the start time of the circular trajectory, and $\phi_x = -pi/2$ and $\phi_y = 0$ are phase shift in x and y directions, respectively.

4.4.2 Performance Evaluation

The effectiveness of the designed FTC system is illustrated by the FDD performance and the tracking performance of following a reference trajectory. First, the FDD performance is depicted by presenting the detection and diagnosis speed and accuracy of the FDD module. Second, the FDD performance comparison of the proposed SAEFK and KF is illustrated with scenarios of tracking circular trajectories with different frequency phrases. The significant performance difference comes when the circular trajectory changes at fast angular frequency. Third, an additional benefit of the SAEKF for state estimation is presented through the comparison of the state estimation with EKF in fault-free and post-fault scenarios. At last, the tracking performance is given to show the tracking capability of the designed controller even under the fault scenarios, and the control efforts are presented also to show the task is fulfilled with the actuator constraints but different magnitudes under three different scenarios.

FDD Performance Evaluation

The injected faults and FDD results for the three scenarios are shown in Fig. 4.1. The dashed line is the injected fault with various magnitudes in 0% LOE (fault-free), 10% LOE, 20% LOE, respectively. The dotted line stands for the detected fault in fault-free scenario,

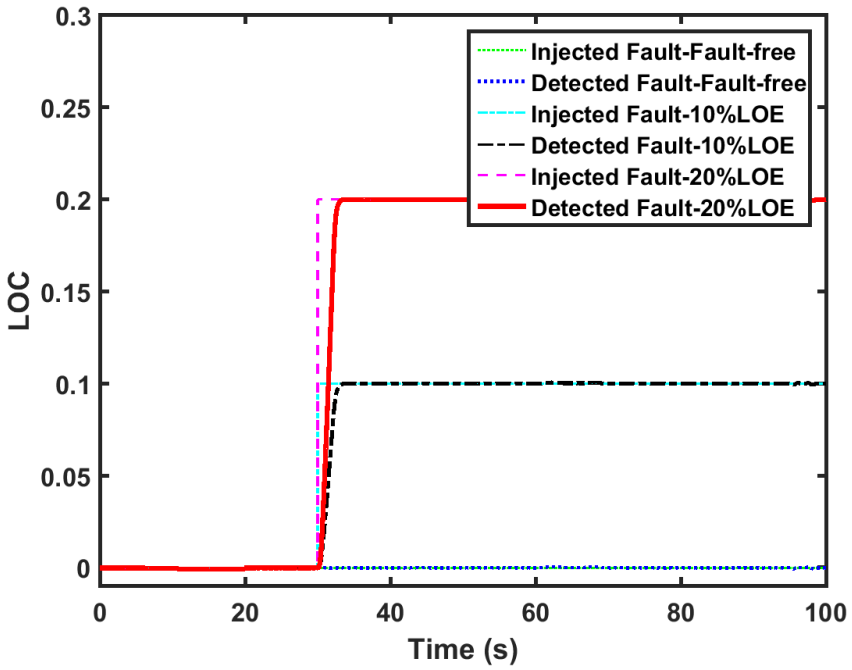

Figure 4.1: Fault detection and diagnosis results

which is around zero in the whole trajectory tracking process. The dash-dot line represents the detected and diagnosed fault in the 10% LOE fault scenario, which follows the injected fault timely (in less than $2s$) and accurately. The solid line stands for detected and diagnosed fault, which is more serious than the first two scenarios, with magnitude in 20% LOE. It shows that the response of the FDD module is considerably fast and accurate to detect and diagnose faults.

FDD Performance Comparison between SAEKF and KF

As mentioned in the subsection 4.4.1, the performance comparison between the proposed SAEKF and KF for FDD purpose is presented by tracking circular trajectory with two different changing rates at $0.2rad/s$ and $1rad/s$, respectively. To evaluate the FDD performance for different fault magnitudes, the tests are carried out under three different fault scenarios. As can be seen from Fig. 4.2(a), Fig. 4.2(b), and Fig. 4.2(c), both SAEKF and KF for FDD perform well with three different fault at the abrupt fault occurring at $30s$ for the trajectory tracking task at rate of $0.2rad/s$. However, when the circular trajectory changes at a faster rate $1rad/s$. The performance of KF for FDD degrades significantly compared to the FDD

performance of the proposed SAEKF methods. This indicates that the nonlinearity of the system dynamics can not be ignored. Since when the circular trajectory changes at a faster rate, the attitude angle changes aggressively. In consequence, the linearized model is not fit for the real situation.

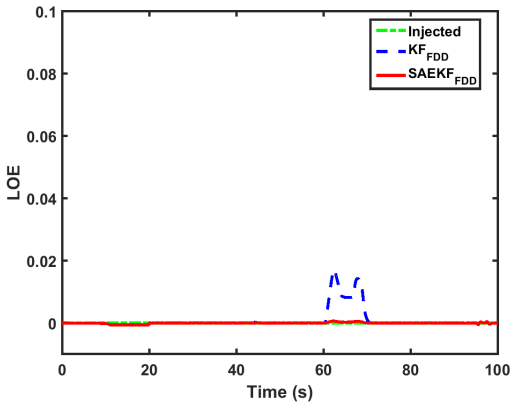

(a) Fault-free scenario

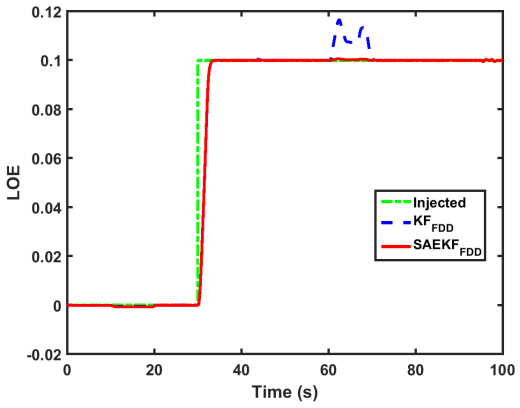

(b) 10% LOE scenario

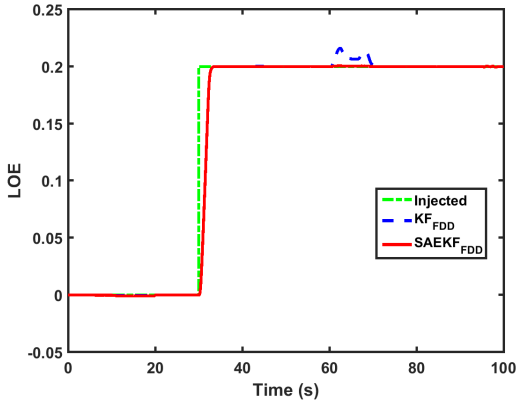

(c) 20% LOE scenario

Figure 4.2: FDD performance comparison between SAEKF and KF

State Estimation

To illustrate the necessity and additional benefit of using FDD for FTC design, the true states (from the model as baseline reference), states obtained from Kalman filter, and states obtained from SAEKF are illustrated and compared in three scenarios: fault-free, the 10% LOE of actuator faults, and the 20% LOE of actuator faults scenarios. The overall compar-

ison is summarized in Table. 4.4. The states includes x_z, v_z, and ν_z as shown in Eq. (3.9). e_{Peak} denotes the peak innovation value of the three mentioned states between the estimated value (either from SAEKF or EKF) and true states. $RMSE$ is the root-mean-square error (RMSE) value of the three states between the estimated value and true states along the whole test period. The performance of state estimation at fault-free scenarios is acceptable.

Table 4.4: Performance comparison between SAEKF and EKF with respect to: height, velocity, and actuator parameter

		Fault-free		10% LOE		20% LOE	
Algorithm	States	e_{Peak}	$RMSE$	e_{Peak}	$RMSE$	e_{Peak}	$RMSE$
EKF	x_z	0.02308	0.11386	0.12172	9.1615	0.26073	20.7592
	v_z	0.12694	1.0958	0.60177	43.311	1.3309	98.8362
	ν_z	0.10623	0.0064661	0.10623	1.2406	0.10623	2.7836
SAEKF	x_z	0.0025942	0.0046448	0.0025958	0.0049069	0.0025978	0.0051485
	v_z	0.017648	3.0726	0.084627	2.9843	0.19604	2.9027
	ν_z	0.10623	0.007423	0.10623	0.015046	0.10623	0.022812

However, the performance of EKF for state estimation is degraded dramatically with the magnitude of faults increasing: 1) $RMSE_{x_z}$ increases from 0.11386, to 9.1615, till 20.7592; 2) $RMSEv_z$ increases from 1.0958, to 43.311, until to 98.8362; 3) $RMSE\nu_z$ increases from 0.0064661, to 1.2406, until to 2.7836. In contrast, the performance of SAEKF stays the same level in terms of three system states x_z, v_z, and ν_z under different fault scenarios.

As can be seen from Fig. 4.3(a), Fig. 4.3(b), and Fig. 4.3(c) for the three scenarios, the height from Kalman filter and FDD block are convergent to the true height in the fault-free case (see Fig. 4.3(a)). However, it is not the case in the other two fault scenarios. There exists significant errors (see Fig. 4.3(b), Fig. 4.3(c)) between the filtered height from EKF and the true states after the fault occurrence. The filtered height from the proposed FDD scheme is still consistent with true height. This problem with EKF for the state estimation arises from the modeling error when faults are not modeled in the state estimation process. However, the estimated hight is reliable and robust to the actuator faults with augmented states related to the faults. Note that with the increasing of LOE from 10% to 20%, the estimation from EKF error also increases, while the estimation from SAEKF still matches the true height. Therefore, the proposed SAEKF as FDD approach can give the right information of the states of the system for both fault-free and fault scenarios. To further examine the performance, the velocity (see Fig. 4.4(a), Fig. 4.4(b), and Fig. 4.4(c)) and parameter about actuator (see Fig. 4.5(a), Fig. 4.5(b), and Fig. 4.5(c)) from Kalman filter and SAEKF are compared with

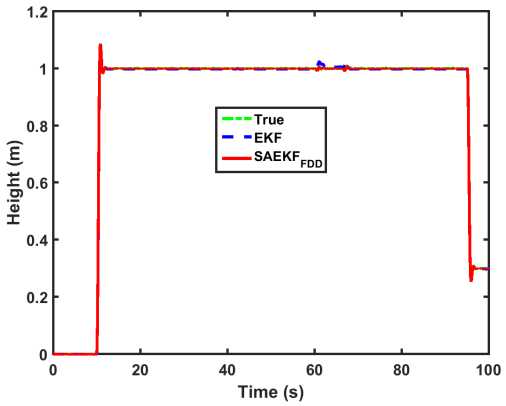

(a) Fault-free scenario

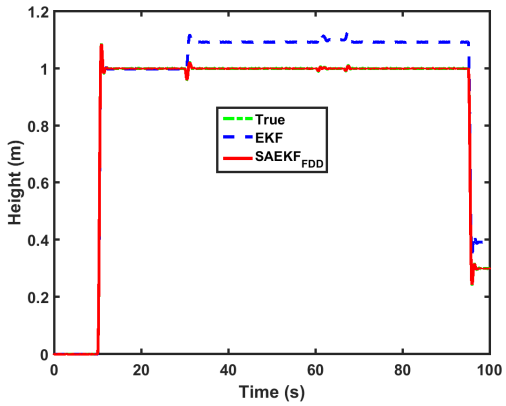

(b) 10% LOE fault scenario

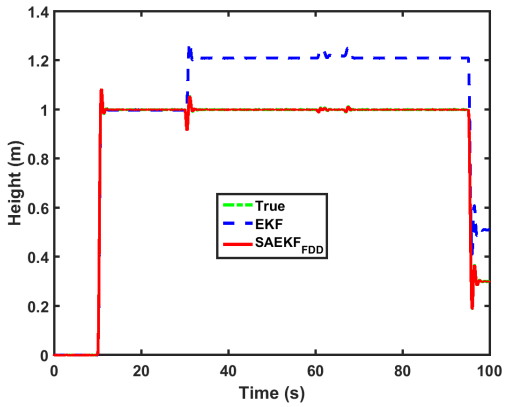

(c) 20% LOE fault scenario

Figure 4.3: Height comparison: true height, height from EKF, and height from SAEKF

respected to the test scenarios. As can be seen from Fig. 4.4(a) and Fig. 4.5(a) in the fault-free scenario, both EKF and SAEKF provide the trusty speed of the Qball-X4 and trusty actuator parameter. However, the performance of EKF is deteriorated significantly when the fault occurs, while the performance of the proposed SAEKF keeps in a robust manner as shown in Fig. 4.4(b) and Fig. 4.5(b) for the 10% LOE and in Fig. 4.4(c) and Fig. 4.5(c) for the 20% LOE scenarios. The performance of EKF for state estimation decreases when the fault increases, while the performance of the proposed SAEKF is satisfactory.

Overall, the comparison results are summarized in Table 4.5. As can be seen from Table 4.5, the proposed FDD approach estimates the right states, which are close to the true states, in fault-free and post-fault scenarios.

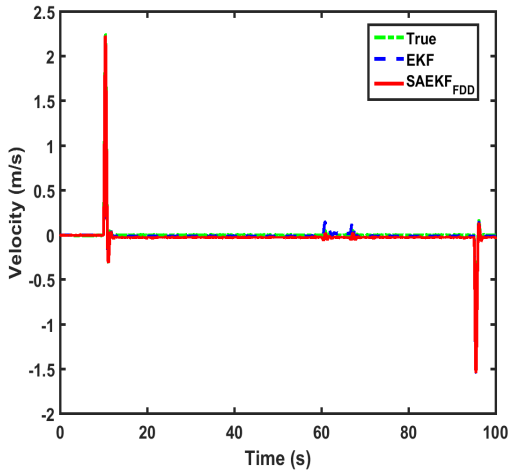

(a) Fault-free scenario

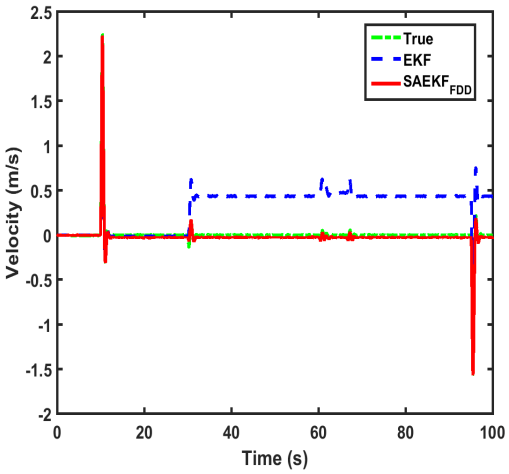

(b) 10% LOE fault scenario

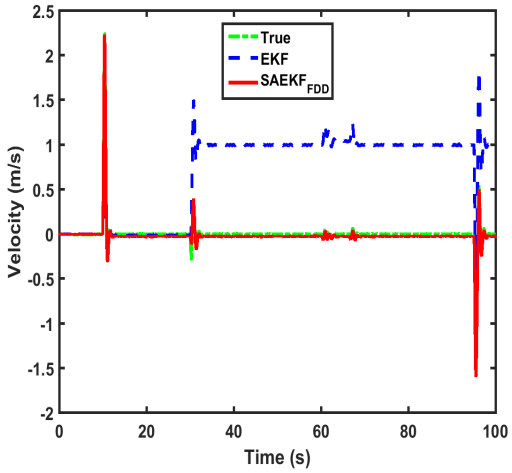

(c) 20% LOE fault scenario

Figure 4.4: FDD performance comparison of velocity of the Qball-X4

Performance and Assessment

Based on the scenarios described in Table 4.3, the tracking performance of the system is presented in Fig. 4.6(a), Fig. 4.6(b), and Fig. 4.6(c). The dotted line is the reference trajectory, and the solid line stands for the measurement trajectory for all the three scenarios. As can be seen from Fig. 4.6(a), Fig. 4.6(b), and Fig. 4.6(c), the Qball-X4 completes the trajectory tracking task under three different scenarios. In the fault-free case, the circular tracking is considerable smooth. Compared to the fault-free scenario, there are fluctuations starting

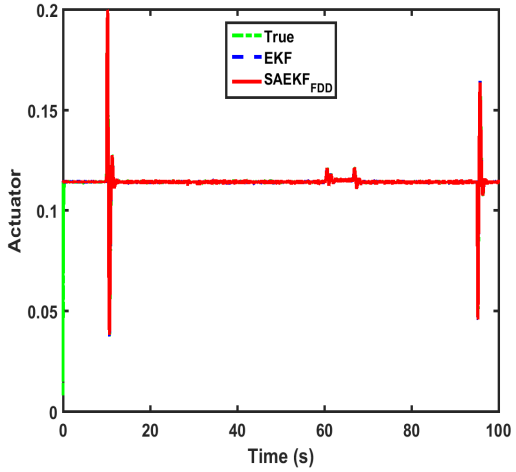

(a) Fault-free scenario

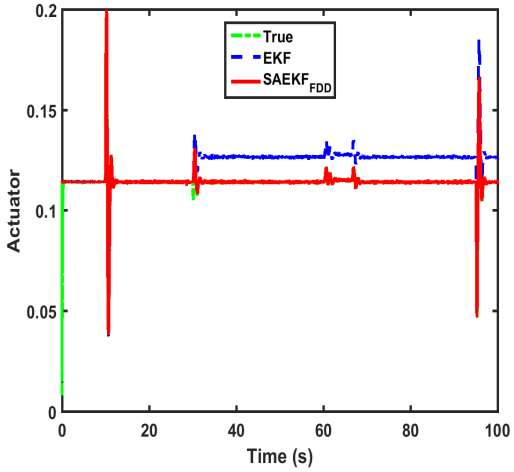

(b) 10% LOE fault scenario

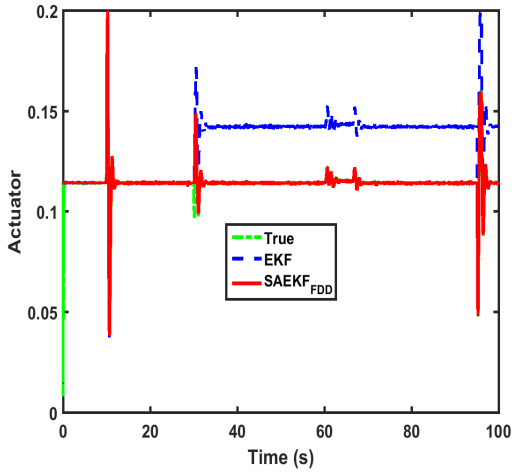

(c) 20% LOE fault scenario

Figure 4.5: FDD performance comparison of actuator parameter

at 30s on the circular tracking process with injected fault with the various magnitude: the 10% LOE and 20% of LOE, respectively. To get a deep insight of the controls in the process, Fig. 4.7 is presented as comparison of control efforts before and after faults. The dotted line is the control efforts in the fault-free case. The dash-dot line is the control efforts in the 10% LOE fault scenario. And the solid line represents the control efforts in the third scenarios, which is under the 20% LOE fault. It is evident that before the fault happens, the control efforts in the three test scenarios are the same value. However, the control efforts increase with the magnitude of LOE increasing to keep the desired performance as close as possible.

Table 4.5: Summary of the comparison of states from: true, SAEKF, and EKF

States in various scenarios / Source	Fault-free			10% LOE			20% LOE		
	height	velocity	actuator	height	velocity	actuator	height	velocity	actuator
True	*	*	*	*	*	*	*	*	*
SAEKF	✓	✓	✓	✓	✓	✓	✓	✓	✓
EKF	✓	✓	✓	⊗	⊗	⊗	⊗	⊗	⊗

* is the true signal, ✓ the well match between the estimation and true signal, and ⊗ the inconsistent match of estimation with true signal.

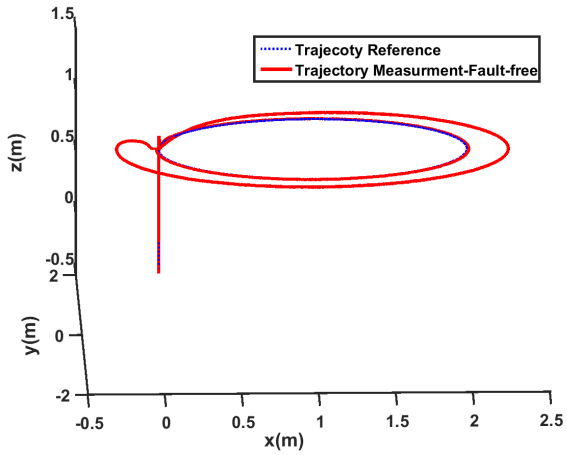

(a) Fault-free scenario

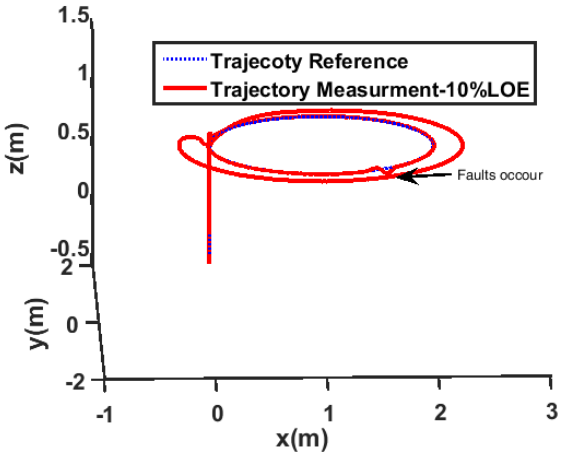

(b) 10% LOE fault scenario

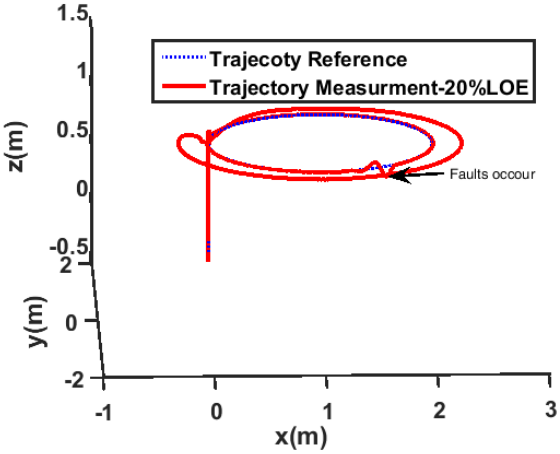

(c) 20% LOE fault scenario

Figure 4.6: Performance of trajectory tracking task

Overall, the control efforts still keep in the range of actuator's limitations.

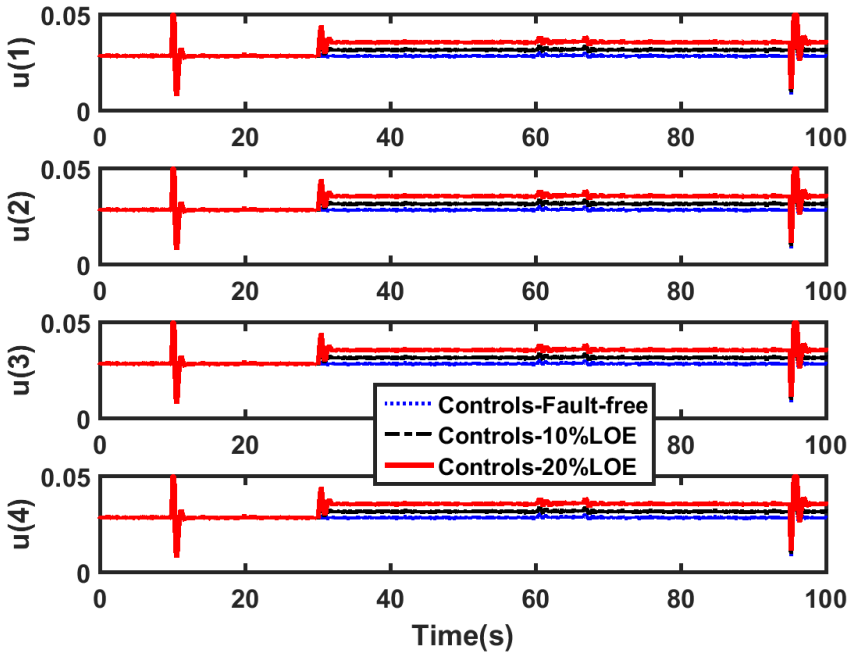

Figure 4.7: Control efforts in three scenarios before and after faults

4.5 Summary

This chapter develops a FTC scheme for a quadrotor UAV with the proposed FDD module using SAEKF approach and controller using improved LQ technique. The test results of the designed FTC shows that the proposed SAEKF can detect and diagnose faults timely and accurately and has better performance compared to the variant of KF when the non-linearity has to be considered. The additional benefit of using the proposed FDD is that it can provide the trusty state estimation even in the faulty situation. With the overall tracking performance of the system, the proposed FTC system works in a considerable good manner. In addition, the improved LQ technique can be further developed with the combination of MPC for FTC design.

Part II

Application to a Fixed-Wing Aerial Vehicle

Chapter 5

Modeling of Boeing 747-100/200

5.1 Introduction

For the assessment of new fault-tolerant flight control techniques, a simulation benchmark was developed based on the reconstructed and validated Flight 1862 aircraft model performed in the Action Group as described in Section 5.2. The benchmark model of Flight 1862 aircraft was constructed based on the record data of a Boeing 747-200F freighter aircraft. Section 5.3 presents a Boeing 747-100/200 non-linear model with an emphasis on longitudinal motion model for the FTC design purpose. Since the primary objective of an airplane is to safely land in the presence of faults and the lateral motion of a commercial airplane is always designed with high degree of static stability, it is assumed that the airplane can be landed safely if the system is longitudinally stable in the event of elevator faults. Based on the stability recognition of longitudinal and lateral channels of a Boeing 747-100/200, the linearized model of longitudinal channel is obtained by linearizing the non-linear model around the trim conditions presented in Section 5.4. Furthermore, the model validation is carried out by the performance comparison to non-linear model of a Boeing 747-100/200 based on each the available control effort. Section 5.5 summaries this chapter.

5.2 GARTEUR Benchmark Description

The GARTEUR RECOVER software package [1] is equipped with several simulation and analysis tools, all centered around a generic nonlinear aircraft model for six-degrees-of-

freedom non-linear aircraft simulations. The simulation of any specific aircraft with various fault types is possible by just applying user-defined aircraft model and fault models. The software architecture of the RECOVER simulation benchmark comprises a generic aircraft model and aircraft specific modules including aerodynamics, flight control system, and engines. The baseline flight control system model reflects the hydro-mechanical system architecture of the Boeing 747-100/200 aircraft. All modeled control surfaces are subjected to aerodynamic effects and mechanical limits throughout the flight envelope. The original aircraft model of the RECOVER benchmark was based on the classical Boeing 747-100/200 aircraft (See Fig. 5.1) with a hydro-mechanical flight control system and the pilot cockpit controls as inputs. A fly-by-wire version of the Boeing 747-100/200 aircraft was created for

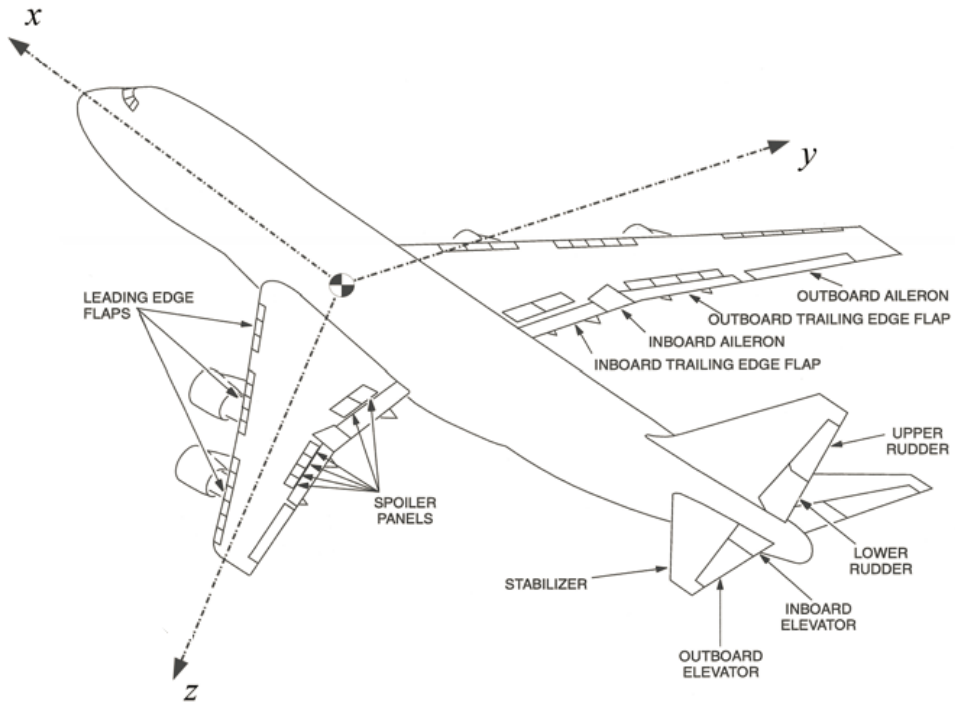

Figure 5.1: Boeing 747-100/200 configuration and flight control surface arrangements

the FTC design and test purposes where all twenty-six aerodynamic control surfaces and four engines can be controlled individually, which allows a newly designed FTC system to have the capability to completely reconfigure the available flight control effectors. Meanwhile, the flexibility of utilizing all the control surfaces and engines also brings challenges in configuring control resources with different FTC strategies. A schematic overview of the

GARTEUR RECOVER benchmark is presented in Fig. 5.2 including relationships among different components of the benchmark. The basic aircraft model contains airframe, actu-

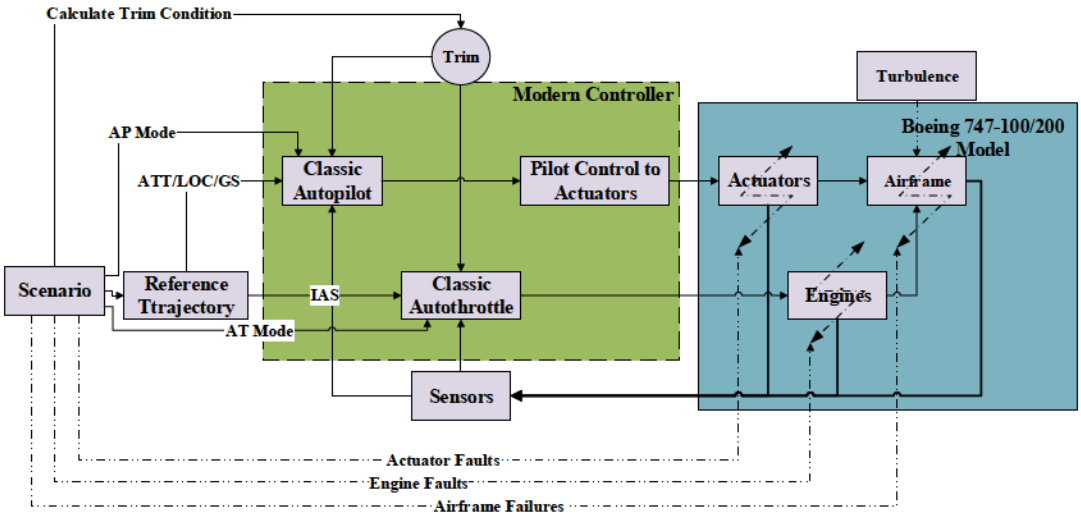

Figure 5.2: Schematic overview of the GARTEUR RECOVER benchmark

ator, engines, and turbulence models. The input of this model was initially based on the pilot's control inputs, which have a fixed linkage to the control surfaces. To control the surfaces separately, as required for the reconfigurable control algorithms, the pilot controls to actuators block is separated from the baseline aircraft model. A basic classic controller is available in the benchmark, based on the Boeing 747-100/200 classic autopilot including auto throttle (AT) to serve as a reference for new adaptive control algorithm designs.

The newly designed FTC system to be evaluated with the benchmark model, is to replace the classic autopilot and auto throttle. The control surfaces should be driven separately or with a certain combination based on the control strategies. Although the new designed FTC system drives the control surfaces distinguished to the conventional control system, the reference commands to the FTC system are still the same, such as altitude hold (ATT) mode, localizer capture mode, glide-slope (GS) capture, and instrument airspeed (IAS). In order to operate the benchmark, a scenario and failure model generator is added. The scenario consists of commands fed into the autopilot and auto throttle, while the failures are directly introduced into the airframe, flight control system, and propulsion models.

5.3 Boeing 747-100/200 Model in Longitudinal Direction

A Boeing 747-100/200 is a four-engines wide-body commercial jet airliner and cargo aircraft with a range of $10,000km$ and maximum level speed $975km/hr$ and design ceiling of $137,166m$. High lift for low speed flight is obtained with wing triple-slotted flaps and Krueger type leading edge flaps. The longitudinal control for aircraft is provided by a movable stabilizer and 4 elevator segments. The lateral control is obtained with 5 spoiler panels, an inboard aileron between the inboard and outboard flaps, and an outboard aileron which only operates when flaps are down. The five spoiler panels on each wing which are used for lateral control also operate symmetrically as speed-brakes in conjunction with the sixth spoiler panels. Directional control is obtained with a two-segment rudder [83].

The benchmark model includes aircraft aerodynamic models and engines. In addition, actuator and sensor characteristics are taken into account, together with models for wind, atmospheric turbulence and faults. The aerodynamic forces and moments are defined in terms of aerodynamic coefficients, which are given in the form of look-up tables. They are functions of a wide set of parameters, such as pitch angle, angle of attack, true airspeed, and altitude. The dimension of the aircraft output vector is 142. However, all these output signals are not necessary to control the aircraft. The dynamical behavior of the aircraft is described by the following nonlinear state representation:

$$\begin{cases} \dot{x}_{NL} = f(x_{NL}(t), u_{NL}(t)) \\ y_{NL}(t) = g(x_{NL}(t), u_{NL}(t)) + \nu(t), \end{cases} \tag{5.1}$$

where x_{NL}, u_{NL}, y_{NL} are the state, input, and output vectors of the full aircraft nonlinear model. The signal vector ν stands for the measurement noise. More particularly, the model of Boeing 747-100/200 can be formulated in the following equations with respected to dynamics equations and kinematic equations. The force equations are:

$$\begin{cases} \dot{\alpha} = \dfrac{-F_x s_\alpha + F_z c_\alpha + m(-p c_\alpha s_\beta + q c_\beta - r s_\alpha s_\beta) V_{TAS}}{m V_{TAS} c_\beta + C_{L_{\dot{\alpha}}} \bar{q} S \frac{\bar{c}}{V_{TAS}}} \\ \dot{\beta} = \dfrac{-F_x c_\alpha s_\beta + F_y c_\beta - F_z s_\alpha s_\beta + m(-p s_\alpha + r c_\alpha) V_{TAS}}{m V_{TAS}} \\ \dot{V}_{TAS} = \dfrac{1}{m}(F_x c_\alpha c_\beta + F_y s_\beta + F_z c_\beta s_\alpha). \end{cases} \tag{5.2}$$

The moment equations are:

$$\begin{cases} \dot{p} = (c_1 r + c2p)q + c_3 M_x + c_4 M_z \\ \dot{q} = c_5 pr - c_6(p^2 - r^2) + c_7 M_y \\ \dot{r} = (c_8 p - c_2 r)q + c_4 M_x + c_9 M_z. \end{cases} \tag{5.3}$$

The kinematics equations are:

$$\begin{cases} \dot{\phi} = p + t_\theta(q s_\phi + r c_\phi) \\ \dot{\theta} = q c_\phi - r s_\phi \\ \dot{\psi} = (q s_\phi + r c_\phi)\dfrac{1}{c_\theta}. \end{cases} \tag{5.4}$$

The navigational equations are:

$$\begin{cases} \dot{h}_e = -(-u s_\theta + v c_\theta s_\phi + w c_\phi c_\theta) \\ \dot{x}_e = u c_\psi c_\theta + v(-c_\phi s_\psi + c_\psi s_\phi s_\theta) + w(s_\phi s_\psi + c_\phi c_\psi s_\theta) \\ \dot{y}_e = u s_\psi c_\theta + v(c_\phi c_\psi + s_\psi s_\phi s_\theta) + w(-c_\psi s_\phi + c_\phi s_\phi s_\theta). \end{cases} \tag{5.5}$$

The true airspeed is denoted in the body axes as:

$$\begin{cases} u = V_{TAS} c_\alpha c_\beta \\ v = V_{TAS} s_\beta \\ w = V_{TAS} s_\alpha c_\beta. \end{cases} \tag{5.6}$$

The products and moments of inertia coefficients are given by:

$$\begin{cases} c_1 = \dfrac{(I_{yy} - I_{zz})I_{zz} - I_{xz}^2}{\Gamma} & c_2 = \dfrac{(I_{xx} - I_{yy} + I_{zz})I_{xz}}{\Gamma} \\ c_3 = \dfrac{(I_{zz})}{\Gamma} & c_4 = \dfrac{I_{xz}}{\Gamma} \\ c_5 = \dfrac{I_{zz} - I_{xx}}{I_{yy}} & c_6 = \dfrac{I_{xz}}{I_{yy}} \\ c_7 = \dfrac{1}{I_{yy}} & c_8 = \dfrac{I_{xz}}{I_{yy}} \\ c_9 = \dfrac{I_{xx}}{\Gamma} & \Gamma = I_{xx} I_{zz} - I_{xz}^2. \end{cases} \tag{5.7}$$

The forces and moments in body-axes for the Boeing 747-100/200 are given by:

$$
\begin{cases}
F_x = \bar{q}SC_{X_b} + \sum_{i=1}^{4} T_{n_i} - mgs_\theta \\
F_y = \bar{q}SC_{Y_b} + 0.0349[T_{n_1} + T_{n_2} - (T_{n_3} + T_{n_4})] + mgc_\theta s_\phi \\
F_z = \bar{q}SC_{Z_b} - 0.0436 \sum_{i=1}^{4} T_{n_i} + mgc_\theta c_\phi \\
M_x = \bar{q}Sb[C_{l_b} + \frac{1}{b}(C_{Y_b}\bar{z}_{cg} - C_{Z_b}\bar{y}_{cg}) - \frac{\bar{c}\dot{\alpha}}{bV_{TAS}}C_{Z_{\dot{\alpha}_b}}\bar{y}_{cg}] \\
\qquad + 0.0436[T_{n_1}y_{eng1} + T_{n_2}y_{eng2} - (T_{n_3}y_{eng3} + T_{n_4}y_{eng4})] \\
M_y = \bar{q}S\bar{c}[C_{m_b} + \frac{1}{\bar{c}}(C_{Z_b}\bar{x}_{cg} - C_{X_b}\bar{z}_{cg}) + \frac{\bar{c}\dot{\alpha}}{bV_{TAS}}(C_{m_{\dot{\alpha}_b}} + \frac{\bar{x}_{cg}}{\bar{c}}C_{Z_{\dot{\alpha}_b}})] \\
\qquad + \sum_{i=1}^{4} T_{n_i} zeng_i \\
M_z = \bar{q}Sb[C_{n_b} + \frac{1}{b}(C_{X_b}\bar{y}_{cg} - C_{Y_b}\bar{x}_{cg}) + \frac{\bar{b}\dot{\beta}}{V_{TAS}}C_{n_{\dot{\beta}_b}}] \\
\qquad + T_{n_1}y_{eng1} + T_{n_2}y_{eng2} - (T_{n_3}y_{eng3} + T_{n_4}y_{eng4}).
\end{cases}
\tag{5.8}
$$

Since the aerodynamic coefficients are obtained directly in the wind coordinate and constructed in the stability coordinate, transformation of aerodynamic coefficients in stability reference frame to body-fixed frame are considerable necessary and given by:

$$
\begin{bmatrix} C_{X_b} \\ C_{Y_b} \\ C_{Z_b} \end{bmatrix} = \begin{bmatrix} -c_\alpha & 0 & s_\alpha \\ 0 & 1 & 0 \\ -s_\alpha & 0 & -c_\alpha \end{bmatrix} \begin{bmatrix} C_D \\ C_Y \\ C_L \end{bmatrix}, \tag{5.9}
$$

$$
\begin{bmatrix} C_{l_b} \\ C_{m_b} \\ C_{n_b} \end{bmatrix} = \begin{bmatrix} c_\alpha & 0 & -s_\alpha \\ 0 & 1 & 0 \\ s_\alpha & 0 & c_\alpha \end{bmatrix} \begin{bmatrix} C_l \\ C_m \\ C_n \end{bmatrix}, \tag{5.10}
$$

where $C_L, C_D, D_Y, C_m, C_l, C_n$ are aerodynamic coefficients available from [84].

The 12 rigid body states of the Boeing 747-100/200 aircraft can be divided into 6 longitudinal and 6 lateral and directional states, which are all determined from the 6-degree of freedom equations of motion. For the longitudinal channel, the states are pitch rate q, true airspeed V_{TAS}, angle of attack α, pitch angle θ, altitude h_e, and x-directional displacement

x_e; while for the lateral and directional channel, the states are roll rate p, yaw rate r, slide slip angle β, yaw angle ϕ, roll ψ, and y-directional displacement y_e. The control surface, as aforementioned in RECOVER benchmark model description, comprises 4 ailerons (inner and outer on each wing), 12 spoilers (2 inner spoilers and 4 outer spoilers on each wing), 2 rudder (upper and lower), 4 elevators (an inner and outer on each left and right elevator), a horizontal stabilizer, and 4 engine thrust, which can be controlled individually for a new FTC design compared to the configuration of the true Boeing 747-100/200 aircraft.

The body-axes longitudinal motion of the Boeing 747-100/200, not including flexible effects, can be described by the following differential equations with parameters $[\dot{\alpha}\ \dot{q}\ \dot{\theta}\ \dot{V}_{TAS}\ \dot{h}_e]$ [83–86]:

$$\begin{cases} \dot{\alpha} = \dfrac{-F_x s_\alpha + F_z c_\alpha}{m V_{TAS}} + q \\ \dot{q} = c_7 M_y \\ \dot{\theta} = q \\ \dot{V}_{TAS} = \dfrac{1}{m}[F_x c_\alpha + F_z s_\alpha] \\ \dot{h}_e = V_{TAS} c_\alpha s_\theta - V_{TAS} s_\alpha c_\theta = V_{TAS} s_\gamma, \end{cases} \tag{5.11}$$

where α (rad) is angle of attack, q (rad/s) is pitch rate, V_{TAS} (m/s) is true velocity, θ (rad/s) is pitch angle, and h_e (m) is altitude. c_α and c_θ are cosine of α and θ, while s_θ and s_α are sine of α and θ. The aerodynamic force along X-axis, Z-axis, and the pitching moment are given by F_x, F_y, and M_y, respectively. The body-axes aerodynamic forces and moments are given by:

$$\begin{cases} F_x = -\bar{q} S [C_D c_\alpha - C_L s_\alpha] + \sum_{i=1}^{4} T n_i - m g s_\theta \\ F_z = -\bar{q} S C_D s_\alpha + C_L c_\alpha - 0.0436 \sum_{i=1}^{4} T n_i + m g c_\theta \\ M_y = \bar{q} S \bar{c} \{ C_m - \dfrac{1}{\bar{c}} [(C_D s_\alpha) + C_L c_\alpha) \bar{x}_{xg} - (C_D c_\alpha - C_L s_\alpha) \bar{z}_{cg}] + \dfrac{\bar{c} \dot{\alpha}}{V_{TAS}} [C_{m_{\dot{\alpha}}} - \dfrac{\bar{x}_{cg}}{\bar{c}} C_{L_{\dot{\alpha}}} c_\alpha] \} \\ \qquad + \sum_{i=1}^{4} T n_i z e n g_i, \end{cases} \tag{5.12}$$

where C_D, C_L, and C_m are dimensionless aerodynamic coefficients about drag force, lift force and pitch moment in wind axis; $\bar{q}$ (N/m^2) is flight dynamic pressure.

Table 5.1: Trim condition for the model linearization

Variables	Normal Value
Altitude	$609.6m(2,000ft)$
True Airspeed	$92.6m/s$
Landing gear	up
Mass	$263,000kg$
X_{cg}	$25\%MAC$
Y_{cg}	0
Z_{cg}	0
Flap setting	$20deg$

5.4 Performance of Linearized Model

The non-linear aircraft model can be linearized for the fault-tolerant controller design. The linearized model with 12 states and 29 control inputs (25 control surfaces and 4 engines) is obtained and represented in the state space form:

$$\begin{cases} \dot{x}_t = A_{lin}x_t + B_{lin}u_t \\ y_t = C_{lin}x_t \end{cases} \tag{5.13}$$

where $A_{lin} \in \mathbb{R}^{12\times12}$, $B_{lin} \in \mathbb{R}^{12\times29}$,

$$\begin{aligned} &x_{lin} \in \mathbb{R}^{12} = [p\ q\ r\ V_{TAS}\ \alpha\ \beta\ \phi\ \theta\ \psi\ h_e\ x_e\ y_e] \\ &u_t \in \mathbb{R}^{29} = [\delta_{air}\ \delta_{ail}\ \delta_{aor}\ \delta_{aol}\ \delta_{sp1-12}\ \delta_{eir}\ \delta_{eil}\ \delta_{eor}\ \delta_{eol}\ \delta_{ih}\ \delta_{ru}\ \delta_{rl}\ \delta_{fo}\ \delta_{fi}\ \delta_{TN1-4}]. \end{aligned} \tag{5.14}$$

x_{lin} is the state vector of the linearized model, u_{lin} is the control input vector of a Boeing 747-100/200, and B_{lin} comprises 6 sets:

$$B_{lin} = [B_{lin_a} \quad B_{lin_{sp}} \quad B_{lin_e} \quad B_{lin_r} \quad B_{lin_{fp}} \quad B_{lin_{T_n}}]$$

where B_{lin_a} is related to 4 ailerons, $B_{lin_{sp}}$ is related to 12 spoilers, B_{lin_e} is related to 4 elevators and 1 horizontal stabilizer, B_{lin_r} is related to 2 rudders, $B_{lin_{fp}}$ related to 2 flaps, and $B_{lin_{T_n}}$ is related to 4 engines. The 12 states can be classified into two sets: 6 longitudinal states and 6 lateral states. The linearized model of the aircraft is under the flight condition with trim value listed in Table 5.1.

For the longitudinal fault-tolerant control design, the state of the longitudinal motion is se-

Table 5.2: Flight condition for the model linearization

Flight Path Angle (γ)	$0deg$
Heading Angle (χ)	$180deg$
Yaw (ψ)	$180deg$
Pitch Angle (θ)	$5.1deg$
Roll (ϕ)	$0deg$

lected as $x_{long} = [q\ V_{TAS}\ \alpha\ \beta]^T$, and the controls are selected to be 4 elevators $[\delta_{eir}\ \delta_{eil}\ \delta_{eor}\ \delta_{eol}]$, 1 horizontal stabilizer δ_{ih}, and 4 individual thrust $[\delta_{TN1}\ \delta_{TN2}\ \delta_{TN3}\ \delta_{TN4}]$, which are comprised as $u_{long} = [\delta_{eir}\ \delta_{eil}\ \delta_{eor}\ \delta_{eol}\ \delta_{ih}\ \delta_{TN1}\ \delta_{TN2}\ \delta_{TN3}\ \delta_{TN4}]^T$.

To investigate and validate that the control law design is acceptable, the time responses of nonlinear model and linearized model are compared with respect to three types of control efforts: elevator, stabilizer, and thrust, respectively.

The deflection of elevator starts at 5 s from the trim value of 2 deg to the final value of 1 deg while all the other controls stay in trim values. The elevator deflection process is shown in Fig. 5.3 and the performance is presented in Fig. 5.4. The deflection of horizontal

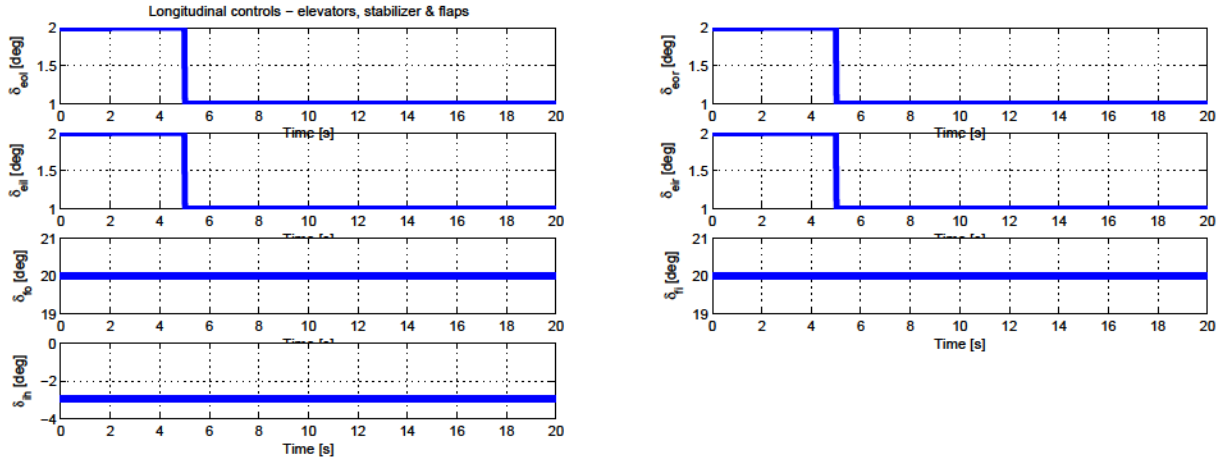

Figure 5.3: Elevator deflections for comparison of linearized model and nonlinear model

stabilizer starts at $5s$ from the trim value of -2.9464 deg to the final value of -1.9464 deg while all the other controls stay in trim values. The stabilizer deflection process is shown in Fig. 5.5 and the performance is presented in Fig. 5.6. The control input of thrust starts also at $5s$ from the trim value of 5.4677×10^4 to the final value of 1.54677×10^5 while all the other controls stay in trim value. The thrust input is shown in Fig. 5.5 and the time responses of the nonlinear model and linearized model are presented in Fig. 5.8.

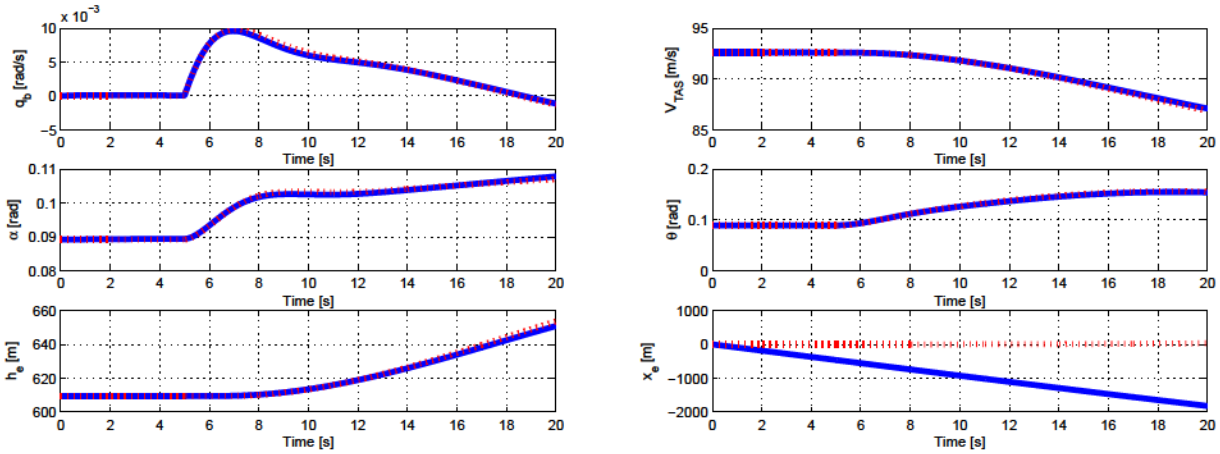

Figure 5.4: Performance with elevator deflections for comparison of linearized and nonlinear model

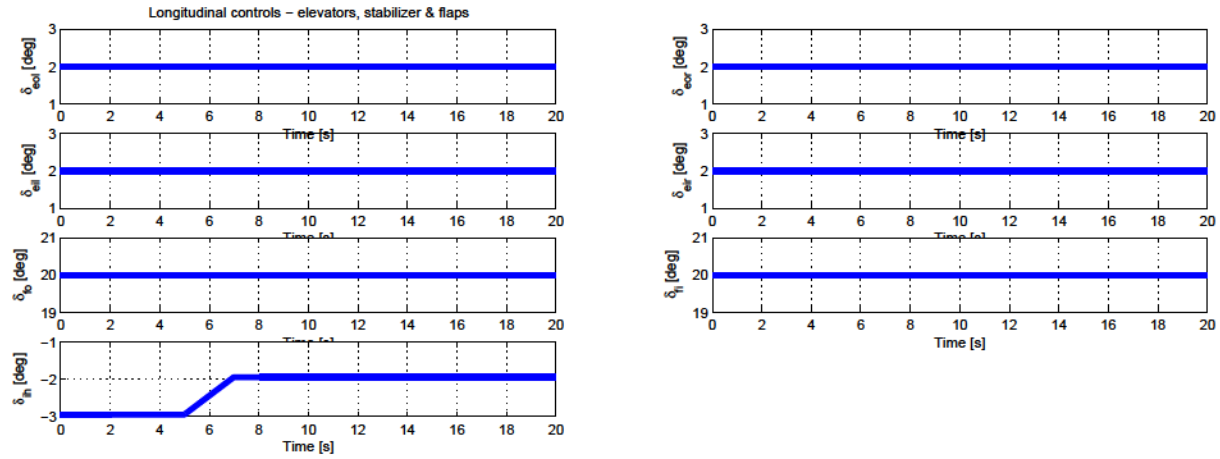

Figure 5.5: Stabilizer deflections for comparison of linearized model and nonlinear model

Remark 5.1. *The blue lines in Fig. 5.4, Fig. 5.6, and Fig. 5.8 stand for the time response of nonlinear model with respect to the corresponding control inputs; while the red dotted lines are the time responses of the linear model. Based on the performance comparison shown in Fig. 5.4, Fig. 5.6, and Fig. 5.8, the linearized model is appropriate to perform FTC control design for aircraft.*

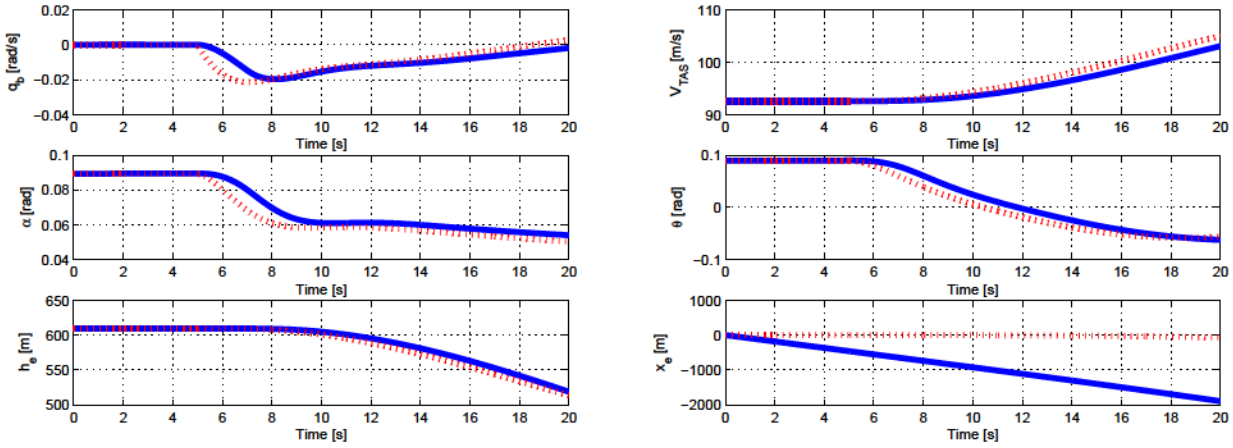

Figure 5.6: Performance with stabilizer deflections for comparison of linearized model and nonlinear model

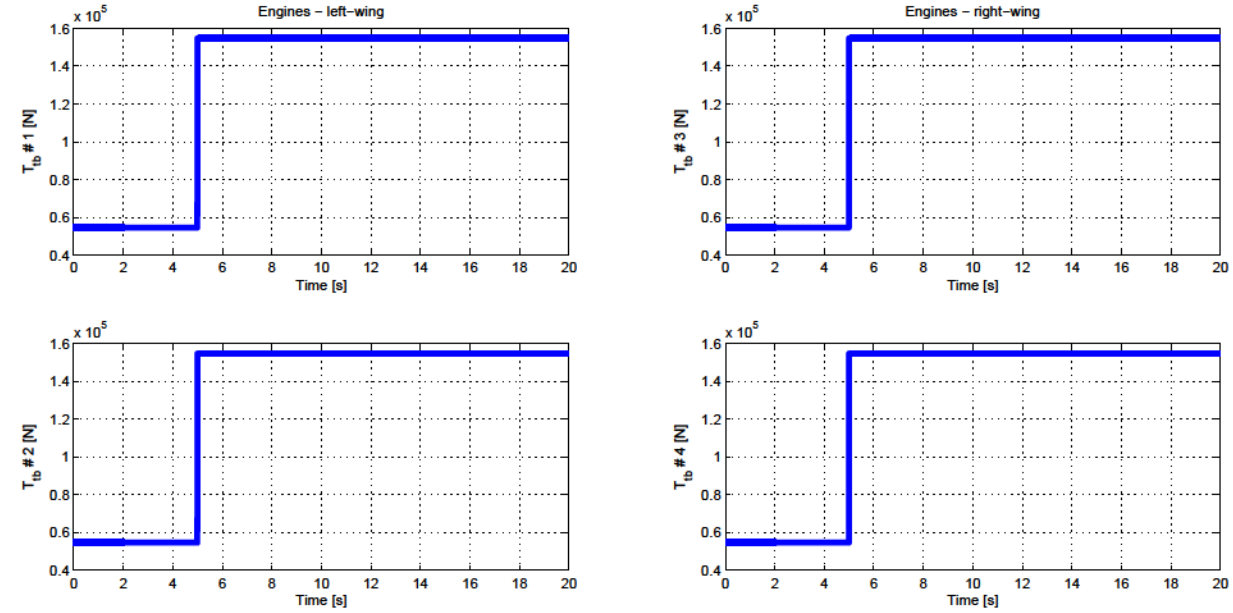

Figure 5.7: Thrust input for comparison of linearized model and nonlinear model

5.5 Summary

This chapter introduces the RECOVER benchmark model of a Boeing 747-100/200 as the platform to evaluate the designed FTC strategies. The schematic diagram of benchmark is presented to illustrate the working scheme and the connections among different modules.

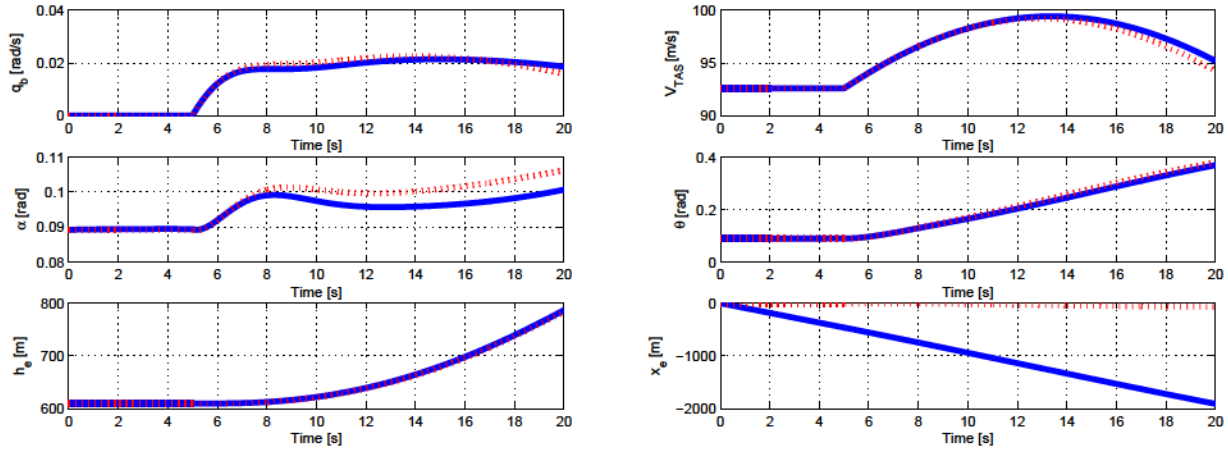

Figure 5.8: Performance with thrust input for comparison of linearized model and nonlinear model

Particularly, the new fault-tolerant controller is to replace the conventional flight control system for the effectiveness and performance evaluation of fault-tolerant capability. Further more, the high fidelity nonlinear longitudinal model of a Boeing 747-100/200 is presented to illustrate the aircraft dynamics. For the sake of fault-tolerant controller design, a linearized model is obtained with specific trim conditions and flight conditions. The linearized model is verified by comparing the time response between linear and non-linear model respected to the different longitudinal inputs: elevator, horizontal stabilizer, and the engines.

Chapter 6

Fault-Tolerant Control of Boeing 747-100/200 Using LF-MPC

6.1 Introduction

LOC during flight contributes one of the major factors for the flight accidents [1, 17]. Learning from previous experience, the faulty aircraft can land safely to avoid a fatal accident by well-trained pilot and a FTC system could be helpful for the success of safe landing [1]. A great amount of works have been done to explore the possibility of improving the survivability of crippled aircraft. With the help of the RECOVER benchmark model of a Boeing 747-100/200, a FTC system is designed and tested to achieve stability and a certain level of performance requirements in the event of different faults/failures. The final goal of a FTC system is to increase the survivability of aircraft and help the pilot to land aircraft for the safety purpose.

MPC is widely used in the industry mainly because of its facets of dealing with multiple variables and handling the constraints [52–54]. MPC was primarily applied to the relatively slow process since this technique requires considerable computational effort to generate control signals. Benefiting from the rapid development of computational power, MPC can be used for the fast sampling time system such as aircraft [4]. MPC possesses an inherent fault-tolerant facet to address faults in non-complex and systematic way. A subspace predictive control [51] is proposed for the design of a FTC system and validated based on a Boeing 747-100/200 benchmark model. This type of technique [51] is a data-driven approach, which

utilizes the updated on-line estimation to deal with faults implicitly. However, this property increases computational burden on the modeling of the predictor in addition to the cost of the on-line optimization. An efficient alternative model predictive control approach named LF-MPC is proposed and presented in this chapter used to design a FTC system. The idea behind LF-MPC based FTC is to improve the on-line fault-tolerant capability with fewer optimization parameters, which are used to model the whole control trajectory. Compared to reducing control horizon in conventional manner, LF-MPC has moderate control efforts and better stability performance. The advantages of the LF-MPC for FTC lie in preserving the architecture of MPC in addressing faults, reducing the computational cost without decreasing the control window. The contributions of this chapter are 1) demonstrating the effectiveness of a LF-MPC based FTC strategy, 2) designing a FTC landing system of aircraft using the LF-MPC, 4) improving the on-line fault-tolerant capability with LF-MPC technique, 4) formulating the fault problem in the framework of LF-MPC.

The objective of the FTC in this design is to stabilize a faulty aircraft and perform safe landing of aircraft in the event of a major actuator fault/failure. The scenarios considered in the validation process are inner elevators stuck at different landing phases, which have major impacts on the stability of the longitudinal channel of aircraft. It is reasonable to assume that the aircraft can land safely in the longitudinal channel with assistance of banking turn maneuver, if the designed FTC system can stabilize aircraft and keep some performance of trajectory tracking ability. The rest of this chapter is organized as follows. Section 6.2 illustrates the FTC design process. Section 6.3 presents the simulation results based on the inner elevators stuck scenarios in level flight, descending, and climbing phases. At last, section 6.4 summarizes this chapter.

6.2 Fault-Tolerant Control Design

This section introduces the design process of a fault-tolerant controller for the longitudinal of aircraft. The FTC design objectives are listed as follows: 1) to provide an automatic pitch stabilization for the aircraft in landing mode; 2) to achieve automatic trajectory tracking for landing; 3) to fulfill automatic speed following task; 4) to preserve the task 1) , 2) , and 3) and achieve safe landing in the presence of elevator stuck faults.

Due to the complexity of the control configuration of a Boeing 747-100/200, it is a challenging task to manage the redundancy configuration for FTC application. In [87], 4 elevators

are controlled individually to compensate the trimmable horizontal stabilizer fault. The trim condition is based on

$$\begin{cases} \dot{x}_t = Ax_t + Bu_t \\ y_t = Cx_t + v_t, \end{cases} \tag{6.1}$$

The longitudinal state vector here is $[q\ V_{TAS}\ \alpha\ \theta\ h_e]$, and the control input is $[\delta_{e_{1-4}}\ \delta_{ih}]$. The 4 elevators are treated as 1 segment. The stabilizer is as the redundancy of the 4 elevators. This configuration utilizes the horizontal stabilizer as the redundancy of elevators, while the 4 elevators are not configured as redundancy for each other. Authors in [86] choses 5 states $[q\ V_{TAS}\ \alpha\ \theta\ h_e]$ and two control inputs $[\delta_e\ \delta_{Tn}]$. The stabilizer is not selected as a control redundancy. The elevator faults are compensated by effectively manipulating the thrust. Such a combination control prevents exploiting the existing freedom of using healthy surfaces which can compensate the performance degradation induced by faulty control surfaces. Authors in [88] argues the configuration of 5 states $[q\ V_{TAS}\ \alpha\ \theta\ h_e]$, but $[\delta_{e_{1-4}}\ \delta_{ih}\ \delta_{EPR_{1-4}}]$. The 4 elevators are still be controlled in a combined manner. Authors in [16] utilizes the 4 elevators as 1 segment, 1 horizontal stabilizer, and 4 individual engines $\delta_{long} = [\delta_e\ \delta_s\ e_{1long}\ e_{2long}\ e_{3long}\ e_{4long}]$. The longitudinal states are $[q\ V_{TAS}\ \alpha\ \theta\ h_e\ x_e]$. For the controller design, the state for the longitudinal channel is chosen as $q,\ V_{TAS},\ \alpha,\ and\ \theta$. To utilize the controls effectively, distinguished from the aforementioned control configurations, the controls configuration are 4 elevators ($\delta_{eir}\ \delta_{eil}\ \delta_{eor}\ \delta_{eol}$), 1 horizontal stabilizer δ_{ih}, and 4 thrust $\delta_{TN1}\ \delta_{TN2}\ \delta_{TN3}\ \delta_{TN4}$. Particularly, δ_{eir} and δ_{eil} are grouped as one segment, δ_{eor} and δ_{eol} are combined as one segment, δ_{ih} is controlled independently, and δ_{TN1-4} are controlled as one segment. Based on the design objective and the control configuration analysis in the literature, the longitudinal model for the design of a fault-tolerant controller is presented as:

$$\begin{cases} \dot{x}_{long} = Ax_{long} + Bu_{long} \\ y_{long} = Cx_{long}, \end{cases} \tag{6.2}$$

where $A \in \mathbb{R}^{4\times4}$ and $B \in \mathbb{R}^{4\times4}$, $x_{long} = [q\ V_{TAS}\ \alpha\ \theta]^T$, and $u_{long} = [\delta_{ei}\ \delta_{eo}\ \delta_{ih}\ \delta_{TN_{1-4}}]$. $[\gamma\ V_{TAS}]$ are two parameters to be tracked. Since $\gamma = \theta - \alpha$, therefore, C is defined as:

$$C = \begin{bmatrix} 0 & 1 & 0 & 0 \\ 0 & 0 & -1 & 1 \end{bmatrix}. \tag{6.3}$$

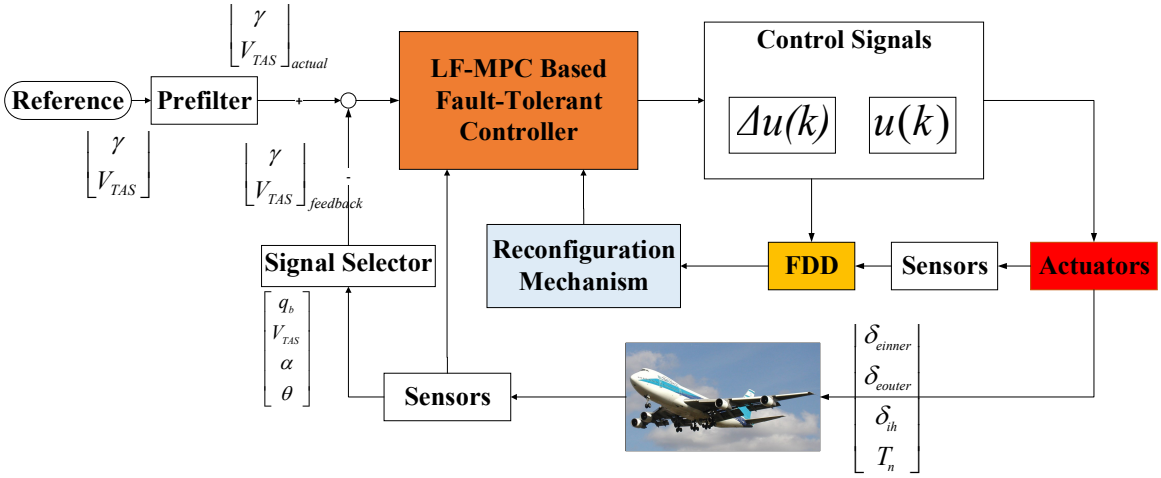

Figure 6.1: Fault-tolerant control scheme using MPC

6.2.1 Fault-Tolerant Control Design Based on MPC

The proposed FTC scheme is presented in Fig. 6.1 with MPC as reconfigurable controller. The reference signals are flight path angle γ and true airspeed V_{TAS}. It is not necessary to apply FDD to track references in a fault-free case. However, for the control reconfiguration purpose, a fault-tolerant controller demands both the measurements of aircraft and fault information available from FDD. The measurements are $[q,\ V_{TAS},\ \alpha,\ \theta]$ and fault information refers to the new limitations of faulty actuators. The discrete model used for the FTC design purpose is obtained from Eq. (6.2):

$$\begin{cases} x_{k+1} = A_d x_k + B_d u_k \\ y_k = C_d x_k, \end{cases} \tag{6.4}$$

where $x_k \in \mathbb{R}^n$ is the discrete state of the system, $u_k \in \mathbb{R}^l$ is the control input, and $y_k \in \mathbb{R}^m$ is the output to be tracked. Taking a difference operation on both sides of Eq. (6.4), one obtains:

$$x_{k+1} - x_k = A_d(x_k - x_{k-1}) + B_d(u_k - u_{k-1}). \tag{6.5}$$

Define $\Delta x_{k+1} = x_{k+1} - x_k$, $\Delta x_k = x_k - x_{k-1}$, and $\Delta u(k) = u_k - u_{k-1}$, which are incremental variables with respect to x_d and u_d, then the state-space equation turns into:

$$\Delta x_{k+1} = A_d \Delta x_k + B_d \Delta u_k. \tag{6.6}$$

Note that the input to the space-space model is changed to Δu_k. To get the system output y_k, the augmented state is set to be $[\Delta x_k^T \ e_k^T]^T$, where $e_k = y_k - r_s$, r_s is the reference to be tracked $[V_{TAS} \ \gamma]^T$, and superscript T stands for the matrix/vector transpose. The finalized state model with input Δu_k and output y_k is formulated as:

$$\begin{cases} \begin{bmatrix} \Delta x_{k+1} \\ e_{k+1} \end{bmatrix} = \begin{bmatrix} A_d & 0 \\ C_d A_d & I \end{bmatrix} \begin{bmatrix} \Delta x_k \\ e_k \end{bmatrix} + \begin{bmatrix} B_d \\ C_d B_d \end{bmatrix} \Delta u_k \\ y_k = [0 \ I] \begin{bmatrix} \Delta x_k \\ e_k \end{bmatrix} + r_s. \end{cases} \tag{6.7}$$

Define $x(k) = [\Delta x_{k+1}^T \ e_{k+1}^T]^T$, $\Delta u(k) = \Delta u_k$, the state model in Eq. (6.7) is rewritten as:

$$\begin{cases} x(k+1) = Ax(k) + B\Delta u(k) \\ y(k) = Cx(k) + r_s, \end{cases} \tag{6.8}$$

where

$$A = \begin{bmatrix} A_d & 0 \\ C_d A_d & I \end{bmatrix}, B = \begin{bmatrix} B_d \\ C_d B_d \end{bmatrix}, C = \begin{bmatrix} 0 & I \end{bmatrix}. \tag{6.9}$$

In the framework of discrete LQR with new model as shown in Eq. (6.8), the cost function to be optimized is formulated as:

$$J_0(x(k), \Delta u(.), k) = \sum_{i=0}^{\infty} x(k+i|k)^T Q x(k+i|k) + \Delta u(k+i|k)^T R \Delta u(k+i|k). \tag{6.10}$$

The control trajectory is obtained by optimizing Eq. (6.10) subjected to the constraints of system dynamics as shown in Eq. (6.8). The solution of this discrete-time regulator problem is determined as $\Delta u(k) = -Kx(k)$, where $K = (R + B^T P B)^{-1} B^T P A$, and P is obtained through the algebraic Riccati equation (ARE):

$$A^T (P - PB(R + B^T P B)^{-1} B^T P) A + Q - P = 0. \tag{6.11}$$

Discrete LQR has a fixed control gain, even if it is obtained with robustness design, which still limits the capability of fault tolerance since the control effort can only be tuned off-line by choosing the weighting matrices Q and R to adapt the physical limitations in nominal case. This problem is well solved in the framework of MPC via composing the physical limitations as constraints and solving the on-line optimization problem. MPC can be used to design a

fault-tolerant controller based on the properties of reformulating constraints, updating the inertial model, and redefining the cost function. Instead of two separate horizons, the cost function of MPC is formulated in a uniform horizon for prediction and control as follows:

$$J(x(k), \Delta u(.), k) = \sum_{i=1}^{N_p} x(k+i|k)^T Q x(k+i|k) + \sum_{j=0}^{N_p-1} \Delta u(k+j|k)^T R \Delta u(k+j|k), \quad (6.12)$$

where N_p stands for the prediction horizon and the control horizon. When $N_p \to \infty$, Eq. (6.12) approximates Eq. (6.10).

Considering the relationship between discrete LQR and MPC with respect to the cost function and an optimization process, the preliminary parameters of MPC in this chapter is tuned based on discrete LQR technique.

Based on the state-space model shown by Eq. (6.8), the state vector is presented with respect to the current state and the incremental control trajectory in the control horizon.

$$\begin{cases} x(k+1|k) = Ax(k) + B\Delta u(k) \\ x(k+2|k) = Ax(k+1|k) + B\Delta u(k+1|k) \\ \qquad\qquad = A^2 x(k) + AB\Delta u(k) + B\Delta u(k+1|k) \\ \qquad\qquad \vdots \\ x(k+N_p|k) = A^{N_p} x(k) + A^{N_p-1} B\Delta u(k) \\ \qquad\qquad + A^{N_p-2} B\Delta u(k+1|k) + \cdots \\ \qquad\qquad + B\Delta u(k+N_p-1|k) \end{cases} \quad (6.13)$$

The differences in the prediction horizon between the references and the system outputs in the prediction horizon are obtained from:

$$E = Fx(k) + \Phi \Delta U, \quad (6.14)$$

where

$$E = [e(k)^T \; e(k+1)^T \; \cdots e(k+N_p)^T]^T, \quad (6.15)$$

$$F = \begin{bmatrix} CA \\ CA^2 \\ CA^3 \\ \vdots \\ CA^{N_p} \end{bmatrix}, \tag{6.16}$$

$$\Phi = \begin{bmatrix} CB & 0 & 0 & \cdots & 0 \\ CAB & CB & 0 & \cdots & 0 \\ CA^2B & CAB & CB & \cdots & 0 \\ \vdots & \vdots & \vdots & \vdots & \vdots \\ CA^{N_p-1}B & CA^{N_p-2}B & CA^{N_p-3}B & \cdots & CB \end{bmatrix}. \tag{6.17}$$

The cost function for the trajectory tracking is

$$\begin{aligned} J(x(k), \Delta u(.), k) &= E^T Q E + \Delta U^T R \Delta U \\ &= \sum_{i=1}^{N_p} (r_s(k+i) - y(k+i|k))^T Q_i (r_s(k+i) - y(k+i|k)) \\ &+ \sum_{j=0}^{N_p-1} (\Delta u(k+j|k)^T R_j \Delta u(k+j|k)), \end{aligned} \tag{6.18}$$

where $r_s(k+i)$ is the reference at time instant i of the prediction horizon. Q and R are the block diagonal matrix with $Q_i (i \in [1, N_p])$ and $R_j (j \in [0, N_p - 1])$ block, respectively. $Q_i \in \mathbb{R}^{m \times m}$ is semidefinite diagonal matrix and $R_j \in \mathbb{R}^{l \times l}$ is a definite diagonal matrix to balance the state and the input in the cost function. Recall the nominal control, the cost function is formulated in the form in Eq. (6.12). First considering the fault-free scenario, the control problem can be addressed in the LQ framework and the control efforts are obtained by solving Eq. (6.12) with dynamics constraints in Eq. (6.8):

$$\Delta U = (\Phi^T \Phi + \bar{R})^{-1} \Phi^T E. \tag{6.19}$$

The receding horizon control strategy is applied, thereby the real incremental control effort can be obtained:

$$\Delta u(k) = [I \ 0 \ \cdots \ 0][\Phi^T \Phi + R]^{-1} \Phi^T E. \tag{6.20}$$

To simplify the cost function by dropping the constant values, the optimization problem in Eq. (6.18) can be further simplified as:

$$J_u(x(k), u(.), k) = \Delta U^T E_J \Delta U + \Delta U^T F_J, \tag{6.21}$$

where $E_J = \frac{1}{2}(\Phi^T \Phi + \bar{R})$ and $F_J = -\Phi^T E$.

Since faults can be treated as new constraints for the post-fault system, the faulty actuators can be formulated as constraints of the system presented as:

$$M\Delta U \leq N, \tag{6.22}$$

where M and N are parameters to constrain the incremental control efforts. To solve the optimization problem with actuator constraints as shown in Eq. (6.21) under constraints in Eq. (6.22), Lagrangian multiplier is applied. Therefore, the new optimization cost function becomes:

$$J(x(k), u(.), k) = \frac{1}{2}\Delta U^T E_J \Delta U + \Delta U^T F_J + \lambda^T (M\Delta U - N). \tag{6.23}$$

Note that only $M\Delta U = N$, which means aircraft is in post-fault condition, the cost function can be formulated with constraints in Eq. (6.23). The control efforts are obtained as:

$$\begin{aligned} \Delta U =& - E_J^{-1} F_J - E_J^{-1} M^T \lambda \\ =& (\Phi^T \Phi + \bar{R})^{-1} \Phi^T E - E_J^{-1} M^T \lambda. \end{aligned} \tag{6.24}$$

Compared to Eq. (6.19), the post-fault control effort denoted by Eq. (6.24) comprises the nominal and the correction terms:

$$U_{postfault} = U_{nominal} + U_{correction}, \tag{6.25}$$

where $U_{nominal} = (\Phi^T \Phi + \bar{R})^{-1} \Phi^T E$ is the control without active constraints and $U_{correction} = E_J^{-1} M^T \lambda$ is the control under active constraints.

6.2.2 Fault-Tolerant Control Using LF-MPC

Based on the basic fault-tolerant facet of MPC illustrated in the previous section, this section introduces a new approach for FTC in the framework MPC. This effort aims to improve the on-line fault-tolerant capability by decreasing the computational burden with

reduced optimization parameters. To this end, the trajectory modeling method is adopted, which is used to model the control trajectory with a few parameters. The technique used in the trajectory modeling is based on a series of Laguerre functions [53].

The advantages of LF-MPC based FTC strategy are summarized as follows: 1) improving computational efficient by reducing the number of optimized parameters, which is critical for the on-line fault-tolerant capability; 2) without sacrificing the stability of MPC in the finite control horizon compared to purely by shortening the control horizon; 3) formalizing the turning process without tunning control N_c.

The following focuses on the modeling of the optimized control trajectory using Laguerre functions. The control vector that is optimized in the design of a predictive controller is as follows:

$$\Delta U = [\Delta u(k)^T, \Delta u(k+1)^T, \cdots, \Delta u(k+N_p-1)^T]^T, \tag{6.26}$$

where $\Delta U \in \mathbb{R}^{lN_p \times 1}$. At the time instant k, any element within the control trajectory ΔU can be represented using the discrete δ-function in conjunction with ΔU:

$$\Delta u(k+i) = [\delta(i), \delta(i-1), \cdots, \delta u(i-N_p+1)]\Delta U, \tag{6.27}$$

where

$$\begin{cases} \delta(i) = diag([\delta_1(i)\ \delta_2(i)\ \cdots \delta_l(i)]) = diag(\underbrace{[1\ 1\ \cdots\ 1]}_{l}) & i = 0 \\ \delta(i) = diag(\underbrace{[0\ 0\ \cdots\ 0]}_{l}) & i \neq 0. \end{cases} \tag{6.28}$$

The δ is used to capture the control trajectory. The idea proposed in [53] is to use a discrete polynomial function (a set of Laguerre functions) to approximate the sequence $[\Delta u(k+i), \Delta u(k+i-1), \cdots, \Delta u(k+i-N_p+1)]$ to reduce the optimization parameters, which is the key for the on-line fault accommodation.

The basic design framework is to replace $\Delta u(k+i)$ by $L(i)^T\eta$ shown as:

$$\Delta u(k+i) = L(i)^T\eta, \tag{6.29}$$

with $L^T(i) = diag([L_1(i)^T, L_2(i)^T, \cdots, L_l(i)^T])$ $(i \in [1, N_p])$, $\eta = [\eta_1^T\ \eta_2^T\ \cdots\ \eta_l^T]^T$.

More particularly, the $L_q(i) = [l_{1_q}(i)\ l_{2_q}(i)\ \cdots\ l_{N_q}(i)]^T$ $(q \in [1,\ l])$ can be calculated iteratively by:

$$L_q(i+1) = A_{ql}L_q(i), \tag{6.30}$$

with $L_q(0)=\sqrt{\beta_q}[1\ -\alpha_q\ \alpha_q^2\ -\alpha_q^3\ \cdots\ (-1)^{N_q-1}\alpha_q^{N_q-1}]$, $\beta_q = 1-\alpha_q^2$ ($\alpha_q \in [0,1)$). N_q is the number of approximation factors of the qth actuator. A_{ql} can be calculated off-line with the parameters α_q, N_q, N_p:

$$A_{ql} = \begin{bmatrix} \alpha_q & 0 & \cdots & 0 \\ \beta_q & \alpha_q & \cdots & 0 \\ -\alpha_q\beta_q & \beta_q & \cdots & 0 \\ \vdots & \vdots & \vdots & \vdots \\ (-\alpha_q)^{N_q-2}\beta_q & (-\alpha_q)^{N_q-3}\beta_q & \cdots & \alpha_q \end{bmatrix}. \tag{6.31}$$

The orthogonal property exists between elements in $L_q(i)$:

$$\begin{cases} \sum_{i=0}^{\infty} l_a(i)l_b(i) = 0, a \neq b \\ \sum_{i=0}^{\infty} l_a(i)l_b(i) = 0, a = b \end{cases}. \tag{6.32}$$

The predictive model in Eq. (6.13) is formulated as Eq. (6.33) with substitution Eq. (6.29):

$$\begin{cases} x(k+j|k) = A^j x(k) + \sum_{p=0}^{j-1} A^{j-p-1}BL(p)^T\eta = A^j x(k) + \phi(j)^T\eta \\ y(k+j|k) = Cx(k) = CA^j x(k) + C\phi(j)^T\eta, \end{cases} \tag{6.33}$$

where

$$\phi(j)^T = \sum_{p=0}^{j-1} A^{j-p-1}BL(j)^T, \quad j \in [1, N_p]. \tag{6.34}$$

The incremental control $\Delta u(k+i)$ is replaced by the $L(i)^T\eta$, thus the parameter $\eta \in \mathbb{R}^{l\times N_q}$ is the only optimized parameter vector instead of the whole control trajectory $\Delta U \in \mathbb{R}^{l\times N_p}$. Note that the dimension of η is much smaller than that of ΔU as N_q is far less greater than N_p. $L(i)$ is determined by Eq. (6.30). Replacing ΔU with the approximation trajectory, the formulation of cost function is represented as follows:

$$J_{0\eta}(x(k), u(.), k) = \sum_{j=1}^{N_p} (r(k+j|k) - y(k+j|k))^T Q_j (r(k+j|k) - y(k+j|k)) + \eta^T R\eta. \tag{6.35}$$

Substituting Eq. (6.33) into the cost function Eq. (6.35), it is obtained that

$$J_{1\eta}(x(k),u(.),k) = \eta^T(\sum_{j=1}^{N_p}\phi(j)Q\phi(j)+R_L)\eta+2\eta^T(\sum_{j=1}^{N_p}\phi(j)QA^j)x(k)+\sum_{j=1}^{N_p}x^T(k)(A^T)^jQA^jx(k). \tag{6.36}$$

The cost function to be optimized can be further simplified by dropping the constant:

$$J_{\eta}(x(k),u(.),k) = \eta^T(\sum_{j=1}^{N_p}\phi(j)Q\phi(j)+R_L)\eta+2\eta^T(\sum_{j=1}^{N_p}\phi(j)QA^j)x(k). \tag{6.37}$$

Constraints Statement in the Framework of LF-MPC

Table 6.1 presents the control surface operating limits, which are used for the fault-tolerant controller design.

1. Constraints on the slew rates

Due to the physical constraints of actuators, the slew rates should not exceed the actuators' limitations as shown in Table 6.1. In particular, the incremental limitations are listed in the last two columns of Table 6.1 with fully and half boost, respectively. The lower and upper

Table 6.1: Boeing 747-100/200 flight control surface operating limits (positive sign: surface deflection down/spoiler panel up) [1]

Control surface	Symbol	Mechanical limit (deg)	Two hydraulic system rate (Full boost, deg/sec)	One hydraulic system rate (Half boost, deg/sec)
Inboard elevator	δ_{ei}	+17/-23	+37/-37	+30/-26
Outboard elevator	δ_{eo}	+17/-23	+37/-37	+30/-26
Inboard aileron	δ_{ai}	+20/-20	+40/-45	+27/-35
Outboard aileron	δ_{ao}	+15/-25	+45/-55	+22/-45
Stabilizer	ih	+3/-12	+/-0.2 to +/-0.5	+/-0.1 to +/-0.25
Upper rudder	δ_{ru}	+45	+75	0
Lower rudder	δ_{rl}	+45	+75	0
Spoiler #1-#4	δ_{sp1-4}	+20	+75	0
Spoiler #9-#12	δ_{sp9-12}	+20	+75	0
Spoiler #5,#8	$\delta_{sp5}, \delta_{sp8}$	+25/-25	+50/-50	+40/-40
Spoiler #6,#7	$\delta_{sp6}, \delta_{sp7}$	+25/-25	+50/-50	+40/-40

limits on $\Delta u(k)$ are Δu_{min} and Δu_{max}, as shown in inequality (6.38):

$$\Delta u_{min} \leq \Delta u(k+i) \leq \Delta u_{max}. \tag{6.38}$$

Inequality (6.38) can be rewritten with η based on Eq. (6.29):

$$\Delta u_{min} \leq L^T(i)\eta \leq \Delta u_{max}. \tag{6.39}$$

2. Constraints on the amplitudes

The actuator magnitude limitations are presented in the mechanical limit column of Table 6.1. All the actuators should respect the limitations when performing the control task. It can be denoted with the incremental controls by $u(i) = \sum_{p=0}^{i-1} \Delta u(p)$, then the inequality constraints for the future time i ($i = 1, 2, \cdots, N_p$) are expressed as:

$$u_{min} \leq S_L(i)\eta + u(i-1) \leq u_{max}, \tag{6.40}$$

where $S_L(i) = diag([\sum_{j=0}^{i-1} L_1(j)^T,\ \sum_{j=0}^{i-1} L_2(j)^T,\ \cdots\ , \sum_{j=0}^{i-1} L_l(j)^T])$ and $u(k-1)$ is the previous control signal vector. With the following definitions:

$$\begin{aligned}
&S_L = [S_L(0)^T\ S_L(1)^T \cdots S_L(N_p-1)^T]^T \\
&\Delta U_{max} = [\Delta u_{max}^T\ \Delta u_{max}^T\ \cdots \Delta u_{max}^T]^T \\
&\Delta U_{min} = [\Delta u_{min}^T\ \Delta u_{min}^T\ \cdots \Delta u_{min}^T]^T \\
&L^T = [L(0)^T\ L(1)^T \cdots\ L(N_p-1)^T]^T \\
&U(k-1) = [u(k-1)^T\ u(k-1)^T \cdots\ u(k-1)^T]^T,
\end{aligned} \tag{6.41}$$

in the prediction horizon N_p, the actuator constraints with respect to η are formulated as:

$$\begin{bmatrix} M_1 \\ M_2 \end{bmatrix} \eta \leq \begin{bmatrix} N_1 \\ N_2 \end{bmatrix}, \tag{6.42}$$

where

$$\begin{aligned}
M_1 = \begin{bmatrix} L^T \\ -L^T \end{bmatrix}, N_1 = \begin{bmatrix} \Delta U_{max} \\ -\Delta U_{min} \end{bmatrix}, M_2 = \begin{bmatrix} S_L \\ -S_L \end{bmatrix}, \\
N_2 = \begin{bmatrix} U_{max} - U(k-1) \\ U_{min} + U(k-1) \end{bmatrix}.
\end{aligned} \tag{6.43}$$

Overall, the FTC strategy design using LF-MPC is to solve the cost function Eq. (6.37) with respect to the constraints in Eq. (6.42) (fault-free and post-fault scenarios). Moreover, actuator faults can be treated as constraints of the optimization problem, therefore, the fault-tolerant controller is designed to solve the constraints problem in Eq. (6.42) subjected to the system dynamics.

Remark 6.1. *From the design process elaborated above, the MPC-based FTC strategy is contributed from two control efforts: the nominal control effort and an additional correction term induced by the active constraints. The constraints are not only from the physical limitations of fault-free actuators but also obtained based on the fault information, which is available from a FDD module. LF-MPC has the same structure with conventional MPC but the control effort optimization form. Instead of optimizing the whole control horizon, LF-MPC optimizes a few coefficients which are used to model the control trajectory. Therefore, it preserves the on-line optimization property of conventional MPC and increases the on-line fault-tolerant capability by reducing the optimized parameters.*

6.3 Simulation Results

The closed-loop system should satisfy the performance criteria during all the flight duration in both fault-free and post-fault conditions. The RMSE criteria for the airspeed V_{TAS} and the flight path angle γ are used to evaluate the performance of the designed FTC system in the presence of inner elevators stuck fault as presented in Table 6.2. The safety margins of parameters are marked on the top and bottom of each figures related to the parameters, which constraints are listed in Table 6.1.

Typically, 3 main phases, including level flight, descending, and climbing, are included in the landing period of longitudinal channel. Therefore, elevator stuck scenarios are tested and evaluated based on the different flight phases when faults occur. The fault-free case is also tested for the performance comparison purpose. Case 1 shows the landing period in normal situation with the criteria mentioned above. There is no fault occurring in the flight duration. Case 2 presents inner elevators stuck at the around trim position when performing a level flight. Case 3 is the scenario when inner elevators stuck at a random non-trim position while performing descending maneuverer. Case 4 illustrates the scenario that the inner elevators of aircraft get stuck when it is in climbing phase. Overall, Case 1 is the fault-free scenario, but the rest of scenarios perform that inner elevators stuck at random

Table 6.2: Tracking performance evaluation

	Stuck Scenarios	**Max Error γ (deg)**	**Max Error V_{TAS} (m/s)**	**RMSE γ**	**RMSE V_{TAS}**
Normal	No Fault	0.76568	1.0015	0.19058	0.3998
Level Flight	Level Flight	3.9086	2.3751	0.34656	0.50077
Descending	Descending	5.3078	2.3164	0.44144	0.48727
Climbing	Climbing	4.8358	5.6811	0.41676	0.87503

positions when aircraft performs straight and level flight, descending, and climbing actions.

Table 6.2 presents 4 scenarios of performance evaluation of the fault-tolerant controller via the landing task of aircraft.

The maximum errors of γ and V_{TAS} are 0.76568 deg and 1.0015 m/s in case 1, showing the tracking performance of the designed FTC in performing the normal duty. Compared to case 1, the rest of cases have larger maximum error with respect to flight path angle γ and true velocity V_{TAS}. In the whole evaluation time horizon, RMSE of γ and V_{TAS} remain the smallest in case 1, showing that the fault has influences on the tracking performance. RMSE γ and RMSE V_{TAS} in case 2, case 3, and case 4 has no significant changes, which demonstrate that the designed controller can fulfill the FTC task of stabilizing the faulty condition aircraft with degraded performance.

The following focuses on the evaluation of the landing performance with a fault-free and 3 faulty scenarios: inner elevators stuck at a random place when performing level flight, descending, and climbing maneuvers, respectively. The FDD unit is integrated into the evaluation process in terms of $2s$ time delay.

6.3.1 Fault-Free Scenario

There are no faults occurring in the whole landing period as shown in Fig. 6.2, in which the vertical axis stands for the altitude of aircraft and the lateral axis stands for the distance from the location where the simulation starts. The safe landing of aircraft with acceptable performance illustrates the success of the designed FTC in performing the normal duty. This landing performance is further illustrated via the tracking capability in terms of flight path angle γ and true airspeed V_{TAS} shown in Fig. 6.3(a) and Fig. 6.3(b), respectively.

To illustrate the performance of the landing from control efforts point of view, the elevator deflections are presented in Fig. 6.4, where the plot with a box is the zoom in value of its respected elevator deflection. In the control process, there are no significant fluctuations in

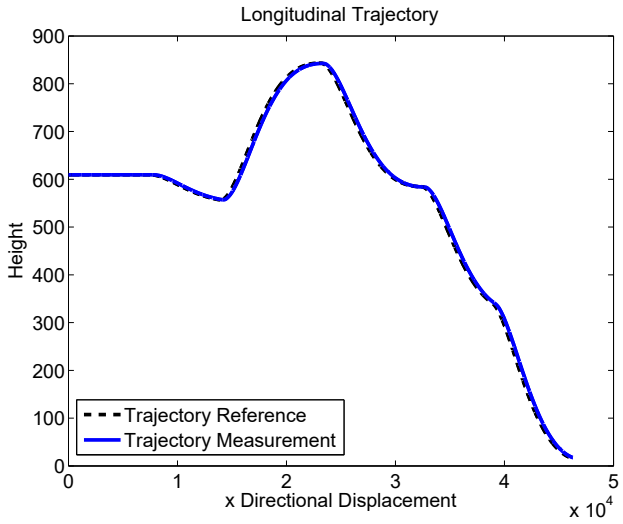

Figure 6.2: Landing trajectory tracking in fault-free scenario

the deflections of inner elevators. The control efforts performance, as shown in Fig. 6.5(b) about elevators, Fig. 6.5(c) about horizontal stabilizer, and Fig. 6.5(d) about thrusts, illustrate the smoothness of control efforts during the whole landing period, which indicate the effectiveness and acceptable performance of the designed FTC in normal flight situation. The objective of the landing in the fault-free case is achieved with the designed FTC.

6.3.2 Fault Scenarios in Landing Process

Elevator Stuck in Level Flight Phase

Fig. 6.6 shows the whole process of landing of aircraft under inner elevators stuck occurring at $30s$ indicated by the red-dashed vertical line in Fig. 6.8(a) and Fig. 6.8(b). The inner elevators stuck starts on the stage of straight flight phase of the landing period. It can be seen from Fig. 6.6 there is a sharp fluctuation at the level flight phase, at which time the stuck fault occurs. Further more, from Fig. 6.7 after the occurrence of faults, the inner elevators are lock in a fixed places of a level flight condition without performing deflections with respect to different flight situations. It indicates a constant pitch moment is placed on aircraft, a counteraction is demanded to neutralize the influence and provide the mandatory moment.

To be more specific, the tracking trajectory of the flight path angle as shown in Fig. 6.8(a) and the true velocity as shown in Fig. 6.8(b) indicate the degradation of the tracking per-

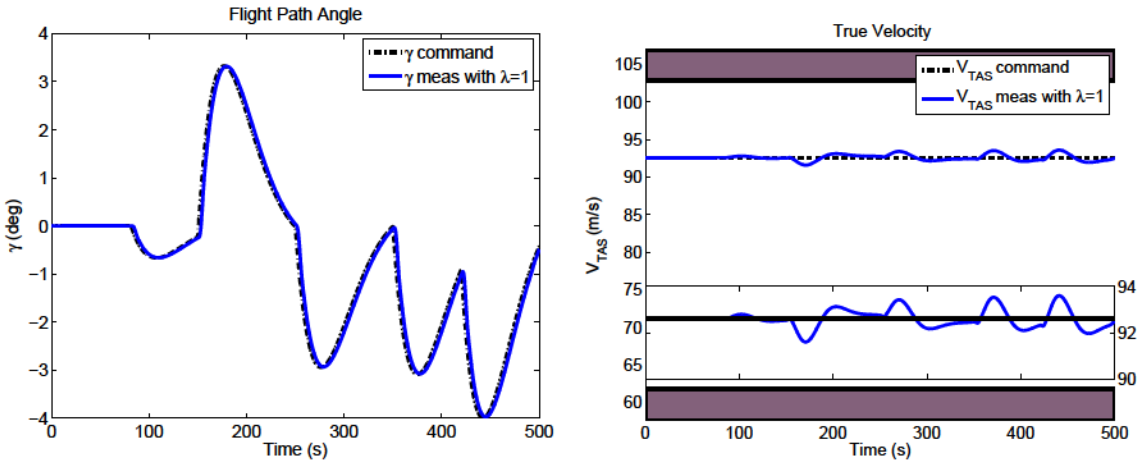

(a) Flight path angle tracking (b) True velocity tracking

Figure 6.3: Reference tracking performance in fault-free scenario

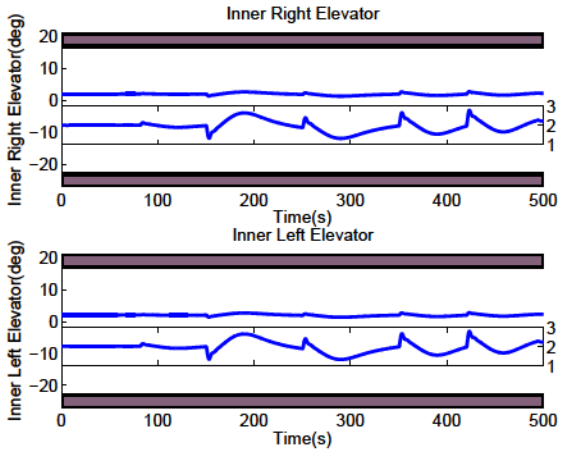

Figure 6.4: Inner elevators deflections in fault-free scenario

formance of these two parameters. However, after the transient period, the flight path angle and true velocity return to track the references again without losing performance significantly. In addition to the deflections of inner elevators stuck presented in Fig. 6.7 and the tracking performance as shown in Fig. 6.8, the control efforts of elevators, horizontal stabilizer, and thrusts are presented in Fig. 6.9 to illustrate the control process of the designed FTC system in the whole landing period. Before the time instant $30s$, the inner elevators follow the desired value to manipulate aircraft altitude and flight path angle. While at the time instant $30s$ at which the fault occurs, the elevators stop following the demanded value but are locked in a fixed place. It can be seen from Fig. 6.9(a) that after the time instant

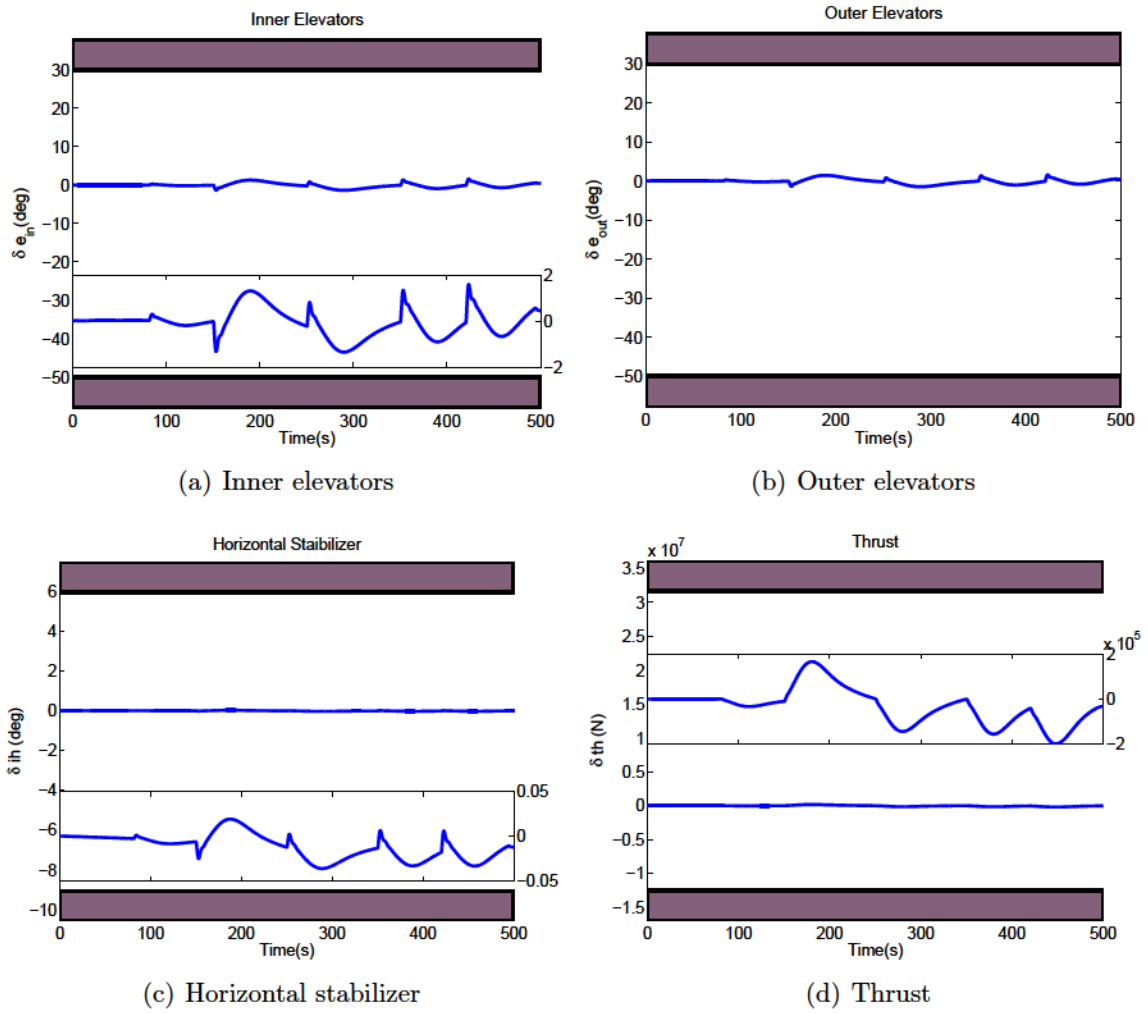

(a) Inner elevators

(b) Outer elevators

(c) Horizontal stabilizer

(d) Thrust

Figure 6.5: Controls in fault-free scenario: inner elevator, outer elevators, horizontal stabilizer, and thrust

of the fault occurs, the command for the inner elevators channel is fixed to be the same command as in the stuck position. However, the command for the outer elevators increases dramatically. This illustrates that the FTC system isolates the stuck channel and drives the rest functional elevators more aggressively to compensate the LOC induced by the stuck of inner elevators. The horizontal stabilizer drops at the transient time of fault occurrence and maintains at a stable level after the control reconfiguration. There is no significant influence on the thrust since it is mainly responsible for the true airspeed.

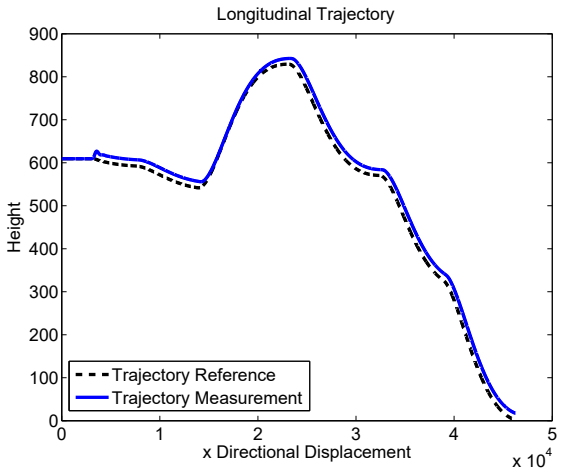

Figure 6.6: Landing trajectory tracking with faults occurring at the levelel flight phase

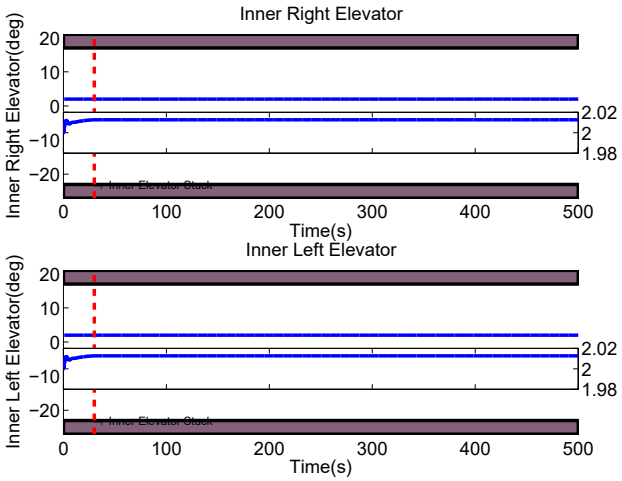

Figure 6.7: Inner elevators deflections with faults occurring at the level flight phase

Elevator Stuck in Descending Phase

Fig. 6.10 shows the whole process of landing under inner elevators stuck at $100s$ as shown in Fig. 6.12(a) and Fig. 6.12(b).

It is clear that when faults occur the flight path angle changes significantly to a maximum value of 4.8358 *deg* in Fig. 6.12(a) and the velocity drops by $5.6811m$ in Fig. 6.12(b). The reason is that when a descending maneuver is performed a slight downward elevator maneuver is required. However, the stuck elevators provide a sustainable relative upward moment inducing aircraft nose up. After the transient time, the flight path angle and true velocity are followed by the faulty aircraft again without losing performance significantly. To illustrate

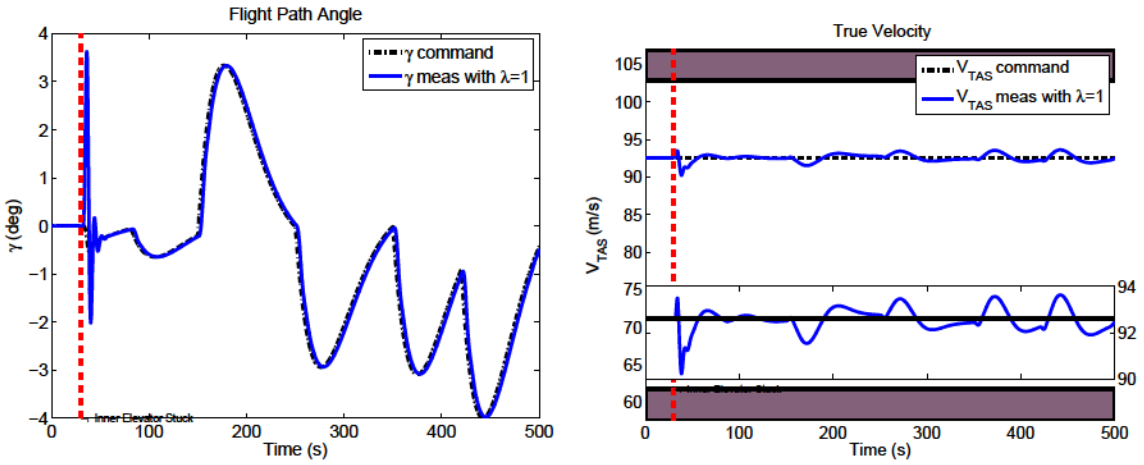

(a) Flight path angle tracking

(b) True velocity tracking

Figure 6.8: Tracking performance with fault occurring at the level flight phase

the process in more details, the fault of elevators stuck is presented in Fig. 6.11. Before the time instant $100s$, the inner elevators follow the desired commands to adjust the state of aircraft. While at the time instant $100s$, the elevators are locked in a fixed place. The tracking performances presented in Fig. 6.12(a) and Fig. 6.12(b) illustrate the validity of the designed fault-tolerant controller. It is noticed that the command for the inner elevators channel is fixed to be the same command as in the stuck position in Fig. 6.13(a). However, it is obviously that the command for the outer elevators changes dramatically due to the faults as shown in Fig. 6.13(b). Note that in the event of stuck transient, the outer elevators' command abruptly jump to the extreme value but not exceed the limitation of actuators. This illustrates that the designed FTC system counts the actuator limitations when performing the control actions. After a short transient period with the help of outer elevators as shown in Fig. 6.13(b) and horizontal stabilizer shown in Fig. 6.13(c), the control signals of outer elevators and horizontal stabilizer return to be moderate. It is clear that to bring aircraft to stable status in the stuck transient, the outer elevators and horizontal stabilizer works more aggressively than that in performing normal duty.

Elevator Stuck in Climbing Phase

For adjusting the altitude purpose during landing phases, aircraft performs climbing maneuvers in some necessary circumstances. Therefore, this kind of scenario is presented with fault occurring during the climbing maneuver in order to validate the effectiveness of the

designed FTC system.

Fig. 6.14 shows the process of the flight path tracking during the landing with faults occurring at the climbing phase. It indicates that the flight path tracking capability keeps in an acceptable manner even when faults occur at the time instant $180s$. In terms of the two tracking parameters γ and V_{TAS} shown in Fig. 6.16, significant deviations only exist at the transient period. There is no significant performance degradation after the recovery transient. The abrupt deviation of flight path angle is obtained from a constant pitch up moment due to the stuck elevators while less pitch up moment is demanded. The conflict of the demanded value and the stuck elevators deteriorates the tracking performance. The recovered tracking performances of γ in Fig. 6.16(a) and V_{TAS} in Fig. 6.16 indicate the effectiveness of the designed fault-tolerant controller. The inner elevators stuck fault is presented in Fig. 6.15 illustrating the inner elevators deflection process before and after fault occurrence.

To elaborate the control process during the evaluation, all the control efforts are presented in Fig. 6.17 in terms of elevators, horizontal stabilizer, and thrusts. Before the stuck occurs the control demand for inner elevators varies with different flight path angles, while it keeps the stuck value after the occurrence of faults, which indicates the designed FTC system calculates the control efforts based on the available control capability. This is further illustrated by Fig. 6.17(b), in which the maximum values on the remaining functional elevators are considered in the reconfiguration process. The stabilizer is reconfigured at a new trim position after the fault occurrence.

6.4 Summary

The objective of this chapter is to safely land aircraft in the event of a major actuator fault/failure. The proposed LF-MPC technique provides a systematic and efficient way to synthesize a FTC system. The saturation of actuators in both fault-free and post-fault scenarios are integrated into the FTC in a seamless way. The time delay of FDD information is also integrated into the validation process. The simulation results of the non-linear aircraft model illustrate the effectiveness and performance of the designed FTC system.

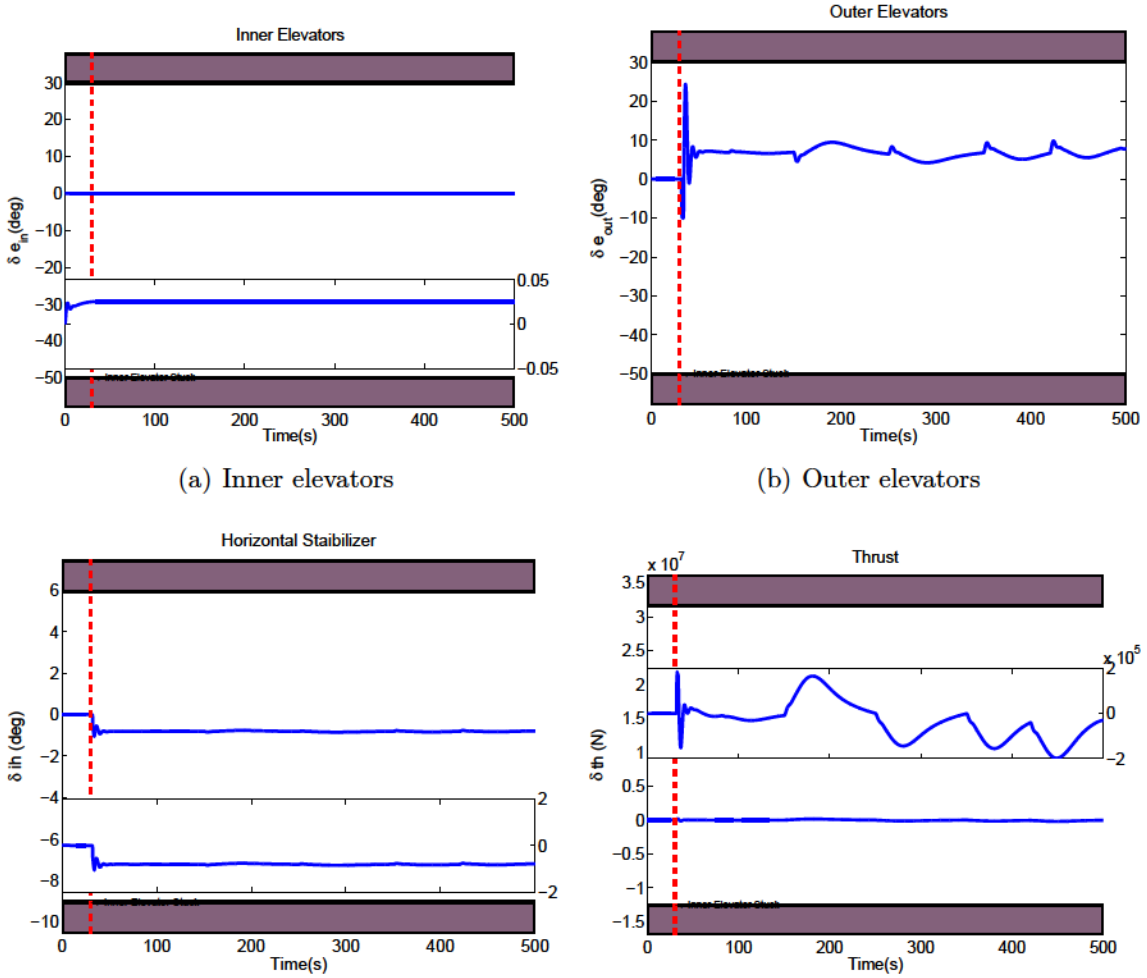

(a) Inner elevators

(b) Outer elevators

(c) Horizontal stabilizer

(d) Thrust

Figure 6.9: Controls with faults occurring at the level flight phase: inner elevators, outer elevators, horizontal stabilizer, and thrust

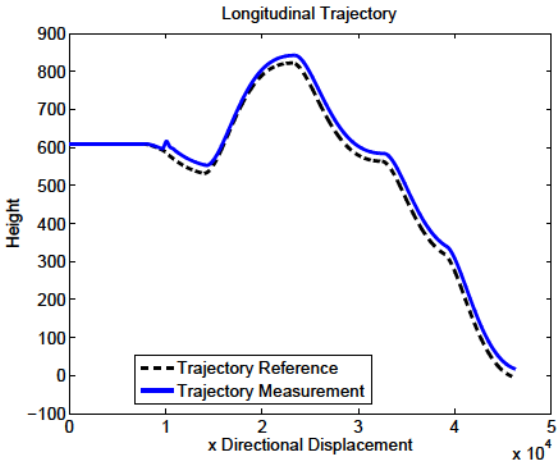

Figure 6.10: Landing trajectory tracking with faults occurring at the descending phase

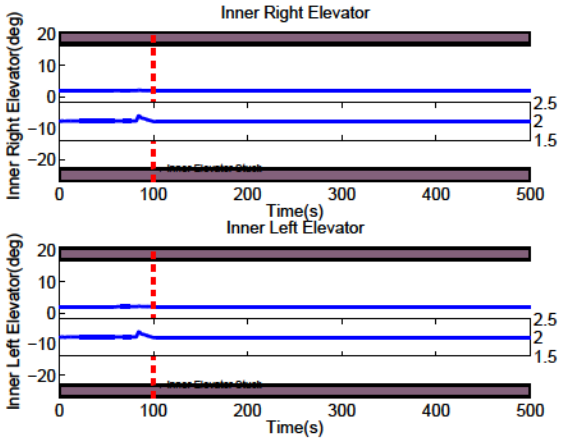

Figure 6.11: Inner elevators deflections

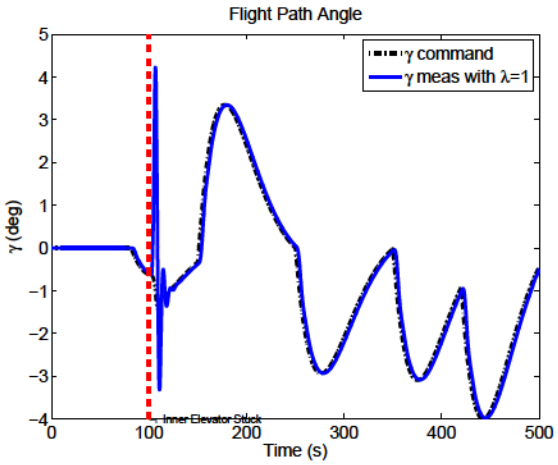

(a) Flight path angle tracking

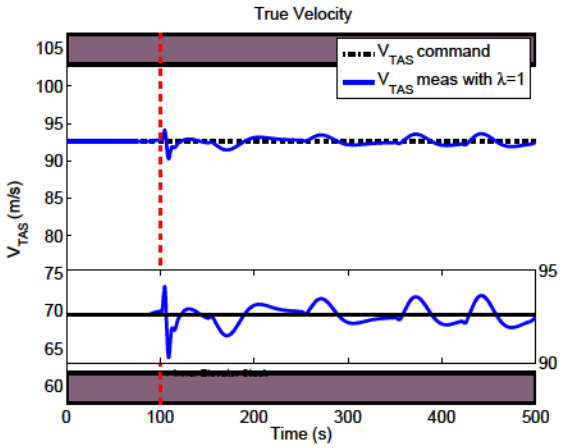

(b) True velocity tracking

Figure 6.12: Tracking performance with faults occurring at the descending flight phase

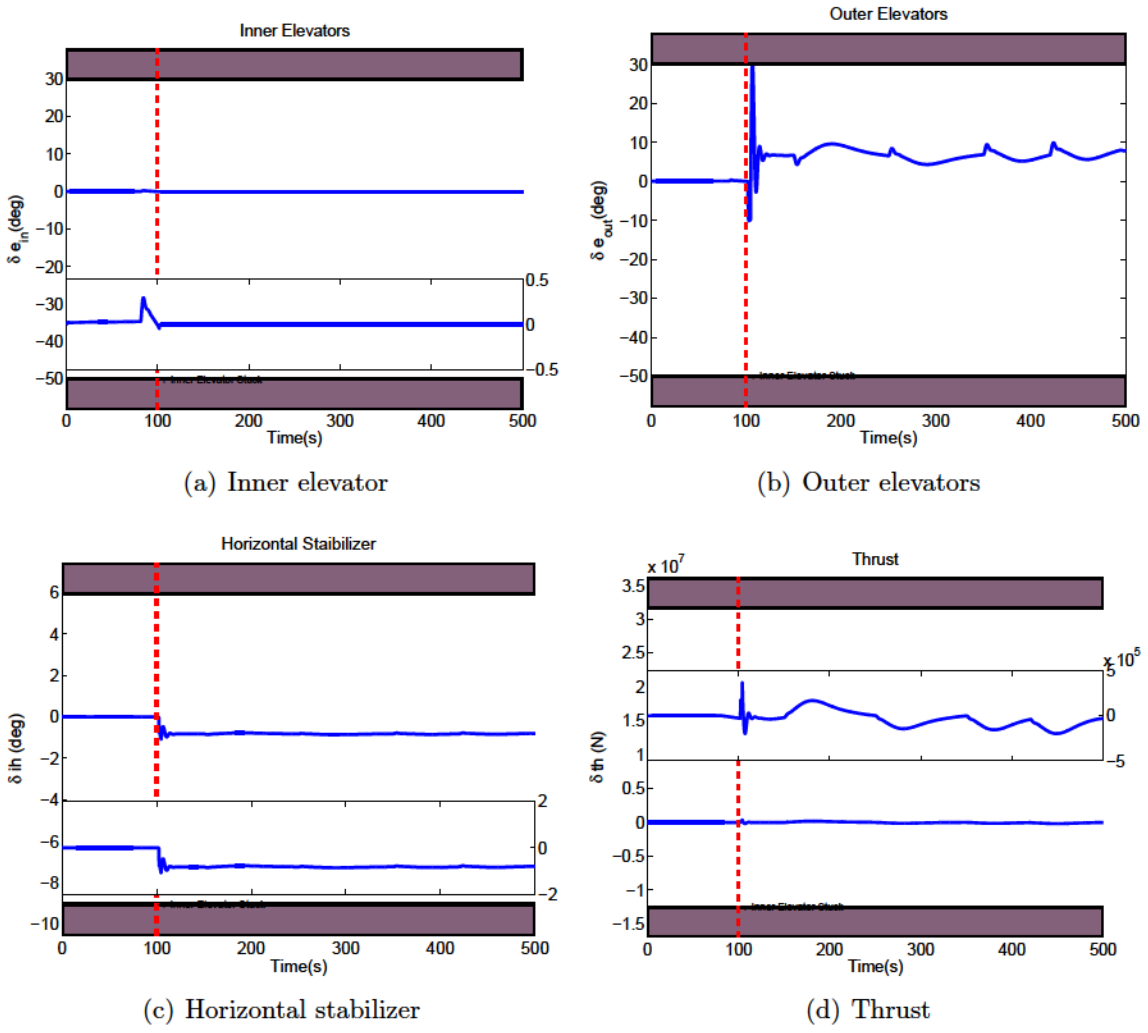

(a) Inner elevator

(b) Outer elevators

(c) Horizontal stabilizer

(d) Thrust

Figure 6.13: Controls: inner elevator, outer elevators, horizontal stabilizer, and thrust

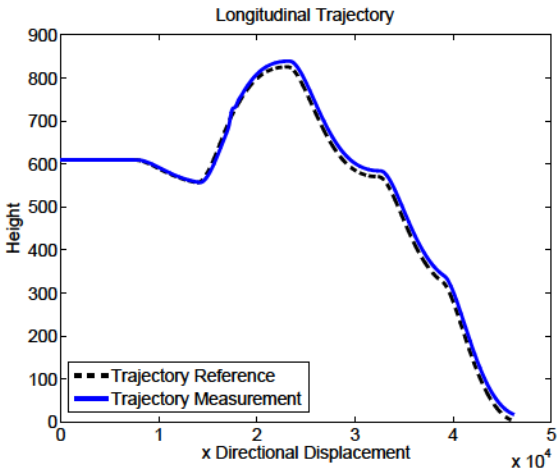

Figure 6.14: Landing trajectory tracking with faults occurring at the climbing phase

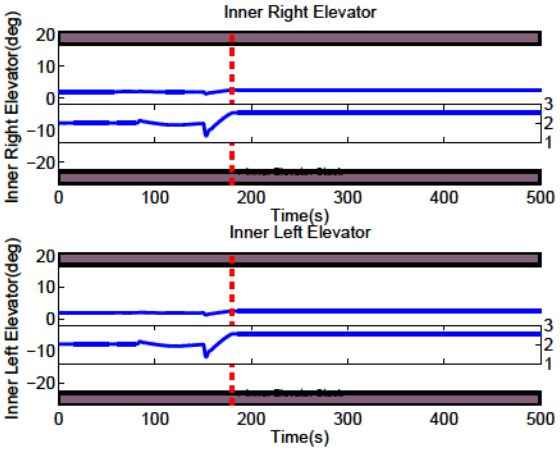

Figure 6.15: Inner elevators deflections

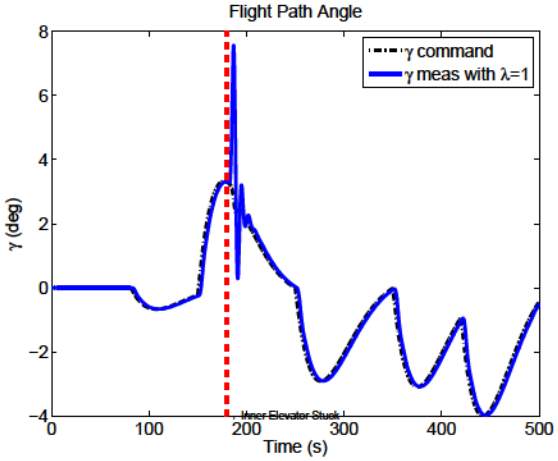

(a) Flight path angle tracking

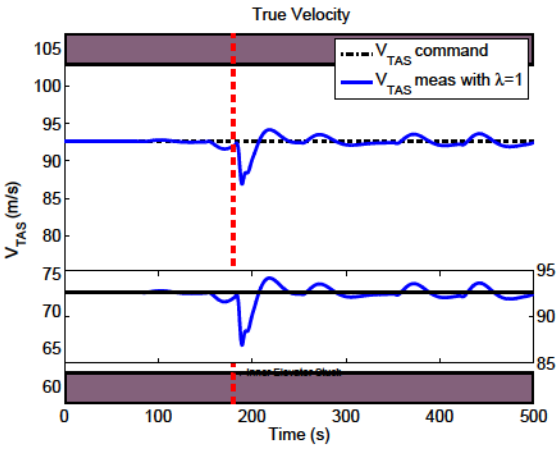

(b) True velocity tracking

Figure 6.16: Reference tracking performance with faults occurring at the climbing phase

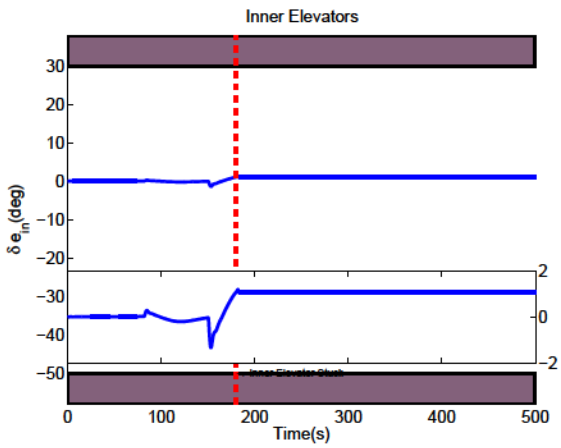

(a) Inner elevators

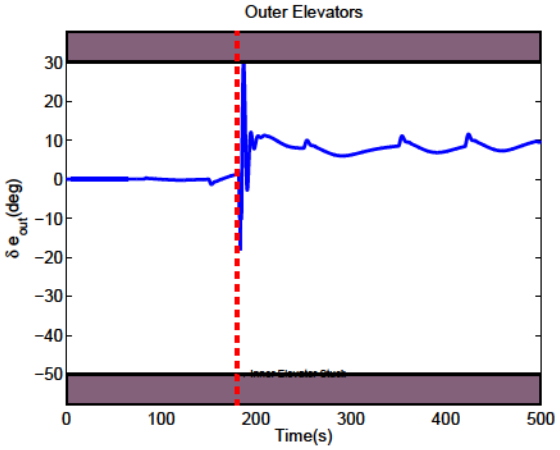

(b) Outer elevators

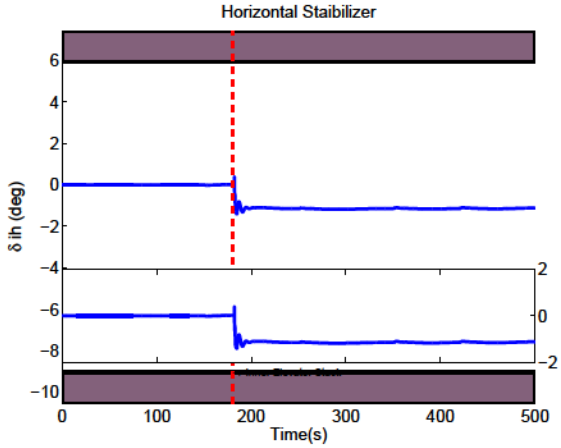

(c) Horizontal stabilizer

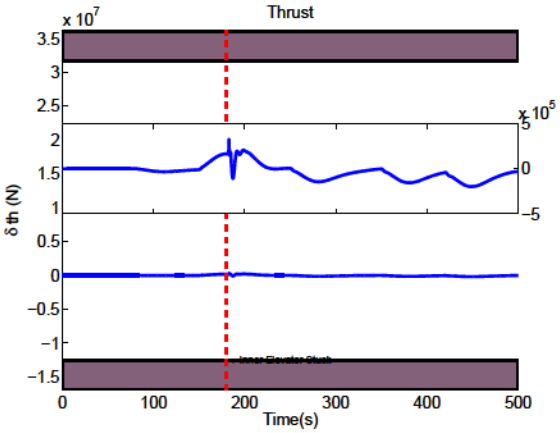

(d) Thrust

Figure 6.17: Controls with fault occurring at the climbing phase

Chapter 7

Fault-Tolerant Control of Boeing 747-100/200 Using Improved LF-MPC

7.1 Introduction

In Chapter 6, a LF-MPC based FTC system is implemented and validated on the benchmark model of a Boeing 747-100/200. As aforementioned, FTC design approaches can be categorized into two types: passive and active FTC approaches [2]. The philosophy of passive FTC is to use the robust property control system to accommodate faults, in which the controller remains the same without reconfiguration. The robustness of the passive FTC can directly be implemented in the control system without extra on-line computational burden. While active FTC adopts the strategy of redistributing control efforts in real time, in which a FDD strategy is often included in the close-loop control system to provide the fault information. Due to the updated fault information available from a FDD module and the flexibility of active FTC in controls reconfiguration, active FTC can handle more complex faults as compared to passive FTC. In consequence, a more complex design of active FTC is demanded than that of passive FTC. It is notice that no matter what control techniques are applied, the performance of the transient period between the fault occurrence and the reconfigurable control action trigged cannot be compensated. This motivates the combination of passive and active FTC strategies. This chapter focuses on improving the performance of designed LF-MPC based FTC strategies during the transient period. Without the constraints activated, the optimization process of MPC is identical to LQR when the internal model is linear. This implies that the control design of MPC can borrow ideas from the well-known

LQR technique. LQR technique is recognized as modern control technology, which presents superior facet at handling multiple input and output system with robust property, such as the control law design for Boeing 767 commercial transport and the Boeing version of Joint Strike Fighter [62, 89]. Generally, the controller performance based on LQR design is determined by the cost functions under the system dynamics constraints. The optimized control law can be tuned by the weighting matrices Q and R. Large values of Q in comparison to R reflect the designer's intent to drive the state to the origin or the tracking error to zero quickly at the expense of large control action. While large values of R compared to Q reduce the control action and decrease the stabilizing rate of the controlled system. However, there is no directly link between the weighting matrix and the control performance in the tuning process, which is also inherently a tuning challenging of MPC. To overcome the drawback, the idea of the prescribed degree of stability is proposed in [82] by adopting exponentially increasing weighting matrices in the cost function of continuous LQ problems. This idea is further developed in literature [53, 90, 91] to improve the performance of MPC. Considering the favorable properties of MPC for FTC design, the prescribed degree of stability is further developed and implemented for FTC of a Boeing 747-100/200 airplane. The contributions are 1) improving the transient performance resisting unpredicted faults with passive FTC technique; 2) improving active FTC ability with the improved decay rate of states and the updated fault information. The performance is investigated and validated throughout the task of safe landing of aircraft in the event of faults. Inner elevators stuck are studied in the evaluation with fault occurring at different landing phases: level flight, descending, and climbing phases.

The rest of this chapter is organized as follows. Section 7.2 illustrates the active FTC strategy and the process of designing active FTC with a prescribed degree of stability. Section 7.3 presents the simulation results of the designed active FTC and the performance comparison of the two control strategy with/without prescribed degree of stability, which are validated on aircraft landing process. Section 7.4 draws the conclusion of this chapter.

7.2 Fault-Tolerant Control Using Improved LF-MPC

The design objective of this chapter is to improve FTC capability for aircraft on both fault-free and post-fault scenarios. Passive FTC strategy is based on the robustness of the controller and active FTC strategy is based on reconfiguration of controls. Therefore, to

improve the FTC performance, there are two approaches accordingly. The proposed LF-MPC based approach focuses on improving 1) the transient performance through increasing the robustness of the fault-tolerant controller, and 2) the on-line fault-tolerant capability in the optimization process. Technically, the closed-loop performance of the predictive control system is specified by the choice of weighting matrix Q and R matrices with specified cost function when the constraints are not activated. Q and R are selected to tune the close-loop response speed. The elements in Q and R are penalties to the corresponding states. A smaller element in Q means less penalty on the corresponding state. A smaller element in R corresponds to less weight on the corresponding controls, hence permitting a larger change in the control increment, and resulting in a faster closed-loop response. With a proper chosen Q and R, the performance of the predictive control system can be adjusted. This is done by changing the eigenvalues in the unit circle. Therefore, the LF-MPC based FTC capability can be improved by changing the eigenvalues of the closed-loop system and solving constraints of the post-fault aircraft when it is activated. Particularly, the parameters to be tracked on the landing process in this design are true airspeed V_{TAS} and flight path angle γ. By formating the eigenvalue of the incremental value of V_{TAS} and γ, the stability degree of V_{TAS} and γ will be improved. With the consideration of the aforementioned time window $[0,\ t_F]$, $[t_F,\ F_{FT}]$, and $[t_{FT}, \infty]$ during the fault-tolerant process, the passive FTC capability is mainly functional in the time interval of $[0,\ t_F]$ and $[t_F,\ F_{FT}]$ before the control reconfiguration. After the transient interval $[t_F,\ F_{FT}]$, the FDD information is available and control reconfiguration is performed with the LF-MPC based active FTC strategy by solving new constraints on-line. The following focuses on the derivation process for improving the transient performance in accommodating faults.

7.2.1 Internal Model

The state space system in the prediction process as shown in Eq. (6.13) is presented in a iterative form as:

$$x(k+j+1|k) = Ax(k+j|k) + B\Delta u(k+j|k), \tag{7.1}$$

where k is the current time instant , j is the time instant in the prediction horizon starting at k, $x(k+j|k)$ is the state at the time instant j of the current prediction horizon, $\Delta u(k+j|k)$ is the incremental control in the prediction horizon j, and A and B are systematic and control matrices, respectively.

7.2.2 Fault-Tolerant Control Design with a Prescribed Degree of Stability

The stability of aircraft in longitudinal channel is guaranteed in the presence of the accuracy of the model since the poles of the closed-loop system is in the unit circle by solving ARE. However, to improve the performance and robustness of the control system for fault-tolerant purpose, it is extremely hard to get the goals by just tuning Q and R matrices. Therefore, the cost function with exponential data weighting matrix [53] is introduced to solve the tuning problem in performance improvement and defined as follows:

$$J_0(x(k), \Delta u(.), k) = \sum_{j=1}^{N_p} \lambda^{-2j} x(k+j|k)^T Q x(k+j|k) + \sum_{j=0}^{N_p-1} \lambda^{-2j} \Delta u(k+j|k)^T R \Delta u(k+j|k), \tag{7.2}$$

$$M\Delta U \leq N, \tag{7.3}$$

subject to the state space equation, where M and N are parameters related to the constraints of the controls ΔU ($\Delta U = [\Delta u(k)\ \Delta u(k+1) \cdots \Delta u(k+N_p-1)]$), and $\lambda \in (0, 1]$.

Theorem 7.1. *1) The minimum solution of the cost function $J_0(x(k), \Delta u(.), k)$ shown by Eq. (7.2) subject to the inequality constraints shown by Eq. (7.3) and dynamics constraints shown by Eq. (7.1)can be found by minimizing:*

$$\hat{J}(\hat{x}(k), \Delta\hat{u}(.), k) = \sum_{j=1}^{N_p} \hat{x}(k+j|k)^T Q \hat{x}(k+j|k) + \sum_{j=0}^{N_p-1} \Delta\hat{u}(k+j) R \Delta\hat{u}(k+j) \tag{7.4}$$

subject to

$$M_\lambda \Delta\hat{U} \leq N, \tag{7.5}$$

where $\hat{x}(k+j|k)$ and $\hat{u}(k+j)$ satisfy the following difference equation:

$$\hat{x}(k+j+1|k) = \frac{A}{\lambda}\hat{x}(k+j|k) + \frac{B}{\lambda}\hat{u}(k+j|k), \tag{7.6}$$

where M_λ and $\Delta\hat{U}$ are defined by:

$$M_\lambda = M \begin{bmatrix} I & 0 & \cdots & 0 & 0 \\ 0 & \lambda I & \cdots & 0 & 0 \\ 0 & 0 & \cdots & \lambda^{N_p-1} I & 0 \\ 0 & 0 & \cdots & 0 & \lambda^{N_p} I \end{bmatrix}, \tag{7.7}$$

$$\Delta\hat{U}^T = [\lambda^{-0}\Delta u(k)^T \ \lambda^{-1}\Delta u(k+1)^T \ \cdots \lambda^{-N_p+1}\Delta u(k+N_p-1)^T]. \tag{7.8}$$

2) With the proper choosing of $\lambda < 1$, the designed FTC system has the ability with guaranteed stability.

Proof. 1) Defining $\hat{x}(k+j|k) = \lambda^{-j}x(k+j|k)$ and $\Delta\hat{u}(k+j|k) = \lambda^{-j}\Delta u(k+j|k)$, the cost function Eq. (7.2) $J_0(x(k), \Delta u(.), k)$ is rewritten using the notation $\hat{x}(k+j|k)$ and $\Delta\hat{u}(k+j|k)$ as follows:

$$\hat{J}(\hat{x}(k), \Delta\hat{u}(.), k) = \sum_{j=1}^{N_p} \hat{x}(k+j|k)^T Q \hat{x}(k+j|k) + \sum_{j=0}^{N_p-1} \Delta\hat{u}(k+j) R \Delta\hat{u}(k+j), \tag{7.9}$$

which is identical to Eq. (7.4).

$$\hat{x}(k+j+1|k) = \lambda^{-(j+1)}x(k+j+1|k) = \lambda^{-1}A\hat{x}(k+j|k) + \lambda^{-1}B\Delta\hat{u}(k+j|k), \tag{7.10}$$

which is identical to Eq. (7.6). To ensure the same constraints with the original constraints shown by Eq. (7.3),

$$M_\lambda \Delta\hat{U} = M\Delta U. \tag{7.11}$$

$\Delta\hat{U}$ is defined in Eq. (7.8), therefore, M_λ equals to

$$M_\lambda = M \begin{bmatrix} I & 0 & \cdots & 0 & 0 \\ 0 & \lambda I & \cdots & 0 & 0 \\ 0 & 0 & \cdots & \lambda^{N_p-1} I & 0 \\ 0 & 0 & \cdots & 0 & \lambda^{N_p} I \end{bmatrix}, \tag{7.12}$$

which is identical to Eq. (7.7).

2) One solves Eq. (7.4) and obtains the closed-loop system:

$$\hat{x}(k+j+1|k) = \lambda^{-1}(A - BK)\hat{x}(k+j|k), \tag{7.13}$$

where $K = (R + \lambda^{-2}B^T P_\infty B)^{-1}\lambda^{-2}B^T P_\infty A$, which is obtained from

$$\frac{A^T}{\lambda}[P_\infty - P_\infty \frac{B}{\lambda}(R + \frac{B}{\lambda}P_\infty \frac{B^T}{\lambda})^{-1}\frac{\bar{B}^T}{\lambda}P_\infty]\frac{A}{\lambda} + Q - P_\infty = 0. \tag{7.14}$$

Therefore, the following is guaranteed:

$$|\lambda^{-1}\lambda_{max}(A - BK)| < 1. \tag{7.15}$$

If $\lambda < 1$, then the maximum eigenvalue of the original system satisfies

$$|\lambda_{max}(A - BK)| < \lambda < 1. \tag{7.16}$$

Therefore, the prescribed degree of stability is guaranteed in the degree of λ, where the variable λ is defined in continuous form in reference [82]. □

Remark 7.1. *With the different cost functions, the constraints remain the same, which implies that the fault-information formulated as constraints remains unchanged.*

Remark 7.2. *With the design of a prescribed degree of stability, the passive fault-tolerant ability is improved. The active FTC strategy is still guaranteed with the inequality constants solved on-line.*

Remark 7.3. *The controls is* $\Delta U = -Kx(k)$ *, where* $K = (\Phi^T\Phi + R)^{-1}(\Phi^T F)$*. F and Φ are defined as:*

$$F = \begin{bmatrix} CA \\ CA^2 \\ CA^3 \\ \vdots \\ CA^{N_p} \end{bmatrix}, \tag{7.17}$$

$$\Phi = \begin{bmatrix} CB & 0 & 0 & \cdots & 0 \\ CAB & CB & 0 & \cdots & 0 \\ CA^2B & CAB & CB & \cdots & 0 \\ \vdots & \vdots & \vdots & \vdots & \vdots \\ CA^{N_p-1}B & CA^{N_p-2}B & CA^{N_p-3}B & \cdots & CA^{N_p-N_c}B \end{bmatrix}, \tag{7.18}$$

The internal model has integral action for trajectory tracking purpose, therefore the maximum eigenvalues of the system matrix A: $\lambda_{max}|A| \geq 1$. Thus, $A^m (m \in [1, N_p])$ induces the numerical problem with m increasing.

The following effort focuses on the solution of numerical problem while keeping the prescribed degree of stability design.

Theorem 7.2. *Subject to the same system state equation by Eq.* (7.1)*,*

the optimal solution of $\Delta u(k+j|k)$ by minimizing the cost function J_{α_w} defined as:

$$J_{\alpha_w} = \sum_{j=1}^{N_p} \alpha_w^{-2j} x(k+j|k)^T Q_{\alpha_w} x(k+j|k) + \sum_{j=0}^{N_p-1} \alpha_w^{-2j} \Delta u(k+j|k)^T R_{\alpha_w} \Delta u(k+j|k) \tag{7.19}$$

is identical to the solution found by minimizing the cost function:

$$J = \sum_{j=1}^{N_p} x(k+j|k)^T Q x(k+j|k) + \sum_{j=0}^{N_p-1} \Delta u(k+j|k)^T R \Delta u(k+j|k), \tag{7.20}$$

where $\lim N_p \to \infty$*, Q_{α_w} and R_{α_w} are selected according to:*

$$\gamma_w = \frac{1}{\alpha_w}, \tag{7.21}$$

$$Q_{\alpha_w} = \gamma_w^2 Q + (1 - \gamma_w^2) P_\infty, \tag{7.22}$$

$$R_{\alpha_w} = \gamma_w^2 R. \tag{7.23}$$

Proof. To prove the identical of the solutions, the identity of the two AREs for Eq. (7.19) and Eq. (7.20) is presented. For a fixed initial condition $x(k)$, the optimal solution to the cost function, when constraints are not activated, is given by the ARE:

$$A^T (P_\infty - P_\infty B (R + B^T P_\infty B)^{-1} B^T P_\infty) A + Q - P_\infty = 0, \tag{7.24}$$

$K = -(R + B^T P_\infty B)^{-1} B^T P_\infty A$. The optimal solution of the exponentially weighted cost function shown by Eq. (7.19) is given by:

$$\frac{A^T}{\alpha_w}[\bar{P}_\infty - \bar{P}_\infty \frac{B}{\alpha_w}(R_{\alpha_w} + \frac{B}{\alpha_w}\bar{P}_\infty \frac{B^T}{\alpha_w})^{-1}\frac{\bar{B}^T}{\alpha_w}\bar{P}_\infty]\frac{A}{\alpha_w} + Q_{\alpha_w} - \bar{P}_\infty = 0. \tag{7.25}$$

Define the $\hat{A} = \frac{A}{\alpha_w}$ and $\hat{B} = \frac{B}{\alpha_w}$, ARE Eq. (7.25) becomes:

$$\hat{A}^T(\hat{P}_\infty - \hat{P}_\infty \hat{B}(R_{\alpha_w} + \hat{B}^T \hat{P}_\infty \hat{B})^{-1})\hat{A} + Q_{\alpha_w} - \hat{P}_\infty = 0. \tag{7.26}$$

To prove the solution for ARE in Eq. (7.24) is identical to that for ARE Eq. (7.26), Eq. (7.24) should be transfered to Eq. (7.26) by changing A to $\hat{A}$ and B to $\hat{B}$.

$$\frac{\hat{A}^T}{\gamma_w}[P_\infty - P_\infty \frac{\hat{B}}{\gamma_w}(R + \frac{\hat{B}}{\gamma_w}P_\infty \frac{\hat{B}^T}{\gamma_w})^{-1}\frac{\hat{B}^T}{\gamma_w}P_\infty]\frac{\hat{A}}{\gamma_w} + Q - P_\infty = 0. \tag{7.27}$$

where $\gamma_w = \frac{1}{\alpha_w}$, which can be further transformed into:

$$\hat{A}^T(P_\infty - P_\infty \hat{B}(\gamma_w^2 R + \hat{B}^T P_\infty \hat{B})^{-1})\hat{A} + \gamma_w^2 Q - \gamma_w^2 P_\infty + P_\infty - P_\infty = 0. \tag{7.28}$$

Compared ARE Eq. (7.25) to Eq. (7.28), if

$$Q_{\alpha_w} = \gamma_w^2 Q + (1 - \gamma_w^2)P_\infty, \tag{7.29}$$

$$R_{\alpha_w} = \gamma_w^2 R, \tag{7.30}$$

then Eq. (7.25) equals to Eq. (7.28) with solutions $\hat{P}_\infty = P_\infty$.

□

Remark 7.4. *The purpose is to scale A with the transformation $\hat{A} = \frac{A}{\alpha_w}$, where $\alpha_w \geq \lambda_{max}|A|$, then the $\lambda_{max}|\hat{A}| < 1$, the state space in the optimization process is stable:*

$$\hat{x}(k + j + 1|k) = \hat{A}x(k + j|k) + \hat{B}\hat{u}(k + j). \tag{7.31}$$

With the transformation of state space, the numerical problem is solved, which comes from the unstable state space equation.

Theorem 7.3. *Subject to the system state equation by Eq.* (7.1)*, the optimal solution of*

$\Delta u(k+j|k)$ by minimizing the cost function J_{α_w} defined by:

$$J_{\alpha_w} = \sum_{j=1}^{\infty} \alpha_w^{-2j} x^T(k+j|k) Q_{\alpha_w} x(k+j|k) + \sum_{j=0}^{\infty} \alpha_w^{-2j} \Delta u^T(k+j|k) R_{\alpha_w} \Delta u(k+j|k) \quad (7.32)$$

is identical to the solution found by minimizing the cost with a prescribed degree of stability:

$$J_{\lambda} = \sum_{j=1}^{\infty} \lambda^{-2j} x^T(k+j|k) Q x(k+j|k) + \sum_{j=0}^{\infty} \lambda^{-2j} \Delta u^T(k+j|k) R \Delta u(k+j|k), \quad (7.33)$$

where $\alpha_w > 1$, $0 < \lambda < 1$, Q_{α_w} and R_{α_w} are defined by

$$\begin{aligned} \gamma_w &= \frac{\lambda}{\alpha_w}, \\ Q_{\alpha_w} &= \gamma_w^2 Q + (1-\gamma_w^2) P_\infty, \\ R_{\alpha_w} &= \gamma_w^2 R, \end{aligned} \quad (7.34)$$

and P_∞ is the solution of the ARE:

$$\frac{\hat{A}^T}{\gamma_w}[P_\infty - P_\infty \frac{\hat{B}}{\gamma_w}(R + \frac{\hat{B}^T}{\gamma_w} P_\infty \frac{\hat{B}}{\gamma_w})^{-1} \frac{\hat{B}^T}{\gamma_w} P_\infty] \frac{\hat{A}}{\gamma_w} + Q - P_\infty = 0, \quad (7.35)$$

where the matrices $\hat{A} = \alpha_w^{-1} A$ and $\hat{B} = \alpha_w^{-1} B$.

Proof. The optimal control of Eq. (7.33) is obtained from the ARE:

$$\frac{A^T}{\lambda}[P_\infty - P_\infty \frac{B}{\lambda}(R + \frac{B^T}{\lambda} P_\infty \frac{B}{\lambda})^{-1} \frac{B^T}{\lambda} P_\infty)] \frac{A}{\lambda} + Q - P_\infty = 0. \quad (7.36)$$

Defining $\hat{A} = \alpha_w^{-1} A$, $\hat{B} = \alpha_w^{-1} B$ and substituting A and B with $\hat{A}$ and $\hat{B}$, Eq. (7.36) turns to be

$$\frac{\alpha_w \hat{A}^T}{\lambda}[P_\infty - P_\infty \frac{\alpha_w \hat{}}{\lambda}(R + \frac{\alpha_w \hat{B}^T}{\lambda} P_\infty \frac{\alpha_w \hat{B}}{\lambda})^{-1} \frac{\alpha_w \hat{B}^T}{\lambda} P_\infty)] \frac{\alpha_w \hat{A}}{\lambda} + Q - P_\infty = 0, \quad (7.37)$$

Defining $\gamma_w = \frac{\lambda}{\alpha_w}$ and substituting γ_w into $\frac{\lambda}{\alpha_w}$,Eq. (7.37) becomes:

$$\frac{A^T}{\gamma_w}[P_\infty - P_\infty \frac{B}{\gamma_w}(R + \frac{B^T}{\gamma_w} P_\infty \frac{B}{\gamma_w})^{-1} \frac{B^T}{\gamma_w} P_\infty)] \frac{A}{\gamma_w} + Q - P_\infty = 0. \quad (7.38)$$

Multiplying both sides of Eq. (7.38) with γ_w^2, and letting

$$Q_{\alpha_w} = \gamma_w^2 Q + (1 - \gamma_w^2) P_\infty, \tag{7.39}$$

$$R_{\alpha_w} = \gamma_w^2 R, \tag{7.40}$$

the following ARE is found:

$$\hat{A}^T (P_\infty - P_\infty \hat{B} (R_{\alpha_w} + \hat{B}^T P_\infty \hat{B})^{-1} \hat{B}^T P_\infty) \hat{A} + Q_{\alpha_w} - P_\infty = 0, \tag{7.41}$$

which is the same ARE for the cost function as shown in Eq. (7.4). Based on Theorem 7.1, the cost function Eq. (7.4) is identical to Eq. (7.32). Therefore, the ARE of Eq. (7.32) and Eq. (7.33) are identical, which lead to the same control gain matrix. □

Remark 7.5.

1. *A prescribed degree of stability is embedded in the FTC design.*
2. *The optimization process is performed using the transformed variables, which solves the numerical problem.*
3. *The active FTC strategy with described degree of stability is implemented based on Theorem 7.3 and the on-line solving the inequality constraints.*

7.3 Simulation Results

The objective is to improve the fault-tolerant performance when actuator faults of aircraft occur during different phases of landing. The evaluation is performed with the same scenarios carried out in Chapter 6 with the application of landing aircraft in the presence of actuators stuck for comparison purpose. In the evaluation process, 4 scenarios are applied to evaluate the performance of the proposed method in improving FTC capability. FTC strategy without ($\lambda = 1$) and with a prescribed degree of stability ($\lambda = 0.9$) are performed, where λ is the parameter of adjusting the robustness of the designed FTC system, and the evaluation criteria are maximum error and RMSE about the difference between references and measurements, which are flight path angle γ and true airspeed V_{TAS}. The fault information is assumed to be provided by an imperfect FDD with $2s$ time delay. The details of the evaluation are shown in Table 6.2 and Table 7.1 with two different designed FTC strategies.

Table 7.1: Tracking performance evaluation with FTC technique based on prescribed degree of stability design

	Stuck Scenarios	**Max Error γ (deg)**	**Max Error V_{TAS} (m/s)**	**RMSE γ**	**RMSE V_{TAS}**
Normal	No Fault	0.7308	0.46369	0.18352	0.16024
Level Flight	Level Flight	3.5217	1.9664	0.3095	0.25644
Descending	Descending	4.555	1.3418	0.37445	0.22118
Climbing	Climbing	3.7879	3.9069	0.32962	0.46312

7.3.1 Performance Comparison

Table 7.2: Tracking performance comparison in the landing period

	Stuck Scenarios	**Max Error γ (deg)**	**Max Error V_{TAS} (m/s)**	**RMSE γ**	**RMSE V_{TAS}**
Normal	No Fault	4.56 %	70.24 %	0.92 %	31.29 %
Level Flight	Level Flight	9.90 %	10.46 %	0.95 %	6.25 %
Descending	Descending	14.18 %	18.36 %	1.26 %	5.01 %
Climbing	Climbing	21.67 %	36.69 %	1.80 %	8.52 %

Table 6.2 shows the FTC performance of compensating elevators stuck fault on aircraft landing process with LF-MPC based FTC strategy without the prescribed degree of stability design. More particularly, in the fault-free scenario, the designed FTC strategy performs in an acceptable manner to fulfill the aircraft landing task. In the post-fault scenarios with fault occurring at different landing phases: level flight, descending, and climbing, the designed FTC strategy can still compensate the actuator faults. Table 7.1 illustrates the performance of the newly designed FTC based on the same scenarios as described in Table 6.2. The FTC strategy is based on the LF-MPC approach with a prescribed degree of stability design, which can also accommodate faults in an acceptable performance and aims to improve the transient performance of the FTC system. The performance comparison results are listed in Table 7.2 demonstrating the performance improvement with respect to two tracking parameters of γ and V_{TAS}.

In the fault-free case, the maximum errors about γ, the maximum error about V_{TAS}, and RMSE about γ, and RMSE V_{TAS} as shown in Table 7.1 are smaller than that shown in the Table 6.2, which imply the tracking performance in different landing phases using the FTC strategy with a prescribed degree of stability is better than the FTC strategy without prescribed degree of stability. The same conclusions are obtained with the criteria about γ and V_{TAS} in 3 post-fault scenarios with fault occurring at level flight, descending, and climbing phases, respectively. It indicates that the active FTC strategy with a prescribed degree of stability improves the fault-tolerant performance comparing to the active FTC

strategy without prescribed degree of stability. More details of stuck fault in various landing phases are presented in the following figures.

7.3.2 Fault-Free Scenario

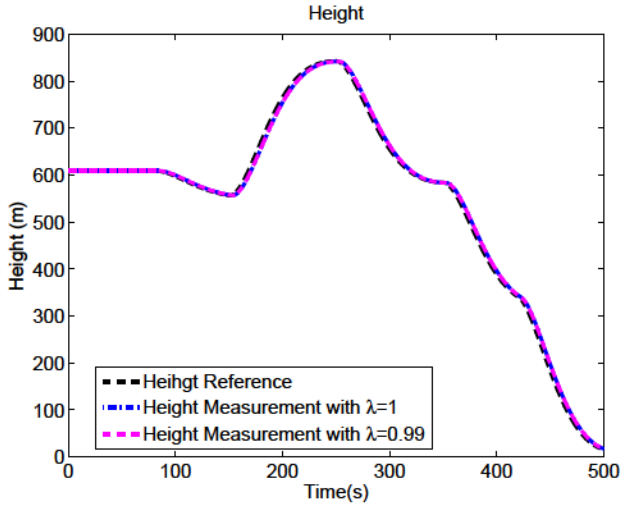

Figure 7.1: Landing trajectory tracking performance comparison in fault-free case

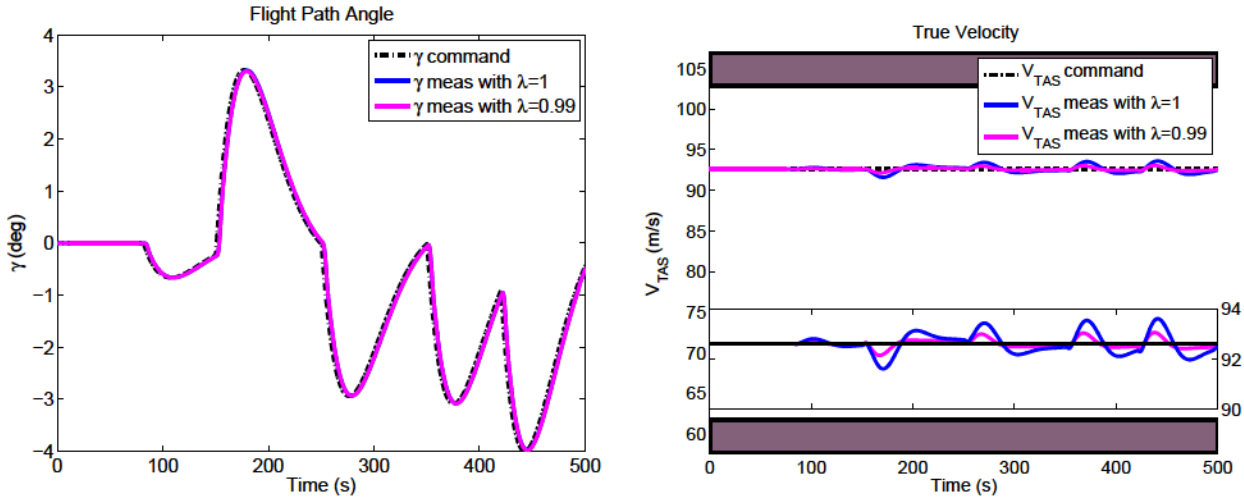

(a) Flight path angle

(b) True airspeed

Figure 7.2: Performance comparison in fault-free scenario: flight path angle and true airspeed

Fig. 7.1 illustrates the tracking performance comparison between active FTC strategies design with and without prescribed degree of stability in the fault-free scenario. The black

bold dashed line is the reference trajectory in the longitudinal plane. The blue dash-dot line stands for the tracking trajectory using active FTC strategy design without prescribed degree of stability. The purple dashed line stands for the tracking trajectory using active FTC strategy design with prescribed degree of stability. It is indicated that both FTC approaches perform in an acceptable manner to perform the fault-tolerant task. Furthermore, flight path angle and true velocity tracking process during landing period are illustrated in Fig. 7.2. In particular, Fig. 7.2(a) illustrates the performance improvement of flight path angle tracking. Fig. 7.2(b) illustrates the performance improvement in terms of true velocity.

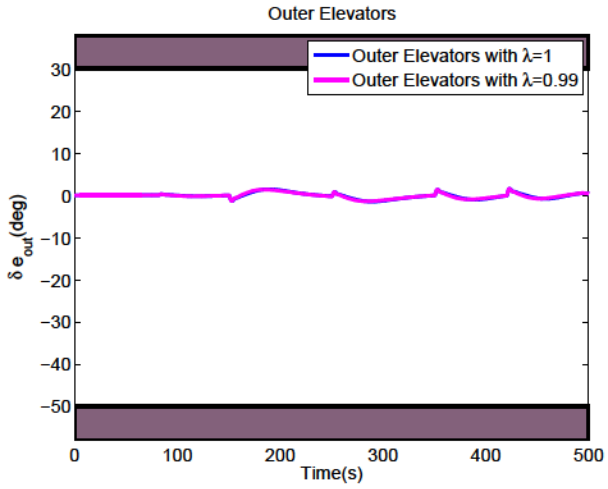

(a) Outer elevators

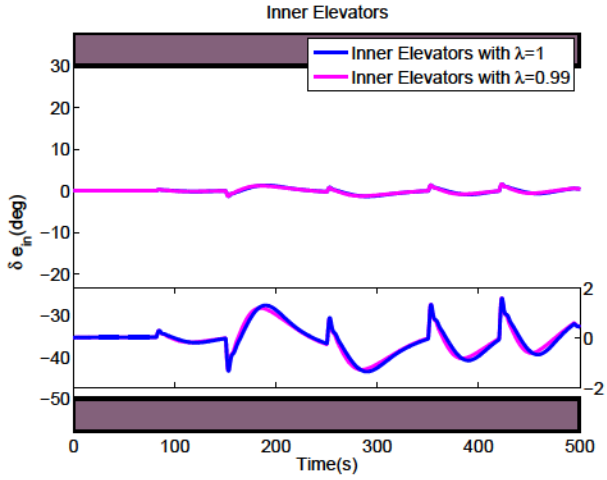

(b) Inner elevator

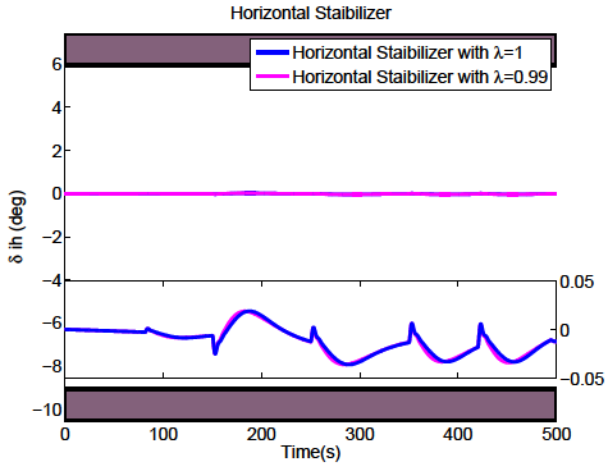

(c) Horizontal stabilizer

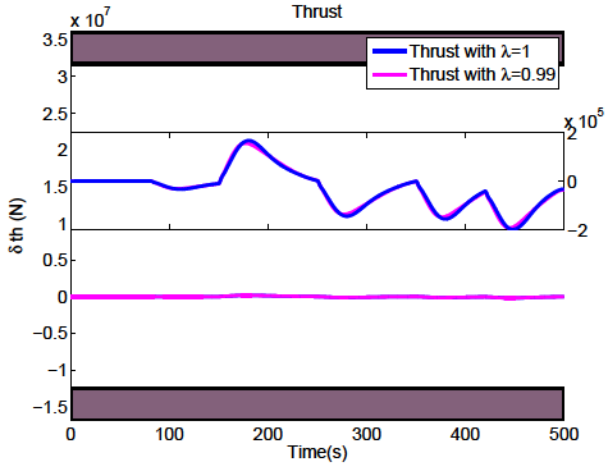

(d) Thrust

Figure 7.3: Control efforts comparison in fault-free scenario: outer elevators, inner elevators, horizontal stabilizer, and engines

The control efforts shown in Fig. 7.3 include outer elevators, inner elevators, horizontal stabilizer, and engines. The control efforts are compared between two active FTC strategies with/without prescribed degree of stability design. The blue lines stand for the controls from the FTC system without prescribed degree of stability design, while the purple lines are the controls from FTC system with the prescribed degree of stability design. The control efforts are very close to each other in outer elevators, inner elevators, horizontal stabilizer, and thrusts with two designed FTC strategies during landing as shown in Fig. 7.3. Note

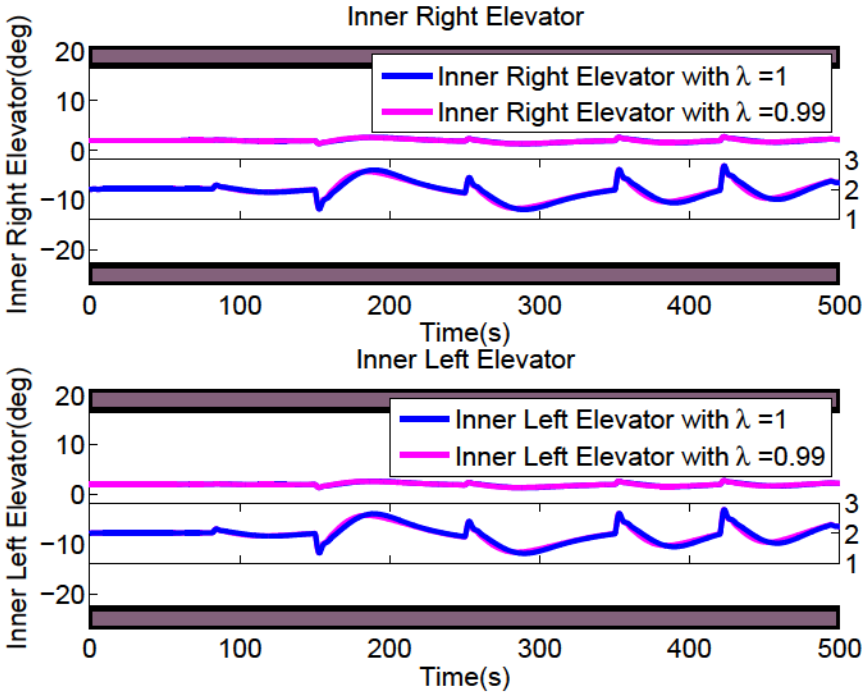

Figure 7.4: Deflections of inner elevators in fault-free scenario

that the deflections of inner elevators shown in Fig. 7.4 copes with the demanded shown in Fig. 7.3(b).

7.3.3 Fault Scenarios in Landing Process

Level Flight Case

Fig. 7.5 illustrates the tracking performance comparison between two aforementioned active FTC strategies in the presence of faults. The post-fault scenario is inner elevators stuck at the level flight phase of landing period. The black bold dashed line, the blue dash-

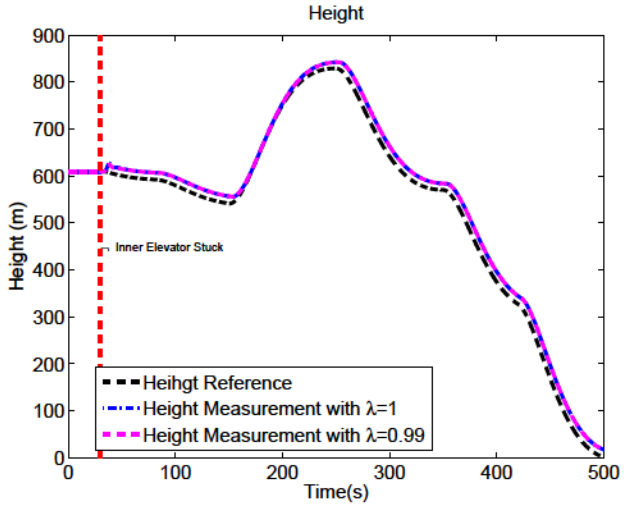

Figure 7.5: Trajectory tracking performance comparison with faults occurring at the levelel flight phase

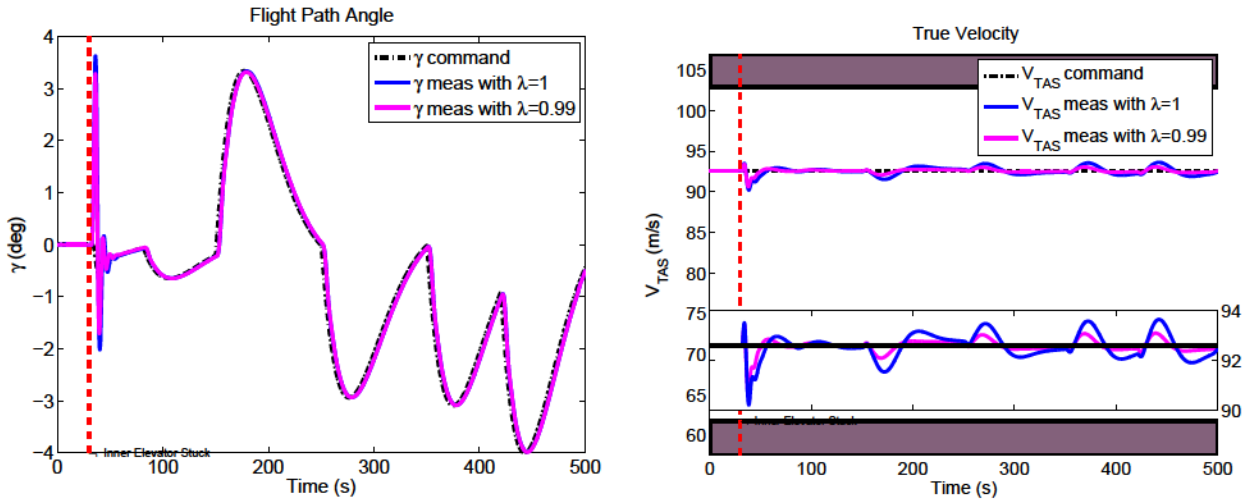

(a) Flight path angle

(b) True airspeed

Figure 7.6: Performance comparison with faults occurring at the levelel flight phase: flight path angle and true airspeed

dot line, and the purple dashed line are the same definition as in Fig. 7.1. The red vertical dashed line marks the time of fault occurrence. The performance of FTC with prescribed degree of stability design is more robust than that without prescribed degree of stability design, particularly at the transient of fault occurrence. Fig. 7.6 illustrates the performance improvement about two tracking parameters: flight path angle γ and true airspeed V_{TAS}. Fig. 7.6(a) illustrates the performance improvement of flight path angle tracking. Before

the fault occurrence, the flight path angle follows the reference trajectory with both active FTC strategies. Both FTC strategies can accommodate elevators stuck fault without the tracking significant performance degradation. However, in the time transient after faults occurrence, the active FTC with prescribed degree of stability design shown in purple line has better performance with less oscillation compared to that without prescribed degree of stability design shown in blue line, which implies the FTC with prescribed degree of stability performs better. The similar performance improvement about true airspeed exits in transient time with elevators stuck shown in Fig. 7.6(b). The true airspeed drops at the presence of actuator fault. The active FTC with prescribed degree of stability design takes less time to stabilize the faulty aircraft and maintain the desired true airspeed as shown in purple line.

Fig. 7.7 illustrates the detail of control efforts to accommodate inner elevators stuck occurring at the level flight phase of landing period. All control efforts in longitudinal channel are compared in terms of two active FTC strategies with/without prescribed degree of stability design. The blue lines stand for the controls from the FTC system without prescribed degree of stability design, while the purple lines are the controls from FTC system with the prescribed degree of stability design. Before the occurrence of actuator faults, there is no significant difference of the control efforts in terms of relevant control channels including outer elevators, inner elevators, horizontal stabilizer, and thrusts with two designed FTC strategies. In the presence of actuator faults, both two control strategies can accommodate elevators stuck faults. However, the control efforts shown in the purple line in Fig. 7.7(a) and Fig. 7.7(c) perturb less in the magnitude than that shown in blue line. There is no significant variation in the thrust before and after faults as shown in Fig. 7.7(d). Note that the controls of the inner elevators in Fig. 7.7(b) are consistent with the deflections of inner elevators shown in Fig. 7.8 after faults occurrence with both two FTC strategies, which imply that the stuck channels are isolated in the control efforts distribution.

Descending Case

Fig. 7.9 illustrates the tracking performance comparison between active FTC strategies design with and without prescribed degree of stability. The scenarios is the post-fault scenario with inner elevators stuck in the descending phase of landing period. The performance of FTC with prescribed degree of stability design is more robust than that without prescribed degree of stability design. The distinguish is clearly illustrated in term of flight path angle γ and true airspeed V_{TAS} shown in Fig. 7.10(a) and Fig. 7.10, respectively. Before the

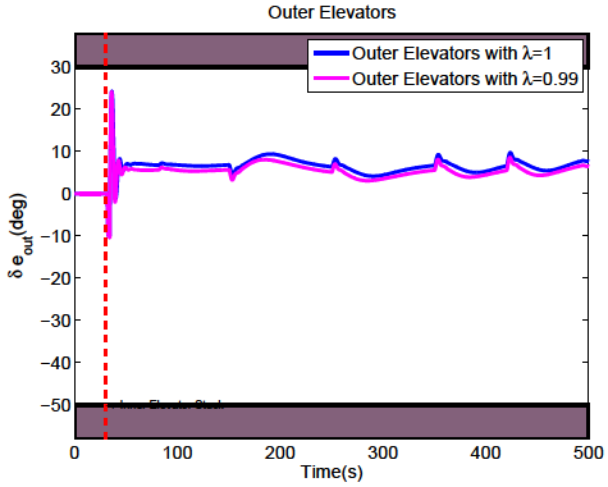

(a) Outer elevators

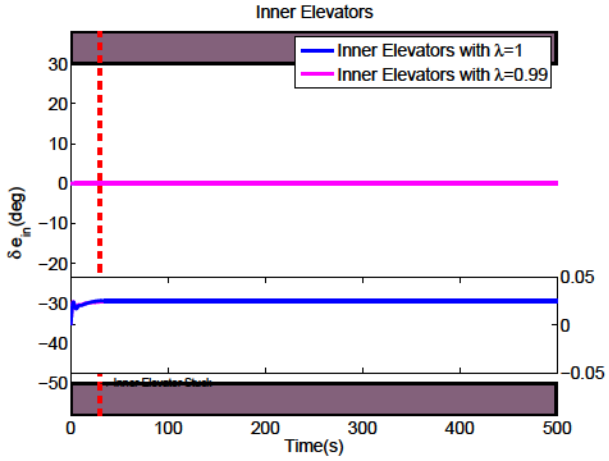

(b) Inner elevators

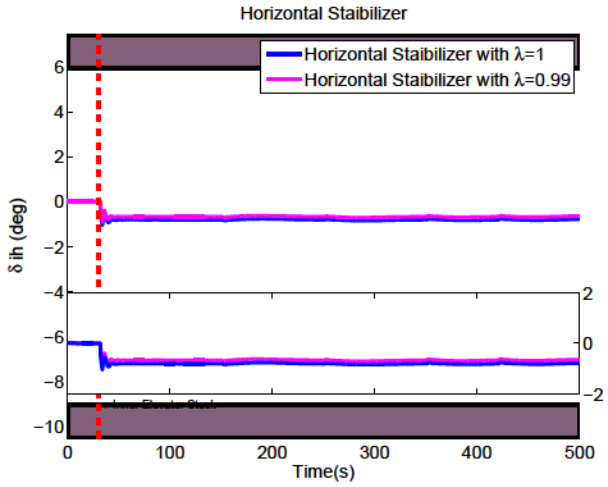

(c) Horizontal stabilizer

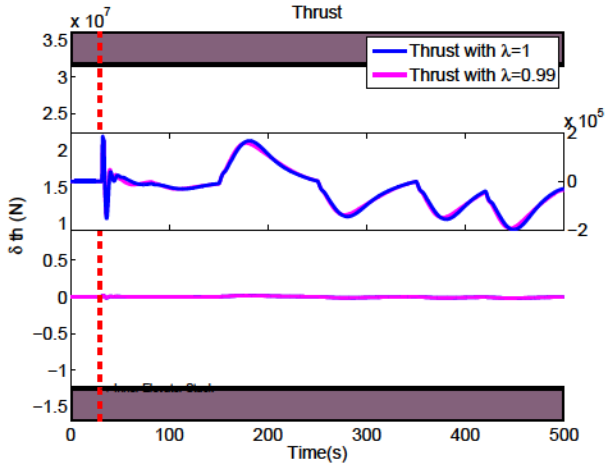

(d) Thrust

Figure 7.7: Control efforts comparison with faults occurring at the levelel flight phase: outer elevators, inner elevators, horizontal stabilizer, and engines

fault occurrence, the flight path angle tracks the reference trajectory with both active FTC strategies. Both FTC strategies can accommodate elevators stuck fault without the tracking significant performance degradation. However, in the time transient after fault occurrence, the active FTC with prescribed degree of stability design shown in purple line shows better performance with less oscillation comparing to that without prescribed degree of stability design shown in blue line, which implies that the FTC with prescribed degree of stability have better fault-tolerant capability in improving transient performance. The similar performance improvement about true airspeed exits in transient time with elevators stuck shown

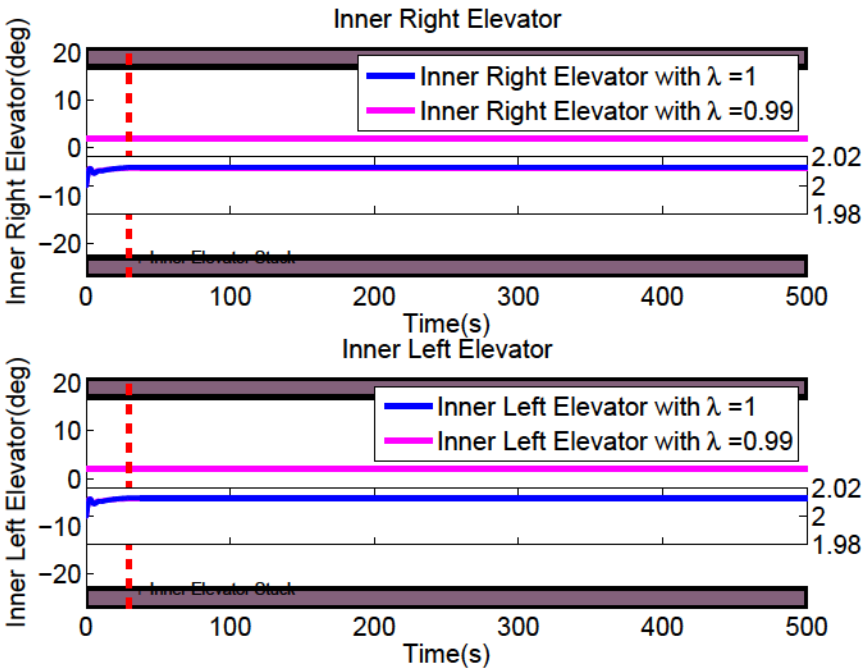

Figure 7.8: Deflections of inner elevators with faults occurring at the levelel flight phase

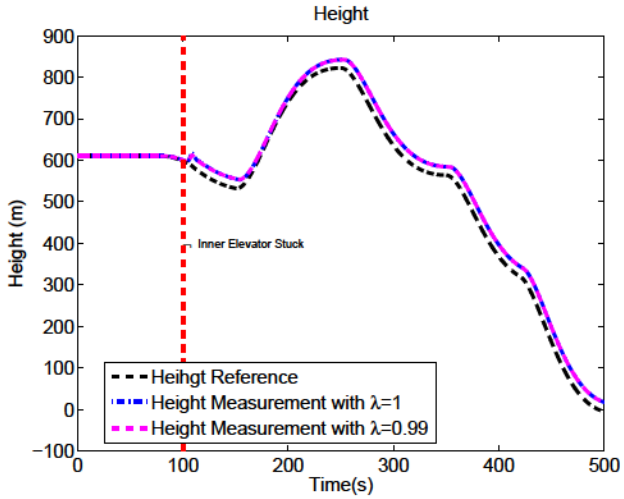

Figure 7.9: Trajectory tracking performance comparison with faults occurring at descending phase

in Fig. 7.10(b). The true airspeed drops at the presence of actuator fault. The active FTC with prescribed degree of stability design takes less time to bring the faulty aircraft back to the desired true airspeed compared to the FTC without prescribed degree of stability design.

Fig. 7.11 illustrates the detail of control efforts to accommodate inner elevators stuck

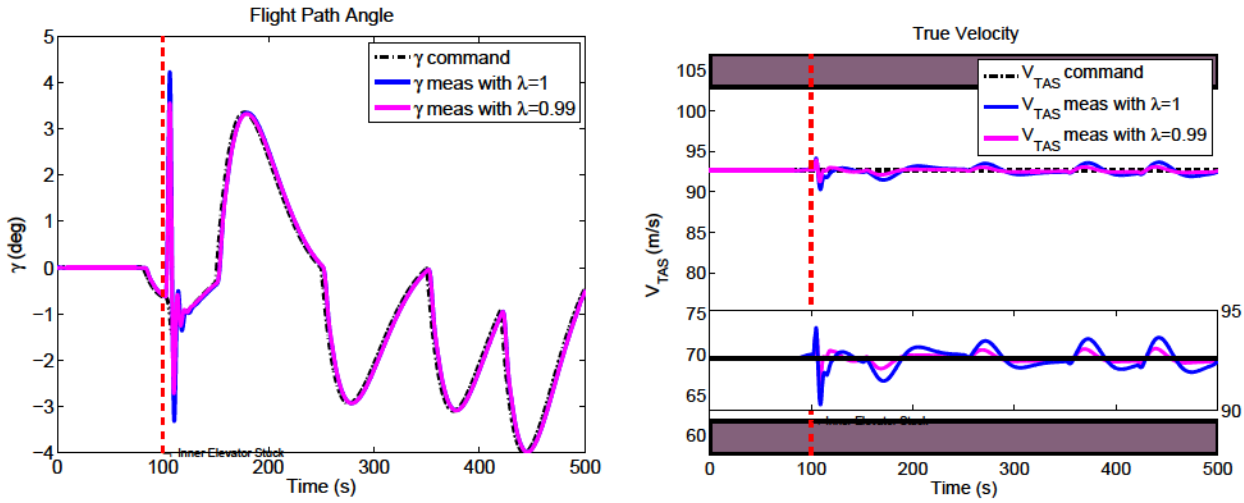

(a) Flight path angle

(b) True airspeed

Figure 7.10: Performance comparison with faults occurring at descending phase: flight path angle and true airspeed

occurring at the climbing landing phase. The control efforts include outer elevators, inner elevators, horizontal stabilizer, and engines. The control efforts are compared between two active FTC strategies with/without prescribed degree of stability design. The blue lines stand for the controls from the FTC system without prescribed degree of stability design, while the purple lines are the controls from FTC system with the prescribed degree of stability design. Before the occurrence of actuator faults, the control efforts are similar in outer elevators, inner elevators, horizontal stabilizer, and thrusts with two designed FTC strategies. In the presence of actuator faults, both two control strategies can accommodate elevators stuck faults. However, the control efforts in the purple line in Fig. 7.11(a) and Fig. 7.11(c) perturb less in the magnitude than that shown in blue line. There is no significant variation in the thrust before and after faults as shown in Fig. 7.11(d). The controls of the inner elevators shown in Fig. 7.11(b) are the same as the inner elevators' deflections shown in Fig. 7.12 after faults occurrence with both two FTC strategies.

Climbing Case

Fig. 7.13 illustrates the tracking performance comparison between active FTC strategies design with and without prescribed degree of stability based on the scenario of inner elevators stuck in the climbing phase of landing period. It can be seen that the performance of FTC with prescribed degree of stability design demonstrates a better robust in the transient

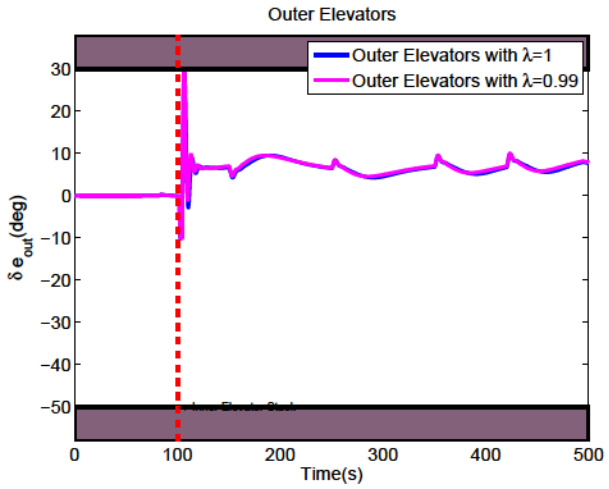

(a) Outer elevators

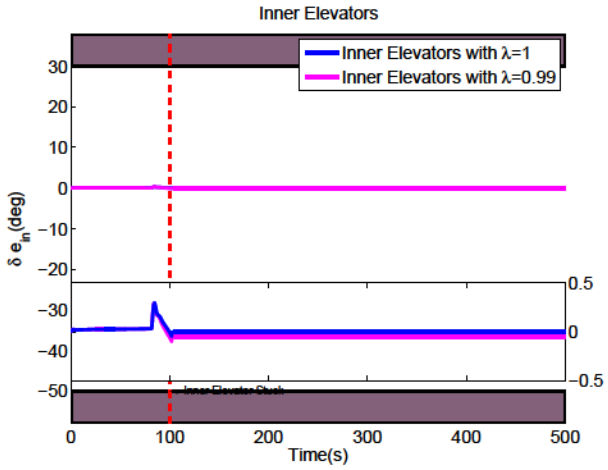

(b) Inner elevators

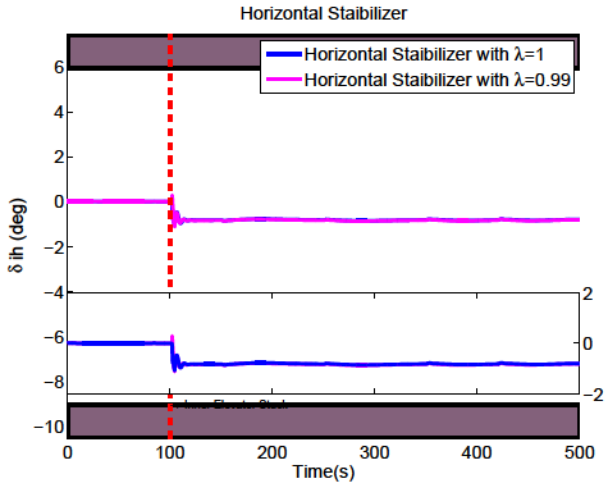

(c) Horizontal stabilizer

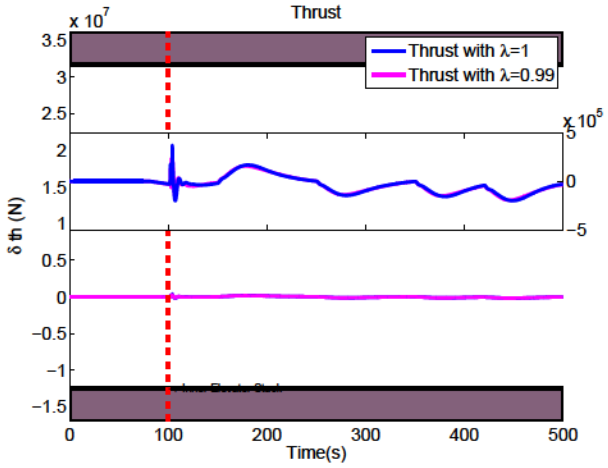

(d) Thrust

Figure 7.11: Control efforts comparison with faults occurring at descending phase: outer elevators, inner elevators, horizontal stabilizer, and engines

period than that without prescribed degree of stability design. Fig. 7.14 illustrates the performance improvement in an direct way in terms of flight path angle γ and true airspeed V_{TAS}. Fig. 7.14(a) illustrates the performance improvement of flight path angle tracking. Before the fault occurrence, the tracking performance is maintained with the two designed active fault-tolerant controller. Both FTC strategies can accommodate elevators stuck fault without the tracking significant performance degradation. However, focusing on the transient period after faults occurrence, the flight path angle controlled by the active FTC with prescribed degree of stability design shown in purple line has less oscillation comparing to

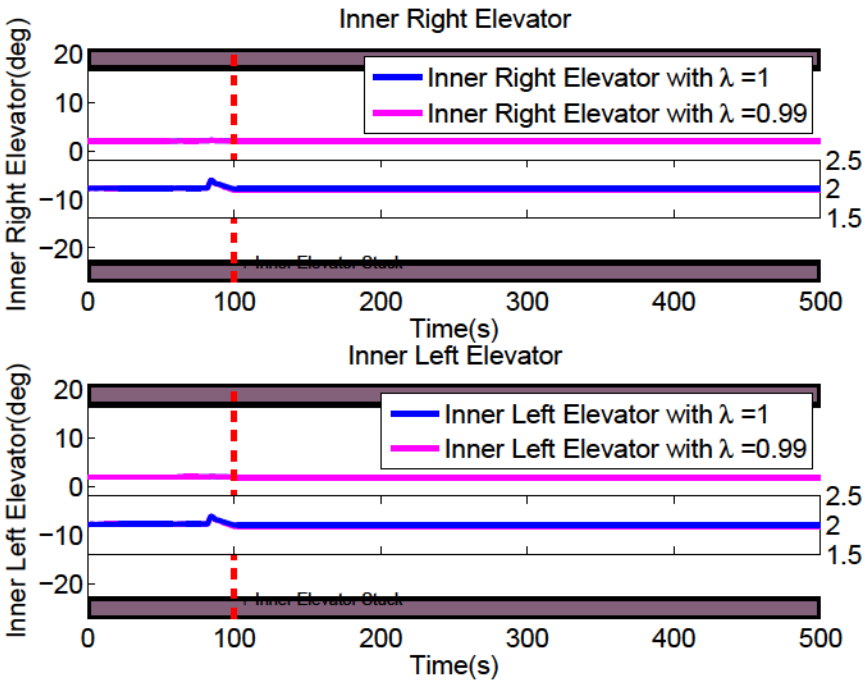

Figure 7.12: Deflections of inner elevators with faults occurring at descending phase

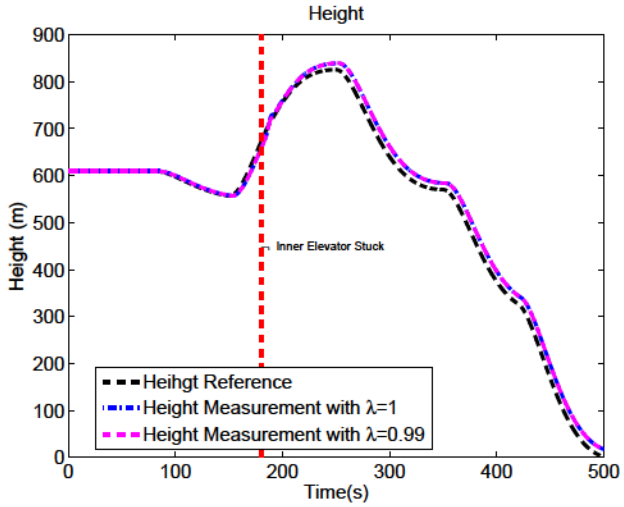

Figure 7.13: Trajectory tracking performance com with faults occurring at the climbing phase

that without prescribed degree of stability design shown in blue line, which implies the FTC with prescribed degree of stability performs better in the transient period. The similar performance improvement about true airspeed exits in transient time with elevators stuck shown in Fig. 7.14(b). The true airspeed drops at the presence of actuator fault. However,

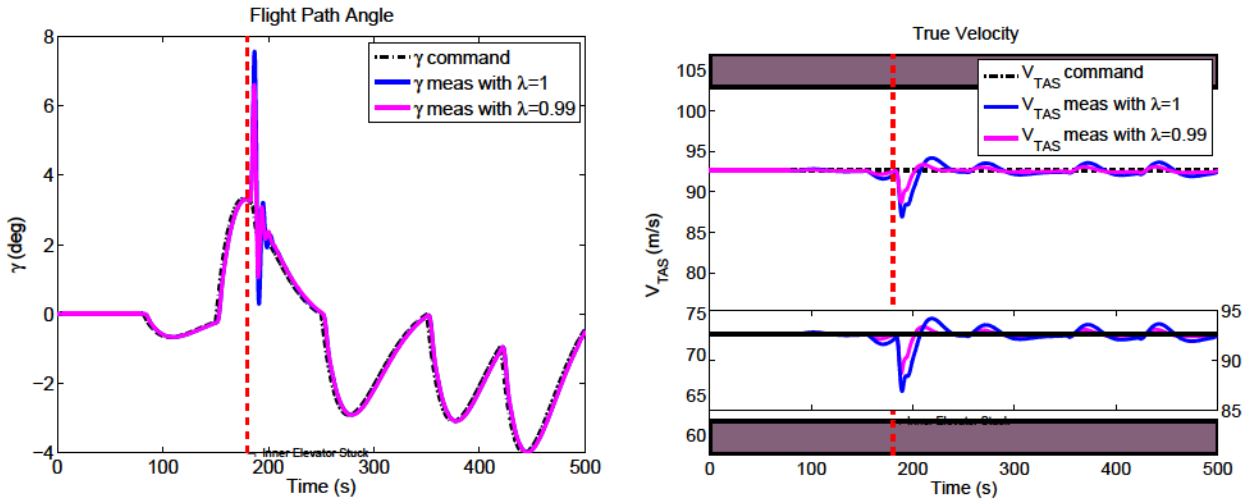

(a) Flight path angle

(b) True airspeed

Figure 7.14: Performance comparison with faults occurring at the climbing phase: flight path angle and true airspeed

the active FTC with prescribed degree of stability design takes less time to stabilize the faulty aircraft and maintain its tracking performance.

Fig. 7.15 illustrates the detail of control efforts to accommodate inner elevators stuck occurring at the climbing landing phase. The control efforts include outer elevators, inner elevators, horizontal stabilizer, and engines. The control efforts are compared between two active FTC strategies with/without prescribed degree of stability design. The blue lines stand for the controls from the FTC system without prescribed degree of stability design, while the purple lines are the controls from FTC system with the prescribed degree of stability design. Before the occurrence of actuator faults, the control efforts are considerable close to each other in outer elevators, inner elevators, horizontal stabilizer, and thrusts with two designed FTC strategies. In the presence of actuator faults, both two control strategies can accommodate elevators stuck faults. However, the control efforts in the purple line in Fig. 7.15(a) and Fig. 7.15(c) perturb less in the magnitude than that shown in blue line. There is no significant variation in the thrust before and after faults as shown in Fig. 7.15(d). Note that the controls of inner elevators shown in Fig. 7.15(b) copes with the deflections of inner elevators shown in Fig. 7.16 indicating the reconfigured controls obtained from the FTC strategies with the consideration of the faulty actuators.

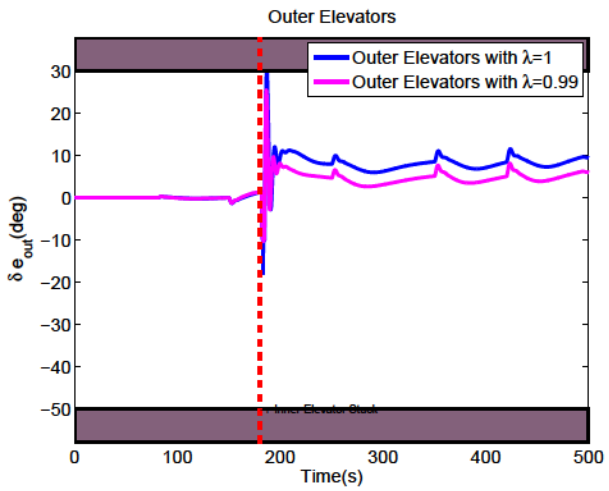

(a) Outer elevator

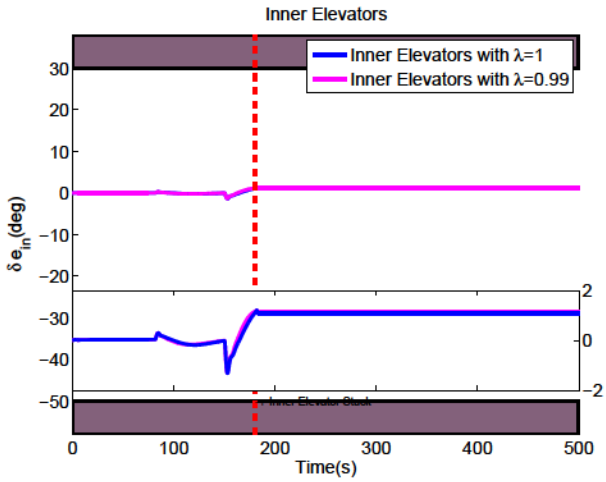

(b) Inner elevator

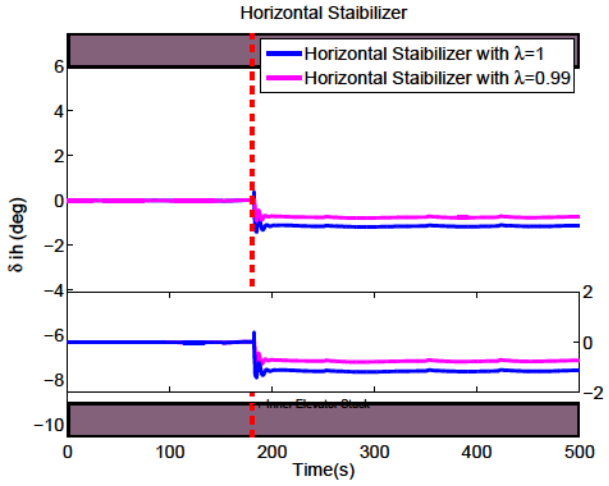

(c) Horizontal stabilizer

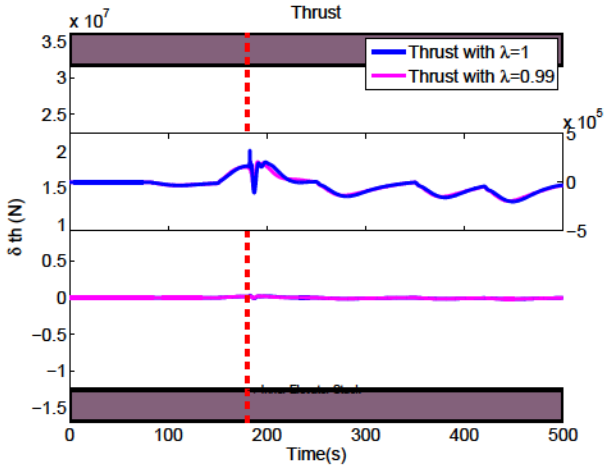

(d) Thrust

Figure 7.15: Control efforts comparison with faults occurring at the climbing phase: outer elevators, inner elevators, horizontal stabilizer, and engines

7.4 Summary

This chapter develops and implements an active FTC strategy using LF-MPC with a prescribed degree of stability. The performance is investigated and validated through the task of aircraft landing process with faults occurrence at different landing phases. The comparison results between the FTC with two different design approaches are presented to demonstrate the effectiveness of the FTC using LF-MPC with a prescribed degree of stability. It also demonstrates that the transient performance improvement with the newly designed

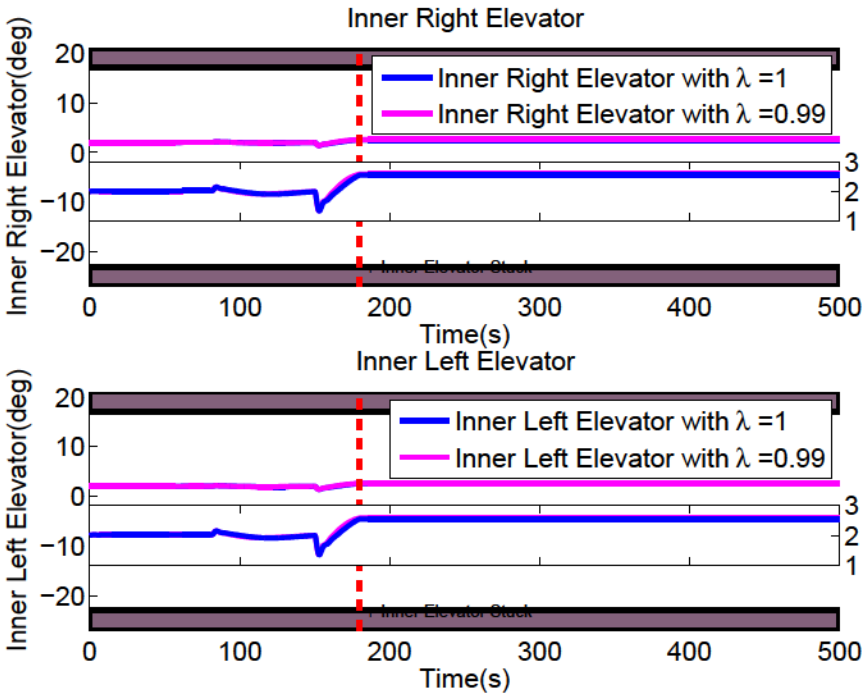

Figure 7.16: Deflections of inner elevators with faults occurring at the climbing phase

FTC with prescribed degree of stability technique comparing to that without the prescribed degree of stability design. Meanwhile, an imperfect FDD with time delay is also considered in the evaluation process, which demonstrates the effectiveness of the designed FTC in a more realistic manner since the time delay of FDD is inevitable in the real application. In the delayed time period, there is no fault information available, which might result in serious consequences without any further actions.

Chapter 8

Conclusions and Future Work

8.1 Conclusions

This thesis proposes a fault-tolerant control (FTC) approach for aircraft in the control design framework of linear quadratic (LQ) programming. The proposed approach adopts LQ technique to address partial or total loss of control (LOC) problems due to the actuator faults, in particular, loss of control effectiveness (LOE) of actuator faults of UAVs and total failure of elevators of a Boeing 747-100/200 airplane.

In the process of solving LOE problem of unmanned aerial vehicles (UAVs), a state-augmented extended Kalman filter (SAEKF), a combination of parameter identification and state estimation techniques, is proposed and implemented to perform fault detection and diagnosis (FDD) task. This approach provides fault information and post-fault system states, in which the unknown fault parameters are estimated by an augmented state vector based on non-linear aircraft model. The performance of diagnosing LOE faults is investigated and validated without any dedicated sensor information. A robust LQ technique with a prescribed degree of stability is implemented as a fault-tolerant controller.

Furthermore, a modified model predictive control (MPC) is implemented to perform FTC for accommodating total failure of actuators of a Boeing 747-100/200 airplane. The modified MPC is based on the modeling method, which is applied to approximate an optimal control trajectory using a series of Laguerre functions. The objective aims to improve the on-line fault-tolerant capability, which is critical for FTC, particularly in the framework of MPC. The Laguerre-function based MPC (LF-MPC) possesses the facets of improving the on-

line fault-tolerant capability and addressing constraints for both fault-free and post-fault scenarios. The emergency task of aircraft in the event of faults is to land aircraft safely as soon as possible. Therefore, the landing scenario is applied to validate the developed FTC system. In addition to the fault scenarios, a fault-free scenario is also used to test the design FTC system in performing a normal duty. Note that the fault information is assumed to be provided by an imperfect FDD with time delay, which further illustrates the effectiveness of the designed FTC system.

Using the FDD information, active FTC strategies satisfactorily perform in the reconfiguration of control efforts. In addition to the development of LF-MPC based fault-tolerant controller, more efforts are carried out to improve the fault-tolerant capability of the designed FTC system during the transient between fault occurrence and the activation of reconfigurable controls. Therefore, the effort focuses on improving the fault-tolerant capability without any FDD information. To this end, a robust LQ technique is further developed and implemented in the MPC framework for fault-tolerant application. The idea is to make a nominal system more robust to compensate the performance deterioration in the transient period before further actions are performed by an active FTC system. The performance of the further developed FTC system is validated through comparing the two designed FTC systems. The validation is performed based on the same landing scenarios without faults and with faults occurring in different phases: level flight, descending, and climbing. In the process of evaluation, the fault information is provided by an assumed FDD with time delay for the robustness test.

Overall, all the validations demonstrate the effectiveness of the proposed FTC schemes, especially the effectiveness in the emergency landing capability of the faulty aircraft.

8.2 Future Work

The objective of the work is to increase the reliability, survivability, and safety of areal vehicles: manned and unmanned aircraft. Therefore the evaluation of the proposed scheme and approaches should further be carried out in real-time platforms.

From the application point of view, as more and more UAVs, especially small UAVs, are presented in the lower airspace. The safety issue is one of the major concerns in the applications. Despite regulations made for the safety operation of UAVs, UAVs should possess the capability of improving the safety and reliability in system level. In this sense,

the application of the proposed approach on UAVs should be further performed under more realistic constraints, such as environmental uncertainty.

For manned aircraft, it is not realistic to test the proposed approach on real commercial aircraft in the near future. However, inspired by NASA generic transport model (GTM) of a scaled Boeing 757 project, the proposed approaches can be further advanced and evaluated in a scaled commercial aircraft.

From the algorithm point of view, LF-MPC improves the fault-tolerant capability by reducing the number of optimized parameters. While it is still costly to optimize the reconfigurable control law at each time intervals. The trade-off of the computational cost and the performance should be further investigated. As indicated in LQ framework, the proposed FTC strategies perform as a normal controller in a fault-free case. A FTC system is activated when FDD information and reconfigurable mechanism are ready. Therefore, the proposed FTC can be used in a standby controller to accommodate faults. The selection of cost function still need to be further investigated regarding the performance and physical meaning. With the consideration of the reconfiguration process, a FDD unit plays a critical role. The reliability of FDD and the integration of FDD with active FTC strategies are still needed further research.

Overall, it is believe that in the LQ framework, more fault-tolerant facets can be explored and advanced. The future work will focus on the real-time application and performance improvement in the framework of LQ design.

Bibliography

[1] C. Edwards, T. Lombaerts, and H. Smaili, *Fault Tolerant Flight Control: A Benchmark Challenge*, vol. 399. Springer, 2010.

[2] Y. M. Zhang and J. Jiang, "Bibliographical review on reconfigurable fault-tolerant control systems," *Annual Reviews in Control*, vol. 32, no. 2, pp. 229–252, 2008.

[3] M. Job, "Air disaster, vol. 2," *Canberra: Aerospace Publications*, 1996.

[4] M. Maciejowski and N. Jones, "MPC fault-tolerant flight control case study: Flight 1862," in *IFAC safeprocess conference*, pp. 121–126, 2002.

[5] C. Edwards, K. Spurgeon, and J. Patton, "Sliding mode observers for fault detection and isolation," *Automatica*, vol. 36, no. 4, pp. 541–553, 2000.

[6] S. M. Adams and C. J. Friedland, "A survey of unmanned aerial vehicle (UAV) usage for imagery collection in disaster research and management," in *9th International Workshop on Remote Sensing for Disaster Response*, 2011.

[7] D. W. Casbeer, D. B. Kingston, R. W. Beard, and T. W. McLain, "Cooperative forest fire surveillance using a team of small unmanned air vehicles," *International Journal of Systems Science*, vol. 37, no. 6, pp. 351–360, 2006.

[8] D. Hausamann, W. Zirnig, G. Schreier, and P. Strobl, "Monitoring of gas pipelines-a civil UAV application," *Aircraft Engineering and Aerospace Technology*, vol. 77, no. 5, pp. 352–360, 2005.

[9] L. Johnson, S. Herwitz, S. Dunagan, B. Lobitz, D. Sullivan, and R. Slye, "Collection of ultra high spatial and spectral resolution image data over california vineyards with a small UAV," in *Proceedings of the 30th International Symposium on Remote Sensing of Environment*, vol. 20, 2003.

[10] M. Nagai, T. Chen, R. Shibasaki, H. Kumagai, and A. Ahmed, "UAV-Borne 3-D mapping system by multisensor integration," *IEEE Transactions on Geoscience and Remote Sensing*, vol. 47, no. 3, pp. 701–708, 2009.

[11] J. Stolaroff, "The need for a life cycle assessment of drone-based commercial package delivery," *Lawrence Livermore National Laboratory*, 2014.

[12] M. Blanke and J. Schrder, *Diagnosis and Fault-tolerant Control*, vol. 691. Springer, 2006.

[13] T. Jordan, W. Langford, C. Belcastro, J. Foster, G. Shah, G. Howland, and R. Kidd, "Development of a dynamically scaled generic transport model testbed for flight research experiments," report, NASA Langley Research Center, Hampton, VA, United States, Jan. 2004.

[14] J. Csank, D. May, S. Litt, and T. Guo, "Control design for a generic commercial aircraft engine," in *Proceedings of the 46th AIAA/ASME/SAE/ASEE Joint Propulsion Conference, Hartford, CT*, 2010.

[15] V. Stepanyan and K. Krishnakumar, "Adaptive control with reference model modification," *Journal of Guidance, Control, and Dynamics*, vol. 35, no. 4, pp. 1370–1374, 2012.

[16] H. Alwi and C. Edwards, "Fault tolerant control using sliding modes with on-line control allocation," *Automatica*, vol. 44, no. 7, pp. 1859–1866, 2008.

[17] H. Alwi, C. Edwards, and C. P. Tan, *Fault Detection and Fault-Tolerant Control Using Sliding Modes*. Springer, 2011.

[18] T. Wang, *Sliding Mode Fault Tolerant Reconfigurable Control against Aircraft Control Surface Failures*. PhD thesis, Concordia University, 2012.

[19] Q. Sang and G. Tao, "Multivariable adaptive piecewise linear control design for NASA generic transport model," *Journal of Guidance, Control, and Dynamics*, vol. 35, no. 5, pp. 1559–1567, 2012.

[20] R. Hallouzi and M. Verhaegen, "Subspace predictive control applied to fault-tolerant control," in *Fault Tolerant Flight Control* (C. Edwards, T. Lombaerts, and H. Smaili, eds.), vol. 399 of *Lecture Notes in Control and Information Sciences*, pp. 293–317, Springer Berlin Heidelberg, 2010.

[21] D. Kufoalor and T. Johansen, "Reconfigurable fault tolerant flight control based on non-linear model predictive control," in *American Control Conference (ACC)*, pp. 5128–5133, 2013.

[22] X. Yu and J. Jiang, "A survey of fault-tolerant controllers based on safety-related issues," *Annual Reviews in Control*, vol. 39, pp. 46–57, 2015.

[23] J. Cieslak, D. Efimov, and D. Henry, "Transient management of a supervisory fault-tolerant control scheme based on dwell-time conditions," *International Journal of Adaptive Control and Signal Processing*, vol. 29, no. 1, pp. 123–142, 2015.

[24] J. Jiang and X. Yu, "Fault-tolerant control systems: A comparative study between active and passive approaches," *Annual Reviews in control*, vol. 36, no. 1, pp. 60–72, 2012.

[25] B. Y. Yi, L. Y. Kang, K. Jiang, and Y. J. Lin, "A two-stage Kalman filter for sensorless direct torque controlled PM synchronous motor drive," *Mathematical Problems in Engineering*, 2013.

[26] N. Djeghali, M. Ghanes, S. Djennoune, and J. P. Barbot, "Sensorless fault tolerant control for induction motors," *International Journal of Control Automation and Systems*, vol. 11, no. 3, pp. 563–576, 2013.

[27] H. Yang, B. Jiang, and M. Staroswiecki, "Supervisory fault tolerant control for a class of uncertain non-linear systems," *Automatica*, vol. 45, no. 10, pp. 2319–2324, 2009.

[28] X. Zhang, M. M. Polycarpou, and T. Parisini, "Adaptive fault diagnosis and fault-tolerant control of mimo non-linear uncertain systems," *International Journal of Control*, vol. 83, no. 5, pp. 1054–1080, 2010.

[29] X. Yang and J. M. Maciejowski, "Fault tolerant control using gaussian processes and model predictive control," *International Journal of Applied Mathematics and Computer Science*, vol. 25, no. 1, pp. 133–148, 2015.

[30] B. Yu, Y. M. Zhang, I. Minchala, and Y. H. Qu, "Fault-tolerant control with linear quadratic and model predictive control techniques against actuator faults in a quadrotor UAV," in *Control and Fault-Tolerant Systems (SysTol)*, pp. 661–666, 2013.

[31] J. M. Maciejowski, "Fault-tolerant aspects of MPC," in *Model Predictive Control: Techniques and Applications - Day 2 (Ref. No. 1999/096), IEE Two-Day Workshop on*, pp. 1/1–1/4, 1999.

[32] R. Isermann and P. Balle, "Trends in the application of model-based fault detection and diagnosis of technical processes," *Control Engineering Practice*, vol. 5, no. 5, pp. 709–719, 1997.

[33] R. Isermann, *Fault-Diagnosis Applications: Model-Based Condition Monitoring Actuators, Drives, Machinery, Plants, Sensors, and Fault-tolerant Systems*. Springer, 2011.

[34] R. Isermann, *Fault-Diagnosis Systems: An Introduction from Fault Detection to Fault Tolerance*. Springer, 2006.

[35] R. Isermann, "Model-based fault-detection and diagnosis status and applications," *Annual Reviews in Control*, vol. 29, no. 1, pp. 71–85, 2005.

[36] F. Gustafsson, "Fault detection terminology," *Adaptive Filtering and Change Detection*, pp. 475–476, 2001.

[37] Y. M. Zhang and J. Jiang, "Active fault-tolerant control system against partial actuator failures," *IEE Proceedings on Control Theory and Applications*, vol. 149, no. 1, pp. 95–104, 2002.

[38] G. J. Ducard, *Fault-Tolerant Flight Control and Guidance Systems: Practical methods for small unmanned aerial vehicles*. Springer Science & Business Media, 2009.

[39] J. Bokor and Z. Szab, "Fault detection and isolation in non-linear systems," *Annual Reviews in Control*, vol. 33, no. 2, pp. 113–123, 2009.

[40] X. Zhao, S. Wang, J. Zhang, Z. Fan, and H. Min, "Real-time fault detection method based on belief rule base for aircraft navigation system," *Chinese Journal of Aeronautics*, vol. 26, no. 3, pp. 717–729, 2013.

[41] P. Lu and E. van Kampen, "Active fault-tolerant control system using incremental backstepping approach," in *AIAA Guidance, Navigation, and Control Conference*, pp. 1–17, 2015.

[42] P. Lu, L. Van Eykeren, E. van Kampen, and Q. Chu, "Selective-reinitialization multiple-model adaptive estimation for fault detection and diagnosis," *Journal of Guidance, Control, and Dynamics*, pp. 1–16, 2015.

[43] P. Lu, L. Van Eykeren, E.-J. van Kampen, C. de Visser, and Q. Chu, "Double-model adaptive fault detection and diagnosis applied to real flight data," *Control Engineering Practice*, vol. 36, pp. 39–57, 2015.

[44] K. S. Narendra and J. Balakrishnan, "Adaptive control using multiple models," *IEEE Transactions on Automatic Control*, vol. 42, no. 2, pp. 171–187, 1997.

[45] N. Swain and S. Manickavasagar, "A combined fault detection, identification and reconfiguration system based around optimal control allocation," in *Fault Tolerant Flight Control* (C. Edwards, T. Lombaerts, and H. Smaili, eds.), vol. 399 of *Lecture Notes in Control and Information Sciences*, pp. 399–422, Springer Berlin Heidelberg, 2010.

[46] A. Sollazzo, G. Morani, and A. Giovannini, *An Adaptive Fault-Tolerant FCS for a Large Transport Aircraft*, pp. 273–291. Springer, 2010.

[47] T. Wang, W. F. Xie, and Y. M. Zhang, "Sliding mode reconfigurable control using information on the control effectiveness of actuators," *Journal of Aerospace Engineering*, vol. 27, no. 3, pp. 587–596, 2014.

[48] T. Wang, W. F. Xie, and Y. M. Zhang, "Sliding mode fault tolerant control dealing with modeling uncertainties and actuator faults," *ISA Transactions*, vol. 51, no. 3, pp. 386–392, 2012.

[49] M. T. Hamayun, C. Edwards, and H. Alwi, "Augmentation scheme for fault-tolerant control using integral sliding modes," *IEEE Transactions on Control Systems Technology*, vol. 22, no. 1, pp. 307–313, 2014.

[50] T. Lombaerts, P. Chu, and J. A. B. Mulder, *Flight Control Reconfiguration Based on Online Physical Model Identification and Non-Linear Dynamic Inversion*, pp. 363–397. Springer, 2010.

[51] R. Hallouzi and M. Verhaegen, "Reconfigurable fault tolerant control of a Boeing 747 using subspace predictive control," in *AIAA Guidance, Navigation and Control Conference and Exhibit*, vol. 6665, p. 2007, 2007.

[52] J. Rawlings and D. Mayne, *Model Predictive Control: Theory and Design*. Nob Hill Pub., 2012.

[53] L. Wang, *Model Predictive Control System Design and Implementation Using MATLAB*. Springer, 2009.

[54] L. Grne and J. Pannek, *Non-linear Model Predictive Control*. Springer, 2011.

[55] A. Yetendje, M. M. Seron, and J. A. De Dona, "Robust multisensor fault tolerant model-following mpc design for constrained systems," *International Journal of Applied Mathematics and Computer Science*, vol. 22, no. 1, pp. 211–223, 2012.

[56] H. Huang, D. W. Li, Z. L. Lin, and Y. G. Xi, "An improved robust model predictive control design in the presence of actuator saturation," *Automatica*, vol. 47, no. 4, pp. 861–864, 2011.

[57] V. Adetola and M. Guay, "Robust adaptive MPC for constrained uncertain non-linear systems," *International Journal of Adaptive Control and Signal Processing*, vol. 25, no. 2, pp. 155–167, 2011.

[58] J. S. Kim, "Recent advances in adaptive mpc," in *International Conference on Control, Automation and Systems (Iccas 2010)*, pp. 218–222, 2010.

[59] C. Liu, W. H. Chen, and J. Andrews, "Explicit non-linear model predictive control for autonomous helicopters," *Proceedings of the Institution of Mechanical Engineers Part G-Journal of Aerospace Engineering*, vol. 226, no. G9, pp. 1171–1182, 2012.

[60] M. Verhaegen, S. Kanev, R. Hallouzi, C. Jones, J. Maciejowski, and H. Smail, "Fault tolerant flight control - a survey," in *Fault Tolerant Flight Control* (C. Edwards, T. Lombaerts, and H. Smaili, eds.), vol. 399 of *Lecture Notes in Control and Information Sciences*, pp. 47–89, Springer Berlin Heidelberg, 2010.

[61] Q. Mayne, B. Rawlings, V. Rao, and O. Scokaert, "Constrained model predictive control: Stability and optimality," *Automatica*, vol. 36, no. 6, pp. 789–814, 2000.

[62] G. J. Balas, "Flight control law design: An industry perspective," *European Journal of Control*, vol. 9, no. 23, pp. 207–226, 2003.

[63] B. Friedland, "Treatment of bias in recursive filtering," *IEEE Transactions on Automatic Control*, vol. 14, no. 4, pp. 359–367, 1969.

[64] M. B. Ignagni, "Separate bias kalman estimator with bias state noise," *IEEE Transactions on Automatic Control*, vol. 35, no. 3, pp. 338–341, 1990.

[65] J. Y. Keller and M. Darouach, "Optimal two-stage Kalman filter in the presence of random bias," *Automatica*, vol. 33, no. 9, pp. 1745–1748, 1997.

[66] Y. M. Zhang and J. Jiang, "Integrated design of reconfigurable fault-tolerant control systems," *Journal of Guidance, Control, and Dynamics*, vol. 24, no. 1, pp. 133–136, 2001.

[67] M. H. Amoozgar, A. Chamseddine, and Y. M. Zhang, "Experimental test of a two-stage Kalman filter for actuator fault detection and diagnosis of an unmanned quadrotor helicopter," *Journal of Intelligent & Robotic Systems*, vol. 70, no. 1-4, pp. 107–117, 2013.

[68] Y. M. Zhang, A. Chamseddine, C. A. Rabbath, B. W. Gordon, C. Y. Su, S. Rakheja, C. Fulford, J. Apkarian, and P. Gosselin, "Development of advanced FDD and FTC techniques with application to an unmanned quadrotor helicopter testbed," *Journal of the Franklin Institute*, vol. 350, no. 9, pp. 2396–2422, 2013.

[69] K. Dalamagkidis, K. P. Valavanis, and L. A. Piegl, "Non-linear model predictive control with neural network optimization for autonomous autorotation of small unmanned helicopters," *IEEE Transactions on Control Systems Technology*, vol. 19, no. 4, pp. 818–831, 2011.

[70] K. Patan and J. Korbicz, "Non-linear model predictive control of a boiler unit: A fault tolerant control study," *International Journal of Applied Mathematics and Computer Science*, vol. 22, no. 1, pp. 225–237, 2012.

[71] M. Saffarian and F. Fahimi, "Non-iterative non-linear model predictive approach applied to the control of helicopters' group formation," *Robotics and Autonomous Systems*, vol. 57, no. 6-7, pp. 749–757, 2009.

[72] B. A. G. Genuit, L. Lu, and W. P. M. H. Heemels, "Approximation of explicit model predictive control using regular piecewise affine functions: An input-to-state stability approach," *IET Control Theory and Applications*, vol. 6, no. 8, pp. 1015–1028, 2012.

[73] D. Q. Mayne and S. Rakovic, "Model predictive control of constrained piecewise affine discrete-time systems (vol 13, pg 261, 2003)," *International Journal of Robust and nonlinear Control*, vol. 15, no. 6, pp. 291–291, 2005.

[74] Y. Y. Zou and S. Y. Li, "Robust model predictive control for piecewise affine systems," *Circuits Systems and Signal Processing*, vol. 26, no. 3, pp. 393–406, 2007.

[75] S. Mollov, T. van den Boom, F. Cuesta, A. Ollero, and R. Babuska, "Robust stability constraints for fuzzy model predictive control," *IEEE Transactions on Fuzzy Systems*, vol. 10, no. 1, pp. 50–64, 2002.

[76] T. Zhang, G. Feng, and J. H. Lu, "Fuzzy constrained min-max model predictive control based on piecewise Lyapunov functions," *IEEE Transactions on Fuzzy Systems*, vol. 15, no. 4, pp. 686–698, 2007.

[77] J. A. Rossiter, B. Kouvaritakis, and M. Rice, "A numerically robust state-space approach to stable-predictive control strategies," *Automatica*, vol. 34, no. 1, pp. 65–73, 1998.

[78] Q. I. Educate, "Quanser Qball-X4 user manual," 2012.

[79] Y. M. Zhang and A. Chamseddine, "Fault tolerant flight control techniques with application to a quadrotor UAV testbed," *Automatic Flight Control Systems-Latest Developments, InTech*, 2012.

[80] M. V. Cook, *Flight Dynamics Principles, Second Edition: A Linear Systems Approach to Aircraft Stability and Control*, vol. 2. Butterworth-Heinemann, 2007.

[81] T. Bresciani, *Modelling, Identification and Control of a Quadrotor Helicopter*. Department of Automatic Control, Lund University, 2008.

[82] B. D. Anderson, J. Pren, and S. Dickerson, *Linear Optimal Control*. Prentice Hall, 1971.

[83] C. R. Hanke, *The Simulation of a Large Jet Transport Aircraft: Mathematical Model*. National Aeronautics and Space Administration, 1971.

[84] C. R. Hanke and D. R. Nordwall, "The simulation of a jumbo jet transport aircraft. volume 2: Modeling data," report, National Aeronautics and Space Administration, 1970.

[85] A. Marcos and G. Balas, "Linear parameter varying modeling of the Boeing 747-100/200 longitudinal motion," in *AIAA Guidance, Navigation and Control Conference, AIAA-01-4347, Montreal, Canada*, 2001.

[86] A. Marcos, S. Ganguli, and G. J. Balas, "An application of H∞ fault detection and isolation to a transport aircraft," *Control Engineering Practice*, vol. 13, no. 1, pp. 105–119, 2005.

[87] J. Cieslak, D. Henry, and A. Zolghadri, "A FTC strategy for safe recovery against trimmable horizontal stabilizer failure with guaranteed nominal performance," in *Fault Tolerant Flight Control* (C. Edwards, T. Lombaerts, and H. Smaili, eds.), vol. 399 of *Lecture Notes in Control and Information Sciences*, pp. 337–361, Springer Berlin Heidelberg, 2010.

[88] A. Varga, "Detection and isolation of actuator/surface faults for a large transport aircraft," in *Fault Tolerant Flight Control* (C. Edwards, T. Lombaerts, and H. Smaili, eds.), vol. 399 of *Lecture Notes in Control and Information Sciences*, pp. 423–448, Springer Berlin Heidelberg, 2010.

[89] J. D. Blight, R. LANE DAILEY, and D. Gangsaas, "Practical control law design for aircraft using multivariable techniques," *International Journal of Control*, vol. 59, no. 1, pp. 93–137, 1994.

[90] L. Wang, "Use of exponential data weighting in model predictive control design," in *Proceedings of the 40th IEEE Conference On Decision and Control*, vol. 5, pp. 4857–4862, 2001.

[91] L. Wang, "Discrete model predictive controller design using laguerre functions," *Journal of Process Control*, vol. 14, no. 2, pp. 131–142, 2004.

Appendix

FTC Test on Qball-X4 Platform

Based on the simulation results, experiments are carried out with the proposed FTC technique validated in the Matlab/Simulink environment. The facilities about the testbed are described in Chapter 3. The parameters of the Qball-X4 are listed in Table 3.1. The fault scenario of 10% of the LOE fault is similar with the fault scenario simulated in the Simulink environment but only including take-off, hovering, and landing. The first $10s$ is the state on the ground with the rotor speeding. At the $10s$ time instant, a step command as a reference for the demanded height feeds into the system. The Qball-X4 works under normal duties until an abrupt 10% LOE occurs at the time instant $30s$. The faulty Qball-X4 lands at $40s$ successfully. The performance is depicted in Fig. 8.1. The dashed blue line is the reference and the red line is the measurement. It can be seen that the proposed fault-tolerant controller possesses the fault accommodation ability and can still work under the actuator faults scenario.

As can be seen from Fig. 8.1, the Qball-X4 follows the height reference on the ground and before $30s$. The time response is fast with very little over shoot. The graph in the first $30s$ shows that the controller performs well in the fault-free mode. The measured height drops in height not significantly showing that the fault has influence on the performance of the Qball-X4. Since, the designed fault-tolerant controller successes accommodate the performance degradation induced by actuator faults.

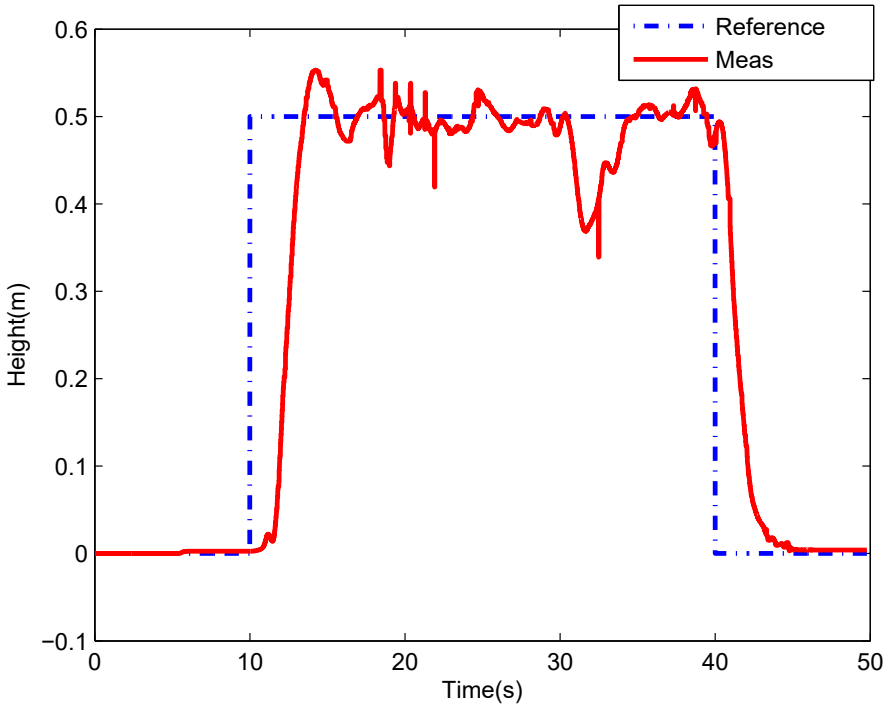

Figure 8.1: Height response for normal and 10% LOE

Full State Model of Boeing 747-100/200

$$B_{lin} = [B_{lin_a} \quad B_{lin_{sp}} \quad B_{lin_e} \quad B_{lin_r} \quad B_{lin_{fp}} \quad B_{lin_{T_n}}] \tag{8.2}$$

$$A_{lin} = \begin{bmatrix} -1.0571 & 0 & 0.1718 & 0 & 0 & -1.647 & 0.0004 & 0 & 0 & 0 & 0 & 0 \\ 0 & -0.5133 & 0 & 0.0003 & -0.5827 & 0 & 0 & 0 & 0 & 0 & 0 & 0 \\ -0.1186 & 0 & -0.2065 & 0 & 0 & 0.2764 & -0.0019 & 0 & 0 & 0 & 0 & 0 \\ 0 & 0 & 0 & -0.0178 & 1.7243 & 0 & 0 & -9.8046 & 0 & 0.0001 & 0 & 0 \\ 0 & 1.0064 & 0 & -0.0021 & -0.6278 & 0 & 0 & 0 & 0 & 0 & 0 & 0 \\ 0.1015 & 0 & -0.9887 & 0 & 0 & -0.0998 & 0.1055 & 0 & 0 & 0 & 0 & 0 \\ 1 & 0 & 0.0895 & 0 & 0 & 0 & 0 & 0 & 0 & 0 & 0 & 0 \\ 0 & 1 & 0 & 0 & 0 & 0 & 0 & 0 & 0 & 0 & 0 & 0 \\ 0 & 0 & 1.004 & 0 & 0 & 0 & 0 & 0 & 0 & 0 & 0 & 0 \\ 0 & 0 & 0 & 0 & -92.5985 & 0 & 0 & 92.5985 & 0 & 0 & 0 & 0 \\ 0 & 0 & 0 & -1 & 0 & 0 & 0 & 0 & 0 & 0 & 0 & 0 \\ 0 & 0 & 0 & 0 & 0 & -92.5985 & 8.2528 & 0 & -92.5985 & 0 & 0 & 0 \end{bmatrix} \tag{8.1}$$

$$B_{lin_a} = \begin{bmatrix} -0.0014515 & 0.0014515 & -0.0039864 & 0.0039864 \\ 0.00018734 & 0.00018734 & -0.0012622 & -0.0012622 \\ -0.00026775 & 0.00026775 & -0.00021456 & 0.00021456 \\ 0 & 0 & 0 & 0 \\ 0 & 0 & -0.00020206 & -0.00020206 \\ 0 & 0 & 0 & 0 \\ 0 & 0 & 0 & 0 \\ 0 & 0 & 0 & 0 \\ 0 & 0 & 0 & 0 \\ 0 & 0 & 0 & 0 \\ 0 & 0 & 0 & 0 \\ 0 & 0 & 0 & 0 \end{bmatrix} \tag{8.3}$$

$$B_{lin_e} = \begin{bmatrix} 0 & 0 & 0 & 0 \\ -0.0026799 & -0.0026799 & -0.0027518 & -0.0027518 \\ 0 & 0 & 0 & 0 \\ 0 & 0 & 0 & 0 \\ -0.00015004 & -0.00015004 & -0.00015718 & -0.00015718 \\ 0 & 0 & 0 & 0 \\ 0 & 0 & 0 & 0 \\ 0 & 0 & 0 & 0 \\ 0 & 0 & 0 & 0 \\ 0 & 0 & 0 & 0 \\ 0 & 0 & 0 & 0 \\ 0 & 0 & 0 & 0 \end{bmatrix} \tag{8.5}$$

$$B_{lin_{sp}} = \begin{bmatrix} -0.0010951 & -0.0011848 & -0.0011848 & -0.0011136 & -0.001182 & 0 & 0 & 0.001182 & 0.0011136 & 0.0011848 & 0.0011848 & 0.0010951 \\ 7.9854e-05 & 0.00011799 & 0.00011799 & 0.0001152 & -9.4011e-05 & -0.00046168 & 0 & -9.4011e-05 & 0.0001152 & 0.00011799 & 0.00011799 & 7.9854e-05 \\ -8.6515e-05 & -7.5066e-05 & -7.5066e-05 & -7.7655e-05 & -9.0698e-05 & 0 & 0 & 9.0698e-05 & 7.7655e-05 & 7.5066e-05 & 7.5066e-05 & 8.6515e-05 \\ 0.00053469 & 0.0026793 & 0.0026793 & 0.0022965 & 0.0010694 & 0 & 0 & 0.0010694 & 0.0022965 & 0.0026793 & 0.0026793 & 0.00053469 \\ 4.2889e-05 & 4.329e-05 & 4.329e-05 & 5.7719e-05 & 9.894e-05 & 0.00022765 & 0 & 9.894e-05 & 5.7719e-05 & 4.329e-05 & 4.329e-05 & 4.2889e-05 \\ 9.8088e-06 & 6.0596e-06 & 6.0596e-06 & 8.0794e-06 & 9.8088e-06 & 0 & 0 & -9.8088e-06 & -8.0794e-06 & -6.0596e-06 & -6.0596e-06 & -9.8088e-06 \\ 0 & 0 & 0 & 0 & 0 & 0 & 0 & 0 & 0 & 0 & 0 & 0 \\ 0 & 0 & 0 & 0 & 0 & 0 & 0 & 0 & 0 & 0 & 0 & 0 \\ 0 & 0 & 0 & 0 & 0 & 0 & 0 & 0 & 0 & 0 & 0 & 0 \\ 0 & 0 & 0 & 0 & 0 & 0 & 0 & 0 & 0 & 0 & 0 & 0 \\ 0 & 0 & 0 & 0 & 0 & 0 & 0 & 0 & 0 & 0 & 0 & 0 \\ 0 & 0 & 0 & 0 & 0 & 0 & 0 & 0 & 0 & 0 & 0 & 0 \end{bmatrix} \quad (8.4)$$

$$B_{lin_r} = \begin{bmatrix} 0.0015433 & 0.0005263 \\ -1.7767e-15 & -5.9225e-16 \\ -0.0024973 & -0.0018245 \\ 1.1066e-14 & 0 \\ 0 & 0 \\ 0.00016595 & 0.00013815 \\ 0 & 0 \\ 0 & 0 \\ 0 & 0 \\ 0 & 0 \\ 0 & 0 \\ 0 & 0 \end{bmatrix} \tag{8.6}$$

$$B_{lin_{fp}} = \begin{bmatrix} -2.7844e-22 & 9.1824e-18 \\ -0.0046546 & 0.0031219 \\ 1.2756e-21 & -6.263e-21 \\ -0.018924 & -0.026714 \\ -0.0012713 & -0.0012799 \\ -6.944e-20 & 9.6089e-20 \\ 0 & 0 \\ 0 & 0 \\ 0 & 0 \\ 0 & 0 \\ 0 & 0 \\ 0 & 0 \end{bmatrix} \tag{8.7}$$

$$B_{lin_{Tn}} = \begin{bmatrix} 6.5041e-08 & 3.7121e-08 & -3.7121e-08 & -6.5041e-08 \\ 2.1638e-08 & 5.7588e-08 & 5.7588e-08 & 2.1638e-08 \\ 3.3541e-07 & 1.914e-07 & -1.914e-07 & -3.3541e-07 \\ 3.7724e-06 & 3.7724e-06 & 3.7724e-06 & 3.7724e-06 \\ -5.6185e-09 & -5.6185e-09 & -5.6185e-09 & -5.6185e-09 \\ 1.433e-09 & 1.433e-09 & -1.433e-09 & -1.433e-09 \\ 0 & 0 & 0 & 0 \\ 0 & 0 & 0 & 0 \\ 0 & 0 & 0 & 0 \\ 0 & 0 & 0 & 0 \\ 0 & 0 & 0 & 0 \\ 0 & 0 & 0 & 0 \end{bmatrix} \tag{8.8}$$

Boeing 747-100/200 Series Operational Data and Geometric Dimensions

Table 8.1: Boeing 747-100/200 operational data and geometric dimensions

	Boeing 747-100/200	Boeing 747-200F
Wing area	511 m^2	511 m^2
Wing mean aerodynamic chord (MAC)	8.324 m^2	8.324m^2
Wing span	59.65 m	59.65 m
Length overall	70.66 m	70.66 m
Height overall	19.33 m	19.33 m
Engines	Pratt Whitney JT9D-3	Pratt Whitney JT9D-7J
Takeoff thrust rating (standard day/sea level)	193 kN	222kN
Maximum takeoff weight	321,995 kg	377,842 kg
Maximum landing weight	255,782 kg	285,763
Maximum zero fuel weight	238,776 kg	267,619 kg
Maximum zero fuel weight	238.776 kg	267.619 kg
Load factor range flaps up	$-1.0/+2.5$	$-1.0/+2.5$
Load factor range flaps down	0/+2	0/+2